SUBTASK 3.4 – FISCHER–TROPSCH FUELS DEVELOPMENT

Final Report

Submitted to:

AAD Document Control

Submitted by:

Joshua R. Strege
Anthony C. Snyder
Jason D. Laumb
Joshua J. Stanislowski
Michael L. Swanson

Energy & Environmental Research Center
University of North Dakota
15 North 23rd Street, Stop 9018
Grand Forks, ND 58202-9018

2012-EERC-06-04   June 2012

(B)   Assumes any liabilities with respect to the use of, or for damages resulting from the use of, any information, apparatus, method, or process disclosed in this report.

Reference herein to any specific commercial product, process, or service by trade name, trademark, manufacturer, or otherwise does not necessarily constitute or imply its endorsement, recommendation, or favoring by the NDIC. The views and opinions of authors expressed herein do not necessarily state or reflect those of the NDIC.

SUBTASK 3.4 – FISCHER–TROPSCH FUELS DEVELOPMENT

ABSTRACT

Under Subtask 3.4, the Energy & Environmental Research Center (EERC) examined the opportunities and challenges facing Fischer–Tropsch (FT) technology in the United States today. Work was completed in two distinct budget periods (BPs). In BP1, the EERC examined the technical feasibility of using modern warm-gas cleanup techniques for FT synthesis. FT synthesis is typically done using more expensive and complex cold-gas sweetening. Warm-gas cleanup could greatly reduce capital and operating costs, making FT synthesis more attractive for domestic fuel production. Syngas was generated from a variety of coal and biomass types; cleaned of sulfur, moisture, and condensables; and then passed over a pilot-scale FT catalyst bed. Laboratory and modeling work done in support of the pilot-scale effort suggested that the catalyst was performing suboptimally with warm-gas cleanup. Long-term trends showed that the catalyst was also quickly deactivating.

In BP3, the EERC compared FT catalyst results using warm-gas cleanup to results using cold-gas sweetening. A gas-sweetening absorption system (GSAS) was designed, modeled, and constructed to sweeten syngas between the gasifier and the pilot-scale FT reactor. Results verified that the catalyst performed much better with gas sweetening than it had with warm-gas cleanup. The catalyst also showed no signs of rapid deactivation when the GSAS was running. Laboratory tests in support of this effort verified that the catalyst had deactivated quickly in BP1 because of exposure to syngas, not because of any design flaw with the pilot-scale FT reactor itself. Based on these results, the EERC concludes that the two biggest issues with using syngas treated with warm-gas cleanup for FT synthesis are high concentrations of CO_2 and volatile organic matter. Other catalysts tested by the EERC may be more tolerant of CO_2, but volatile matter removal is critical to ensuring long-term FT catalyst operation.

TABLE OF CONTENTS

TABLE OF CONTENTS (continued)

LIST OF FIGURES

LIST OF FIGURES (continued)

LIST OF TABLES

NOMENCLATURE

ASF	Anderson–Schultz–Flory (distribution model used to describe FT product composition)
BP	budget period
BYU	Brigham Young University
C_{5+}	pentane and heavier hydrocarbons
CTL	coal to liquids
DCL	direct coal liquefaction
DEPG	dimethyl ether of polyethylene glycol (solvent used for gas sweetening)
DDGS	dried distiller's grains and solubles (by-product of ethanol production)
EERC	Energy & Environmental Research Center
FID	flame ionization detector (with GC)
FT	Fischer–Tropsch
FTS	Fischer–Tropsch synthesis
GC	gas chromatography
GSAS	gas-sweetening absorption system
HDO	hydrodeoxygenation
HHV	higher heating value
HPFBG	high-pressure fluidized-bed gasifier
HPLC	high-performance liquid chromatography
ICP	inductively coupled plasma (tool for measuring metals content)
IGCC	integrated gasification combined cycle
LGA	laser gas analyzer (Raman spectrometer)
MS	mass spectrometer (with GC or as a stand-alone unit)
NDIC	North Dakota Industrial Commission (cost-share partner in BP1)
PFPD	pulsed-flame photometric detector (with GC)
PRB	Powder River Basin
RI	refractive index (with HPLC)
	retention index, particularly Kovats RI (as a measure of a peak's position in a GC or HPLC chromatogram)
SMP	subtask management plan
$STCO_2$	selectivity to CO_2
STLG	selectivity to light gas
TCD	thermal conductivity detector (with GC)
TL	torrefied and leached
TOC	total organic content (refers to carbon molecules dissolved in water)
UV	ultraviolet (with HPLC)
WGS	water–gas shift

SUBTASK 3.4 – FISCHER–TROPSCH FUELS DEVELOPMENT

EXECUTIVE SUMMARY

Fischer–Tropsch (FT) technology allows the United States to domestically produce liquid fuels from existing coal and biomass resources. Under Subtask 3.4 of the Strategic National Energy Security Solutions (SNESS) Program, the Energy & Environmental Research Center (EERC) developed catalysts and processes to improve the technical and economic feasibility of FT synthesis in the United States, enhancing our nation's overall energy security. Work focused on upstream processes such as gasification and syngas cleanup, on the FT process itself, and on the downstream process of fuel upgrading.

Work under Subtask 3.4 occurred in two distinct budget periods (BPs). BP1 began in July 2008 and ended in March 2010. In BP1, a high-pressure fluidized-bed gasifier (HPFBG) was coupled to a small, pilot-scale, packed-bed FT reactor. Two coal types were gasified: a North Dakota lignite and a Powder River Basin subbituminous. In addition, three biomass types were cogasified with the coal and gasified straight. The biomass included switchgrass, dried distiller's grains and solubles, and olive pits. Biomass was gasified untreated, leached, and torrefied.

Syngas was cleaned by using hot sorbent beds to remove H_2S and water-cooled quench pots to remove waters and tars. The gasifier was successfully operated on all coal and biomass types. Biomass pretreatment by leaching helped to prevent ash agglomeration when cofeeding 30% biomass with coal (either subbituminous or lignite), and biomass torrefaction led to higher gasification temperatures. Untreated biomass led to agglomeration, demonstrating that leaching had helped to improve the gasification potential of the biomass. Issues with gasifier operation prevented any clear results as to whether long-term, sustainable gasification of 100% biomass (that is, without coal blending) was feasible on this system.

The packed-bed FT reactor achieved sustained liquid synthesis and temperature control, demonstrating the feasibility of this design for small-scale operation. However, catalyst deactivation was apparent both from reactor operation and product analysis. Laboratory work showed that the catalyst did not perform well under high CO_2 concentrations as seen in the syngas. In the laboratory, the catalyst suffered 80% loss of productivity when feed was switched from an optimum blend of CO and H_2 to simulated syngas containing significant levels of CO_2 and N_2. Light gasifier tars may also have caused coking in the pilot-scale reactor. An attempt to regenerate the catalyst in the pilot-scale reactor had no noticeable impact on catalyst activity.

A process for generating kilogram-scale quantities of pelletized iron-based catalyst was conceived of, constructed, and tested. Although the process was successful, the catalyst was never used in the packed-bed FT reactor. Laboratory testing under BP3 would reveal that this catalyst had very poor mechanical strength and would not be suitable for use in a fixed bed.

Using AspenPlus™ software, a computer-based model was developed that is capable of accurately predicting the gas composition from the gasifier. Early results from laboratory-scale

FT synthesis were used to generate equations for predicting the behavior of the packed-bed FT reactor. However, the syngas composition from the gasifier was sufficiently different from the composition used in the laboratory-scale reactor that the model could not accurately predict the distribution of various components in the FT liquids.

The liquid product from the packed-bed FT reactor was upgraded to improve its fuel qualities. Although not required by the BP1 subtask management plan (SMP), the aim of the upgrading effort was to generate specification-compliant jet fuel. The product quality was much improved by hydrotreating, but product enhancement did not fully convert the FT product into jet fuel. The effort demonstrated the feasibility of a FT product-upgrading process and also identified key issues to be considered if the goal of upgrading FT liquids is to produce jet fuel.

BP2 was initially proposed as a collaborative effort with Albemarle Corporation, a global catalyst company. Albemarle would provide in-kind cost share to develop FT catalysts specific to syngas from biomass-rich feeds. This proposal was ultimately rescinded by the EERC, and the funding originally set aside for BP2 was reallocated to projects with greater commercial cost share in the form of cash rather than in-kind.

BP3 began in October 2010. Since BP1 had shown that both CO_2 and light gasifier tars had a negative impact on catalyst performance, BP3 examined catalyst performance when a gas-sweetening system was used. The basic column design was first modeled using ChemCAD$^{®}$ and AspenPlus to determine operating performance under various conditions. The column design was then finalized based on model results and constructed at the EERC. Lastly, the column was operated using the same HPFBG and FT reactor used in BP1 to see how strong of an effect gas sweetening had on catalyst performance.

The FT catalyst, coal, and operating parameters were nearly identical to those used in BP1 when syngas was only treated by warm-gas sulfur capture and water quench. The results with gas sweetening showed significant improvement in every metric of FT system performance. Carbon monoxide conversion through the FT skid increased by 280% per unit of catalyst; hydrocarbon production increased by 240%; wax collection increased from zero to 20% of the total organic product; and the quality of recovered FT liquids also increased notably as the saturated content increased from 40% to 55% of the liquid organic product. Heavy, saturated hydrocarbons are generally considered more desirable for fuel processing than light, unsaturated hydrocarbons, so the higher production of wax and saturated liquid means that more of the recovered hydrocarbon could be processed into diesel fuel, jet fuel, lubricant, or wax. The FT product quality also held steady during the entire week of operation, whereas the product had become lighter and less saturated over the course of a few days when running with only warm-gas cleanup.

The iron-based catalyst had clearly underperformed with a high CO_2 concentration during BP1. Cobalt-based catalysts might fare better than iron-based catalysts with similar concentrations of CO_2 as long as the H_2/CO ratio of the syngas is acceptable. The EERC produced a suite of cobalt-based FT catalysts to test this theory using bottled gas. The first two catalysts tested showed little if any activity, so ruthenium was added as a modifier. The cobalt catalyst with ruthenium added performed reasonably well. The cobalt-based catalyst showed decreased activity when exposed to simulated syngas, but the decrease in activity was not as

severe as had been the case for iron-based catalysts. This result is not conclusive but does suggest that cobalt may be preferable to iron when CO_2 acts to dilute syngas without changing the H_2/CO ratio.

SUBTASK 3.4 – FISCHER–TROPSCH FUELS DEVELOPMENT

1.0 INTRODUCTION

There has been growing interest in recent years to supplant petroleum-based fuels with alternative transportation fuels. One promising route for domestic production of liquid fuels is Fischer–Tropsch synthesis (FTS). FTS has at least two advantages over other routes to generate synthetic fuels. The first advantage is that the FT process uses gasification, a well-demonstrated commercial process for converting carbon-based material to syngas. Gasification relies on high-temperature reactions with steam, oxygen, and air to fully decompose carbon molecules into H_2, CO, CO_2, CH_4, and other gases while rejecting unusable inorganic material as slag or ashy char. As such, syngas can be produced from any carbon-based material with enough energy to sustain gasification temperatures, including coal, natural gas, petroleum residues, biomass, or waste. Most other routes to synthetic fuels rely on specific chemical characteristics of the feed and do not fully decompose the feed material. This limits the types of feed that can be used for those processes and also limits what fraction of a given feedstock can be converted to fuel. For instance, ethanol can only be fermented from sugar, and direct coal liquefaction (DCL) processes can only use specific ranks of coal.

The second clear advantage for FTS is that the FT process has been successfully demonstrated at the large scale since the Second World War. The process was first described by Frans Fischer and Hans Tropsch in the 1920s (1), and by 1935, Fischer had described processes for generating optimum syngas compositions, removing sulfur, and achieving high FTS conversion (2–4). The process was developed at an industrial scale by Germany and used to generate diesel fuel throughout World War II using cobalt-based catalyst and coal-derived syngas (5). In the decades since, FTS has been practiced on an even larger scale in South Africa by Sasol and PetroSA. Coal-to-liquid (CTL) processes similar to FTS for generating chemicals, such as methanol, from syngas have been practiced commercially in the United States for many years. The long history of successful commercial operation with FTS and related CTL processes offers assurance of its large-scale technical feasibility.

FTS can generate a number of organic compounds, the most prevalent of which are normal or *n*-paraffins (Equation 1); olefins (Equation 2); and primary alcohols (Equation 3). The primary by-product of FTS is water. Iron-based catalysts can catalyze the water-gas shift (WGS) reaction, which converts some of the FT product water into H_2 and CO_2 by Equation 4. The WGS reaction is reversible, so extra product water could also be generated at high CO_2 concentrations and low CO concentrations. Cobalt-based catalysts have no WGS activity and do not consume FT product water or generate extra water.

$$n \cdot CO + (2n+1) \cdot H_2 \rightarrow C_nH_{2n+2} + n \cdot H_2O \qquad \text{[Eq. 1]}$$

$$n \cdot CO + 2n \cdot H_2 \rightarrow C_nH_{2n} + n \cdot H_2O \qquad \text{[Eq. 2]}$$

$$n \cdot CO + 2n \cdot H_2 \rightarrow C_nH_{2n+1}OH + (n-1) \cdot H_2O \qquad \text{[Eq. 3]}$$

$$H_2O + CO \rightleftharpoons H_2 + CO_2 \hspace{4cm} \text{[Eq. 4]}$$
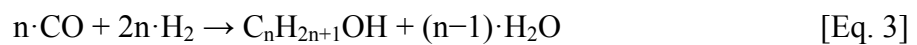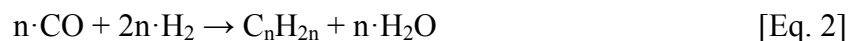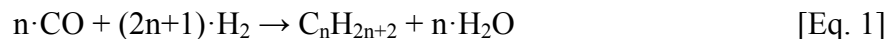
While FTS is well-established and understood, several obstacles have hindered its widespread adoption for synthetic fuel production. The first and perhaps most important factor is cost. At a minimum, FT plants require pressurized gasification, deep gas sweetening to remove contaminants, and FT reactors. Gasifiers and FT reactors are obviously necessary costs, but the gas-sweetening process is also a very expensive part of a FT plant. Large-scale gas sweetening is often done today using physical solvents such as Rectisol® or SELEXOL™. Such solvent-based processes cool the syngas to subzero temperatures so that the solvent can physically absorb carbon dioxide, hydrogen sulfide, volatile matter, and other syngas contaminants. H_2S is of special concern in the FT process because it has been known from the time FTS was first discovered to rapidly and permanently deactivate FT catalysts (1, 4).

Because of the need for cryogenic cooling, the capital and operating costs for traditional cold-gas cleanup are significant. The energy penalty of cooling and reheating both syngas and solvent can also be significant. This limits gas sweetening for synthetic fuel production to very large installations that can benefit from economies of scale. Small-scale CTL plants may operate profitably by generating higher-value chemicals, but given the comparatively low value of transportation fuel, FTS can only operate economically at a large scale.

H_2S and other key contaminants can also be removed using hot- or warm-gas sorbents (6, 7). Warm-gas cleanup is a promising alternative to gas sweetening at the small scale because it requires less maintenance, does not have the significant energy penalty associated with cooling and reheating gas and liquid streams, and has lower utility costs. However, warm-gas cleanup cannot capture all gas contaminants. Some gas cooling is required to condense water and gasifier tars, and gas sweetening remains the only practical way to capture CO_2.

While high costs can potentially be overcome using warm-gas cleanup, another factor that hinders widespread adoption of FTS for liquid fuel production is its environmental impact. CO_2 captured by gas sweetening is often released into the atmosphere, and FTS over iron-based catalyst generates further CO_2 via the WGS reaction (Equation 4). The carbon footprint of a large-scale FT plant is thus quite substantial.

CO_2 emissions can be reduced by cofeeding biomass in the gasification step. Because plant matter consumes as much CO_2 as it releases when burned, the use of biomass can reduce net CO_2 emissions of the FT process. However, there are at least two major issues that limit the use of biomass for FTS. First, many biomass types are rich in alkali and chlorine, species that cause agglomeration and corrosion, respectively. Finding ways to remove or minimize the impact of these species will be critical to incorporating biomass into gasifiers designed for coal or petroleum residues (8, 9). Second, as described above, gasification and FTS do not readily scale down. Biomass gasification plants are likely to be limited in scale to the amount of biomass available in the immediate area (10, 11). Given the massive infrastructure required to not only gasify biomass but then to shift the gas chemistry, sweeten the syngas, and convert the gas to liquid fuels, commercial gasification and FTS will likely require more biomass than can be supplied at a reasonable collection radius in order to operate at a profit.

One way to make biomass gasification more economical while also reducing the impact of alkali and chlorine is by biomass pretreatment. Leaching is an effective pretreatment method for removing water-soluble salts (8, 9, 12). Other pretreatment methods can densify biomass at the collection site, making it easier to transport. Numerous densification options are available, including drying, pelletizing, pyrolysis, and torrefaction. In cofeeding with coal for gasification, torrefaction offers a unique advantage in that the torrefaction product is similar in energy density and physical characteristics to coal, allowing it to achieve similar bed temperatures and to be fed similarly (13, 14). Cofeeding torrefied biomass with coal will likely be an easier proposition than cofeeding raw biomass or pyrolysis oil into a gasifier.

A commercial FT plant might be able to economically operate at a smaller scale, minimize its CO_2 emissions, and reduce capital and operating costs by using warm-gas cleanup while blending torrefied biomass and coal. However, as stated previously, warm-gas cleanup cannot capture all gas contaminants. CO_2 in particular cannot be removed without gas sweetening.

A number of researchers have studied the effects of CO_2 on FTS and have shown that iron-based FT catalysts can synthesize liquids from CO_2 (15–22). The studies referenced used exclusively bottled gas for FTS in laboratory-scale reactors. Given the promising nature of these results, it may not be necessary to remove CO_2 for FTS over iron, and warm-gas cleanup using modern sorbents may be sufficient. However, it is not certain from the laboratory results whether gas sweetening might still be needed to remove other trace contaminants (gasifier tar, ammonia, chlorides, metals, etc.). It is likewise uncertain whether the FT product generated using warm-gas cleanup would present any unique challenges for refining to fuel.

Subtask 3.4 – Fischer–Tropsch Fuels Development was conceived as a project to test these various processes that might encourage more widespread adoption of FTS which, in turn, would increase the use of domestic energy resources, reduce dependence on foreign oil, and provide a reliable, long-term source of alternative transportation fuel. In BP1 of Subtask 3.4, the Energy & Environmental Research Center (EERC) constructed a pilot-scale FT reactor based on design recommendations provided by Brigham Young University (BYU) through its FT Consortium. This FT reactor was coupled to an oxygen-blown, high-pressure, fluidized-bed gasifier (HPFBG). The gasifier was operated using blends ranging from 100% coal to 100% biomass to determine the effects of biomass pretreatment and fuel blending on gasification and FT performance. Warm-gas cleanup was used to remove sulfur from the syngas, and water cooling was used to remove moisture and other condensables from the syngas, but the dry syngas was left unsweetened. The syngas was fed to an iron-based FT catalyst to determine whether warm-gas cleanup is sufficient for long-term FTS using a fluidized-bed gasifier.

In support of the pilot-scale effort in BP1, the EERC also developed a novel iron-based catalyst production method and performed laboratory-scale testing on several batches of catalyst. A model of the HPFBG and FT reactor was developed using AspenPlus® software to predict system performance. FT liquids generated in BP1 were hydrotreated and distilled to jet fuel to determine whether warm-gas cleanup had any impact on refining.

In BP3, a gas-sweetening absorption system (GSAS) was designed, built, and coupled to the HPFBG and pilot-scale FT reactor. The GSAS provided sweetened syngas to the FT reactor

so that its performance using warm-gas cleanup could be compared to performance using gas sweetening. AspenPlus and ChemCAD® were used to design and simulate the GSAS before construction. A cobalt-based FT catalyst was also developed and tested in the laboratory under bottled gas to assess its performance relative to iron-based FT catalyst using simulated warm-gas cleanup. Finally in BP3, a dual-column pilot distillation system was purchased for upgrading DCL liquids that might be blended with FT liquids to generate fungible transportation fuel.

2.0   GOALS AND OBJECTIVES

Subtask 3.4 started in Budget Period (BP) 1 and continued through BP3. In BP1, the goal was to assess the viability of small-scale distributed gasification and FTS using warm-gas cleanup, cofeeding coal with biomass, and biomass pretreatment. The specific objectives were to develop and test FT catalysts using warm-gas cleanup, to test FT catalyst performance under both coal and biomass, and to develop a model for predicting FT system performance under varying conditions. Warm-gas cleanup using packed-bed sorbents is more readily scaled down and requires less energy than cold-gas sweetening, so it is better suited to small-scale distributed gasification. However, little information is available on the feasibility of FTS using modern warm-gas capture sorbents, as existing large-scale FT plants rely on cold-gas sweetening.

BP2 was originally focused on development of novel cobalt-based FT catalysts, particularly catalysts that would better operate using warm-gas cleanup. The project partner, Albemarle Corporation, would also work with the EERC to develop novel catalysts for upgrading FT waxes into fungible fuels. However, BP2 ultimately fell through, and the funds were reallocated to other projects. No work was conducted under BP2, and Activities 5–9 were removed from the subtask management plan (SMP).

The goal in BP3 was to compare catalyst performance using warm-gas cleanup to performance using cold-gas sweetening. The specific objectives were to design and construct the GSAS, compare FT catalyst performance using gas sweetening to performance using warm-gas cleanup, and develop and test novel iron- and cobalt-based FT catalysts that might exhibit better performance using warm-gas cleanup. As will be described in Section 4.0, the results of BP1 demonstrated that the EERC's existing iron-based catalyst performed poorly and quickly deactivated using only warm-gas cleanup. It was hoped that novel catalysts might make warm-gas cleanup more suitable for FTS.

3.0   EXPERIMENTAL METHODS

Subtask 3.4 work included several distinct interrelated activities, some of which spanned both budget periods. During BP1, the main technical activities included Activity 1 – FT System Testing, Activity 2 – Catalyst Development and Production, and Activity 3 – Process Simulation. Activities 1 and 3 continued into BP3. BP3 also included Activity 10 – Distillation of DCL Liquids. This activity involved procurement of a distillation column dedicated to processing liquids generated by DCL. Subtask management was included as a separate activity (Activity 4) throughout the project duration.

The activities were numbered in the order in which they were conceived. However, this was not the order in which work was performed. For instance, Activity 1 was conceived first, but it soon became apparent that the EERC would not have ready access to FT catalysts for testing. Activity 2 was next conceived to generate catalyst in support of Activity 1. Just as catalysts tested under Activity 2 were later used in Activity 1, some of the simulations performed in Activity 3 were used to design equipment under Activity 1. However, fuel upgrading performed under Activity 3 occurred after Activity 1. Activity 4 spanned the project duration but generated no results because it was dedicated purely to subtask management. Because of the comprehensive nature of this report, it is convenient to describe work in the order in which it was performed, not in the order in which the activities were conceived. This is a different order than has been presented in proposals, the SMP, quarterly reports, and other previous documentation. Table 1 lists each activity and the corresponding section in this report. As mentioned in Section 2.0, Activities 5–9 were removed from the SMP after BP2 was canceled.

The single biggest activity was Activity 1 – FT System Testing. As written in proposals and the SMP, this activity included all pilot-scale design and construction work as well as operation. Activity 1 included construction and operation of not only the pilot-scale FT reactor, but also the pilot-scale GSAS.

Activity 2 – Catalyst Development and Production was intended to supplement FT system testing by providing a reliable source of catalyst to test and use in the pilot-scale FT reactor. Small batches of catalyst were also tested in a laboratory-scale FT reactor under this activity to verify performance prior to pilot-scale testing.

Activity 3 – Process simulation was intended mainly as a means to predict gasifier and FT system performance so that optimum test conditions could be selected before pilot-scale operation in BP1. Some FT product upgrading was also performed under Activity 3 during BP1 to examine the obstacles in converting raw FT liquids to fungible transportation fuels.

Project oversight and reporting were carried out under Activity 4 – Subtask Management. This included efforts to ensure that all activities progressed together, as well as preparation of all quarterly reports, progress updates, presentations, and final reports. Because no experimentation was done under Activity 4, it is not described in the experimental section. An account of presentations and travel is given in Section 4.7.

Table 1. Project Activities and Corresponding Sections in Final Topical Report

	Experimental Sections	Results and Discussion
Activity 1 – FT System Testing	3.3.1 and 3.3.2	4.3, 4.4, 4.5.1, and 4.5.2
Activity 2 – Catalyst Development and Production	3.1	4.1
Activity 3 – Process Simulation	3.2 and 3.3.3	4.2 and 4.5.3
Activity 4 – Subtask Management	None	4.7
Activity 10 – Distillation of DCL Liquids	3.4	4.6

The purpose of Activity 10 – Distillation of DCL Liquids was to purchase and install a distillation column. The distillation column is dedicated to processing and upgrading coal liquid generated by the DCL process, which complements the FT process by generating fuel components that are not easily generated by FTS. The following sections provide details on the specific experimental methods used in each of these assorted efforts in the order described in Table 1.

3.1   Catalyst Production and Laboratory Testing

At the start of BP1, one of the primary concerns about running the pilot-scale FT reactor was the need to procure catalyst from vendors with prohibitively high royalty fees or exclusive licensing agreements with larger commercial companies. Activity 2 – Catalyst Development and Production was conceived as a way for the EERC to have a secure supply of catalyst for in-house testing. Small batches of catalyst were also screened in a laboratory reactor under Activity 2 to verify performance before they were tested in the larger pilot-scale FT reactor under Activity 1.

3.1.1   Iron-Based Catalyst Production and Laboratory Testing

3.1.1.1   Production of Novel Iron-Based Catalyst

In BP1, the EERC partnered with BYU by joining the BYU FT Consortium to have access to catalyst formulations. Through this partnership, the EERC tested a novel production method for generating large batches of catalyst for pilot-scale testing.

The process design was based on coprecipitation in a flowing reactor, with a planned production of 1 kg of catalyst per run. Two 15-gal closed-head drums held the Fe–Cu reagent and the base. They were placed inside open-head 30-gal drums, which served as containment. A third closed-head 30-gal drum served as a deionized water reservoir for mixing the solutions and flushing the system. Two peristaltic pumps were used to introduce the reagent and base to the reactor. The pumps were cross-connected to the water reservoir to allow flushing the reactor system and for metering water when mixing the chemicals. Counters added to the pump motor shafts recorded the pump revolutions. Pumping test results showed that total flow could be measured from the total revolutions to within 1.5%. The reagent and base flowed from the pumps through two preheaters to bring their temperatures to the desired 82°C. Temperature was maintained by internal rod heaters and controllers. The reagent and base were mixed in the reactor, which was also heated. A stirrer provided the required mixing. The pump metering the base was manually adjusted to control the pH measured in the reactor. The precipitated product was continuously drained from an overflow outlet near the top of the reactor through a water-cooled heat exchanger for filtering. The washing step, the silication step, and the potassium impregnation step were batch processes carried out in the collection drum. A schematic and illustration of the precipitation process equipment is shown in Figure 1. Further description of the specific methods used and the production results are offered in Section 4.1.1.2.

6
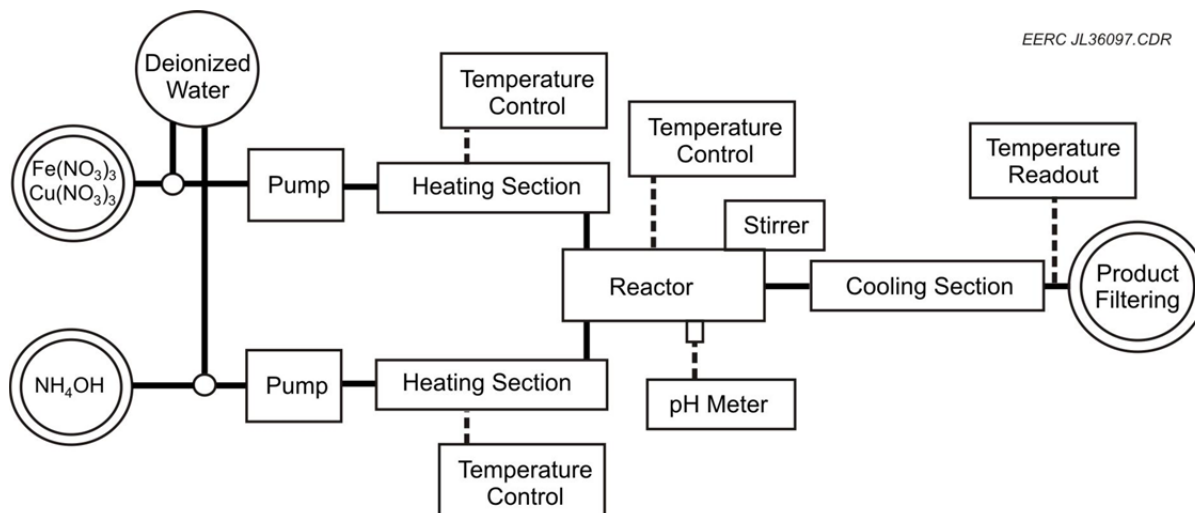
Figure 1. Schematic illustration of catalyst production equipment.

3.1.1.2 *Performance of Novel Iron-Based Catalyst*

3.1.1.2.1 FTR43 – Laboratory Screening Test

The catalyst generated using the coreciptation method was finished too late in BP1 to be tested. Its performance was examined in the laboratory reactor in BP3, with plans to test it in the pilot-scale FT reactor if it showed high activity. The catalyst was diluted 1:1 by volume with Pyrex beads and loaded into the laboratory-scale FT reactor described in Appendix B. The catalyst was activated under a flow of 0.3 slpm CO at just above atmospheric pressure. The reactor temperature was ramped up at 1°C/min to 300°C, then held at 300°C for 12 hours while CO continued to flow to complete activation.

After the catalyst was activated, 0.15 slpm H_2 and 0.2 slpm CO were flowed to the reactor to test catalyst performance. The test identification number was FTR43. Target pressure was 250 psig, but plugging issues caused the actual pressure to vary from 240 to almost 300 psig. Temperature was held at 260°C. These conditions were held for 189 hours, after which the reactor was opened and the contents examined.

3.1.1.3 *Testing Existing Iron-Based Catalyst in Support of Pilot-Scale Work*

3.1.1.3.1 FTR32 – Establishing Baseline Catalyst Performance

Because the catalyst generated in BP1 was produced too late to be used in any pilot-scale testing, the EERC instead used an iron-based catalyst generated under a different project. The same batch of catalyst was also used in pilot-scale testing during BP3, when gas sweetening was used upstream of the FT reactor. The catalyst support was SA31145, an alumina pellet with a diameter of 1/8 in. and a pore size of 20/230 nm that was purchased from Saint-Gobain Norpro. The composition of the catalyst was 17.2 wt% iron, 0.2 wt% copper, 0.5 wt% potassium,

0.7 wt% lanthanum, and the balance alumina. Composition was determined by acid digestion into solution followed by inductively coupled plasma (ICP) metals analysis of the acid solution.

Prior to pilot-scale testing in BP1, catalyst performance was examined in the laboratory reactor. The catalyst was diluted 1:1 by volume with Pyrex beads in the laboratory reactor to control heat release. The catalyst was activated under CO at a flow rate of 0.3 slpm, a pressure of 10–15 psi, and a temperature ramp of 1°C/min up to 300°C followed by a soak at 300°C for 12 hours.

In Test FTR32, the catalyst was run at several sets of conditions to determine both its optimum performance and its behavior under simulated syngas. Optimum conditions were 260°C and 250 psi with the H_2 flow rate at 0.15 slpm and the CO flow rate at 0.2 slpm. The catalyst was also tested at higher flow rates with H_2 at 0.22 slpm and CO at 0.3 slpm.

3.1.1.3.2 FTR40 – Effect of Simulated Syngas

A separate batch of the same catalyst was next run under simulated syngas at 260°C and 250 psi in laboratory Test FTR40. The activation procedure was the same as in Test FTR32, and the catalyst was again diluted 1:1 with Pyrex glass beads. To simulate syngas, the H_2 flow rate set point was 0.12 slpm, the CO set point was 0.11 slpm, the N_2 set point was 0.13 slpm, and the CO_2 set point was 0.29 slpm. These flow rates were chosen to approximate the syngas composition observed in pilot-scale testing during BP1 (see Section 4.5.1). All sets of conditions were held for several days to achieve steady state.

3.1.1.3.3 FTR44 – Effect of Catalyst Aging

The batch of catalyst used for pilot-scale testing in BP3 was generated in mid-2009, but it was stored under air until late 2011. A sample of this batch was diluted 1:1 by volume with Pyrex glass beads and then tested in the laboratory reactor for 278 hours to determine any loss of activity from aging. The test identification number was FTR44. Prior to activation, the aged catalyst was dried in situ under 1 slpm airflow at atmospheric pressure and 250°C for 16 hours to drive off any moisture that had accumulated with age. The catalyst was then activated first by cooling to 60°C, then by flowing 0.2 slpm CO, and ramping the temperature at 1°C/min to 300°C, and holding overnight.

3.1.1.3.4 FTR45 – Effect of Actual Syngas

Although Test FTR40 had determined the effect of simulated syngas on catalyst performance using bottled gas, no laboratory testing had been done using actual syngas during BP1. Pilot-scale results from BP1 suggested that catalyst was affected by more than just CO_2 in syngas. In BP3, a new batch of catalyst with the same formulation used in previous testing was produced, diluted 1:1 by volume with Pyrex glass beads, and loaded into the laboratory reactor for Test FTR45. The drying and activation procedure was the same as in Test FTR44. Following activation, a number of test conditions were examined, as shown in Table 2. The high-pressure test near the end was performed using biomass-derived syngas that had been compressed and

Table 2. Test Conditions Examined in Test FTR45

Test	Pressure, psig	Temperature, °F	H_2 Flow, slpm	CO Flow, slpm	Syngas Flow, slpm	Duration, hours
1	250	250	0.22	0.3	–	24.5
2	250	250	0.15	0.2	–	48.0
3	250	260	0.15	0.2	–	20.4
4	250	260	0.17	0.23	–	24.7
5	250	260	0.19	0.25	–	120.3
6	445	260	–	–	0.35	68.3
7	250	260	0.19	0.25	–	72.5
Total Time on Stream						378.6

collected in a pressurized gas cylinder. This syngas had been generated at low temperature in a fixed-bed gasifier. Similar to the syngas used in pilot-scale testing during BP1, the bottled syngas was sulfur-free but had not been sweetened to remove CO_2 or other contaminants. This syngas contained 15% H_2, 18% CO_2, 15% CO, and the balance N_2 with unquantified amounts of other gases (CH_4, higher hydrocarbons, etc). It should be noted that because this syngas was collected from a different type of gasifier than the pressurized fluidized-bed gasifier used for pilot-scale testing, its bulk composition is somewhat different than that used in Test FTR40 or in any of the pilot-scale tests.

3.1.2 Cobalt-Based Catalyst Production and Laboratory Testing

In BP3, the EERC produced three formulations of cobalt-based catalyst. Two of these contained cobalt and lanthanum on an alumina support. The other also contained ruthenium. Table 3 gives the metal loading on each catalyst as determined by ICP.

In previous attempts to produce cobalt-based FT catalyst, laboratory test results had suggested that the SA31445 alumina pellets used for iron-based FT catalyst support had too small a pore size for cobalt-based catalysis. The cobalt-based catalyst support was instead SA3232, a 6-mm aluminum sphere with a pore size of 1.3 µm that was purchased from Saint-Gobain Norpro. Because 6-mm spheres would not fit into the laboratory reactor, the spheres were broken into thirds or fourths of their original sizes.

Table 3. Cobalt-Based Catalyst Compositions Tested in BP3

Formulation:	1	2	3
Test ID:	FTR46	FTR47	FTR48
Cobalt, wt%	7.1	10.7	13.5
Lanthanum, wt%	2.6	2.3	2.3
Ruthenium, wt%	–	–	1 (est)[1]
Aluminum, wt %	Balance	Balance	Balance

[1] Ruthenium content could not be measured by ICP. Its content is estimated from the solution strength used in ruthenium precipitation.

Catalyst was loaded into the laboratory reactor at 1:1 dilution with Pyrex glass beads and tested under bottled gas. Prior to testing, catalyst was activated using a different procedure than is used for iron-based catalysts. The change in activation procedure was necessary because cobalt is activated by reducing it to a metallic state, while iron is activated by forming iron carbide. Cobalt-based catalyst was first heated to 300°C at 1°C/min under 0.1 slpm H_2 and 0.9 slpm N_2 and held overnight at temperature. The feed was then switched to 0.5 slpm H_2 for several hours to fully reduce the catalyst before cooling to 150°C under N_2. Finally, CO and H_2 were flowed to the reactor at 150 psig to initiate catalyst induction, after which the reactor was slowly brought to temperature and pressure.

Target run conditions were 220°C and 250 psig. In Test FTR47, the temperature was raised to 240°C on the second day of testing to see if the activity would improve. In Test FTR48, the conditions were not attainable because of high catalyst activity, so temperature was kept at only 210°C to prevent a rapid exothermic temperature rise.

Flow rates at steady state were 0.21 slpm H_2 and 0.1 slpm CO. These flow rates are different from those used for iron-based catalysts because iron catalyzes the WGS reaction and will convert H_2O generated by FT synthesis into excess H_2. Cobalt, which has no WGS activity, requires excess H_2 in the feed stream.

Since CO_2 is nonreactive over cobalt, the high CO_2 concentration left after warm-gas cleanup may have a different impact on cobalt-based catalyst performance than on iron-based catalyst performance. The CO_2 tank was found to have been disconnected prior to Test FTR48. Since CO_2 is reported to act mainly as an inert diluent for FTS on cobalt (16, 17, 19), N_2 was selected as a surrogate. Use of N_2 to model CO_2 is probably not entirely valid, since research has shown that CO_2 may appear to compete with CO for absorption on cobalt (16), but N_2 was the only other gas readily available at the time. On the final day of Test FTR48, the feed was switched to 0.15 slpm H_2, 0.1 slpm CO, and 0.4 slpm N_2 until the H_2 cylinder ran empty. This was done to assess the relative impact of simulated warm-gas cleanup on cobalt-based catalyst performance as compared to iron-based catalyst performance in Test FTR40.

3.2 Process Modeling

3.2.1 HPFBG and FT Process Modeling

In BP1, a computer-based process model of the gasifier, cleanup train, and FT system was constructed using AspenPlus software. The model was built to simulate gasification on the HPFBG and FTS in the pilot-scale FT reactor. The purpose was to develop a model that could be used to predict the effect on FT catalyst performance based on changes in gasifier operation.

A screenshot of the AspenPlus model is shown in Figure 2. Coal is entered into the model as a nonconventional component. The user specifies the proximate analysis of the fuel on an as-fired basis and the ultimate analysis of the fuel on a dry basis. These analytical results are used to convert the coal stream into a stream consisting of basic elements, including C, H, N, S, and O,
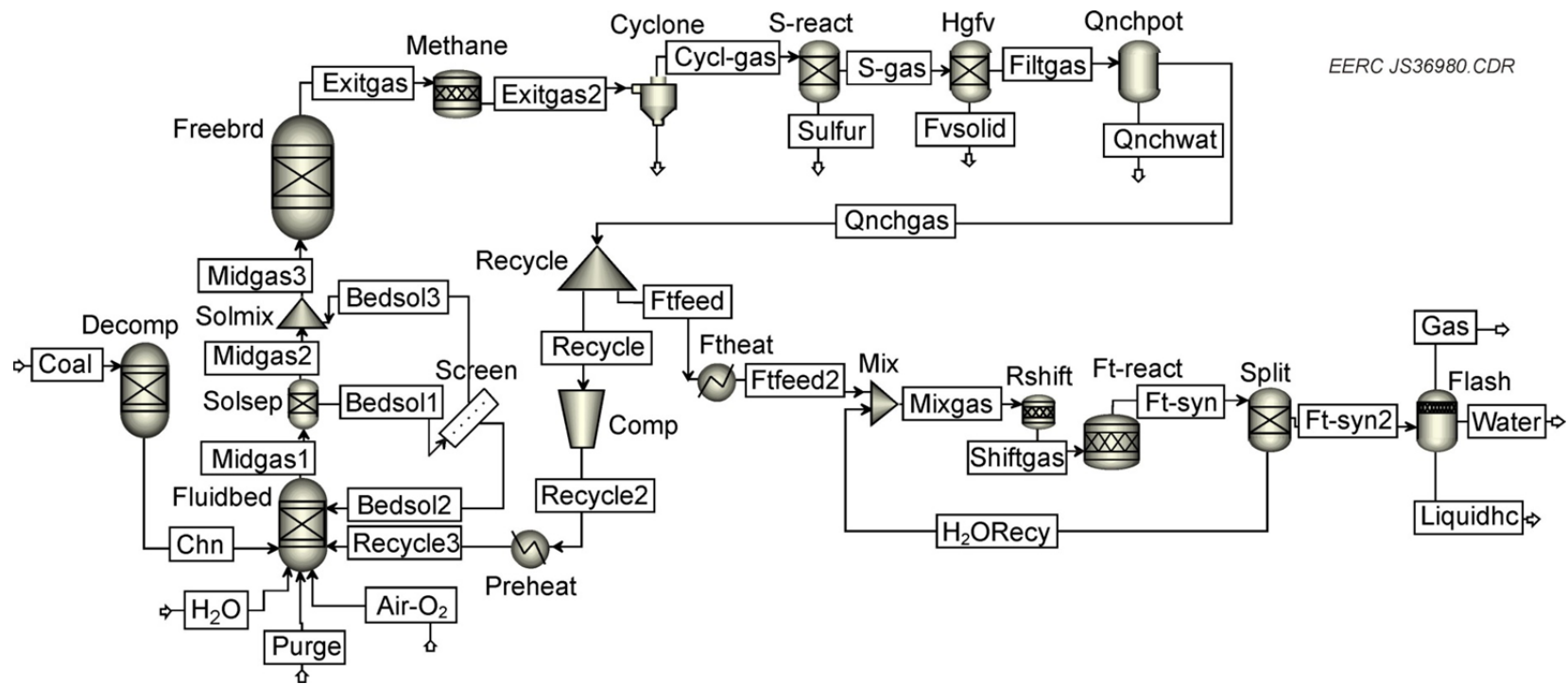
Figure 2. AspenPlus model representation of the HPFBG and FT reactor.

that can be utilized in AspenPlus. The conversion occurs in the "Decomp" unit with the aid of a user-provided code. The basic elements then combine with oxygen ("Air-O$_2$"), steam ("H$_2$O"), purge, and the recycle syngas stream ("Recycle3") in the gasifier.

The HPFBG is simulated as two separate sections: the fluid bed and the freeboard. A phase and chemical equilibrium model called RGIBBS is used in each section to determine the products of gasification. Carbon conversion is limited in each section by user input based on operational data from the actual HPFBG. The "Solsep" and "Screen" blocks separate the solids exiting the fluid bed by particle-size distribution. The larger-sized portion of the solids is sent back to the fluid-bed section as "Bedsol2," while the smaller-sized fraction remixes with the gas and escapes to the freeboard as "Bedsol3." This is similar to solids behavior in the actual HPFBG, in which the reactor diameter expands and the temperature drops in the freeboard to cause large entrained particles to fall back down into the gasifier bed. A methane reactor was added after the freeboard section because an equilibrium model is unable to predict methane presence in the gas stream at the operating temperature of the gasifier. The reactor also allows for the user to specify the water–gas shift reaction to further calibrate the model to operating data. This compensates for the small amount of WGS that occurs in the cyclone and exit piping before the gas cools below 1000°F.

The "Cyclone" block uses a simulated cyclone model to remove the larger particulate from the gas stream. The cyclone model is based on the geometry of the cyclone used with the HPFBG. Sulfur is removed in the gas stream in the "S-react" component separator that simply subtracts all sulfur from the syngas composition. The remaining particulate is captured in the hot-gas filter vessel (HGFV) block. The quench pot ("Qnchpot") block simulates cooling of the gas and uses a two-phase flash to calculate the amount of water removed from the gas stream. The gas flows to a recycle splitter where a portion of the gas is fed to the FT reactor and the remaining gas is compressed, reheated, and sent back to the gasifier.

Feed gas to the FT reactor first passes through a heater that simulates the preheater found on the pilot-scale FT reactor. The FT reactor itself is represented by four blocks that, combined, represent one unit operation. In a FT reactor with an iron-based catalyst, significant WGS occurs simultaneously with the FT reactions. The WGS reactions consume water, and the FT reactions produce water. In the AspenPlus model, these steps must be modeled separately, and in order to maintain a proper mass balance, 50% of the water generated in the FT reactor is recycled back to the shift reactor ("Rshift"). The shift reactor is set to shift the gas to a 2:1 H$_2$/CO ratio. The FT reactor uses an RSTOICH model in AspenPlus along with a calculator block to determine the products of the reaction. The Anderson–Schulz–Flory (ASF) model is used to determine the product distribution. Three separate ASF models are used: one for alkanes, one for olefins, and one for alcohols. The user is required to enter a chain growth probability value (α value) for each product type as well as the CO conversion for each product. The overall concentration of alkanes versus olefins and alcohols was determined from analyzing the product from laboratory tests but is left as a user-specified input that can be modified for different catalysts or conditions. In the last step of the AspenPlus model, the product from the FT reactor is cooled and separated into gas, water, and organic liquids.

The AspenPlus model of the HPFBG and FT reactor was used to simulate the actual run conditions in BP1. As indicated above, input included coal properties; air, steam, and purge flow rates; HPFBG bed temperature and pressure; flow rate to the FT reactor; and α values for the FT catalyst as determined from laboratory testing. The results were compared to actual pilot-scale performance in BP1 to assess the model's accuracy and usefulness for predicting behavior in future pilot-scale tests.

3.2.2   GSAS Process Modeling

The GSAS was designed and built to test gas sweetening in BP3. Prior to beginning construction, the tentative GSAS design was modeled using AspenPlus and ChemCAD. AspenPlus was initially used to assess the overall column design. The model was also used to estimate the appropriate column diameter when using SELEXOL or a similar solvent. The AspenPlus chemical database does not include SELEXOL, so a generic dimethyl ether of polyethylene glycol (DEPG) was used as a substitute in the model. The ChemCAD database includes SELEXOL properties, and the ChemCAD model was used to estimate equilibrium performance of the overall system under varying conditions both for SELEXOL and for methanol (i.e., the Rectisol process).

3.2.2.1   AspenPlus Modeling

AspenPlus has the capability to simulate both equilibrium- and rate-limited separations. Equilibrium-based modeling can provide quick and useful estimates of the effect that changes in process conditions will have on a given column, but it cannot be used to estimate proper column geometry. Rate-limited separations proceed more slowly than predicted by equilibrium and are affected strongly by column geometry. The ability to simulate rate-based separation was used to give some estimate of the effect of column geometry on CO_2 capture performance. Because AspenPlus modeling was performed under the assumption that the initial skid would not include a glycol chiller, AspenPlus modeling was performed at temperatures at or above the freezing point of water (32°F).

Figure 3 provides a screenshot of the AspenPlus model for the GSAS. This is conceptually similar to the actual skid. Lean DEPG solvent enters the top of the "ABSORB" column as "LEAN-IN," strips acid gas out of the "GAS-IN" stream, and exits the column as "RICH-OUT." The rich solvent is heated and flashed in the "FLASH" drum to drive off acid gas ("CO_2") and then pumped through the "COOLER" heat exchanger. The model includes a makeup stream that does not exist in the actual GSAS. In the actual GSAS, a sizable reservoir holds extra solvent between the flash drum and the pump, meaning a makeup stream is not needed.

For equilibrium modeling, the syngas flow rate to the absorption column was held constant at 1000 scfh and 70°F, with column pressure at 250 psig. Table 4 provides the gas composition. Several variables were adjusted to assess their effect on both CO_2 capture efficiency and CO_2 recovery (i.e., the fraction of CO_2 in the "RICH2" rich solvent stream that flashes out in the "CO_2" acid gas stream). Variables included the number of equilibrium stages in the column, lean solvent inlet temperature, flash drum pressure, and flash drum temperature.
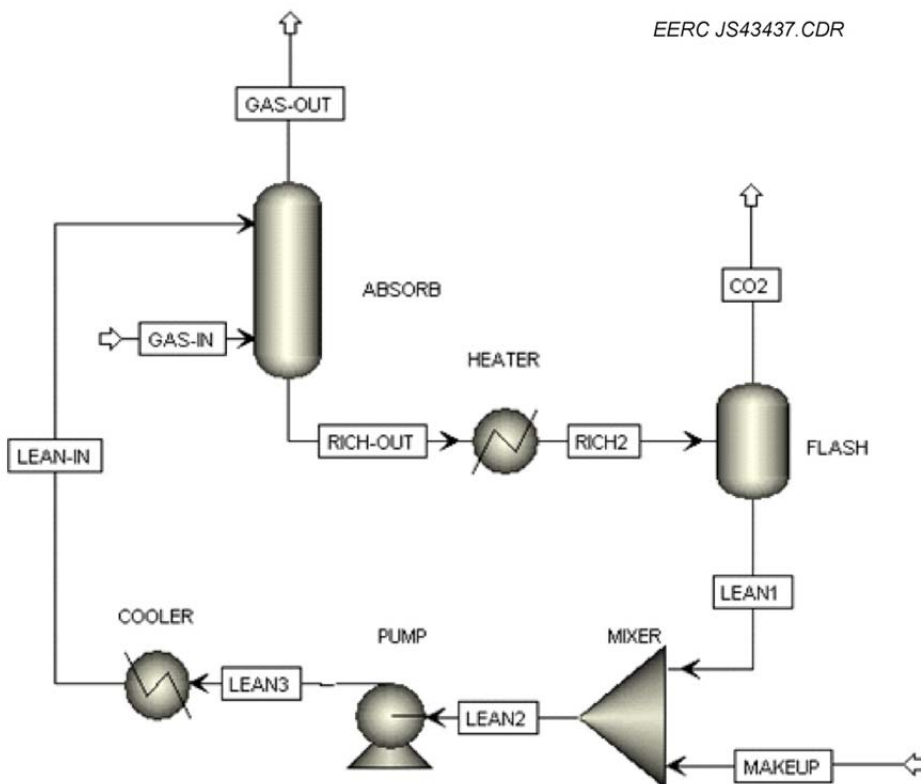
Figure 3. Screenshot of the AspenPlus GSAS model.

Table 4. Gas Composition Used in the AspenPlus GSAS Model

Component	H_2	CO	CO_2	CH_4	H_2O	N_2
Mole Fraction	15%	15%	40%	1%	0.2%	28.98%

The AspenPlus GSAS model was also used for rate-based modeling. This approach is usually used with amines and other chemical sorbents because their ability to absorb CO_2 is dictated by chemical reaction rates instead of equilibrium absorption. However, it can also be useful for sizing physical absorption columns because absorption can sometimes be limited by mass diffusion rather than by equilibrium.

The rate-based model used the Billet and Schultes model [23] for estimating mass transfer coefficients. Syngas flow rate was held constant at 1000 scfh and 70°F. Gas composition was the same as in equilibrium modeling (Table 4). Column height was held at 11 ft, flash drum temperature was held at 70°F, and flash drum pressure was held at 16 psia. Solvent temperature was switched between 30° and 70°F, and column pressure was varied between 250 and 750 psia, as shown in Table 5. The solvent flow rate at each condition was selected by varying flow until the model column flooded and would no longer converge, which indicated maximum CO_2 capture. The column diameter was also varied to achieve suitable flow.

14

Table 5. Conditions Tested in the AspenPlus GSAS Rate-Based Model

Simulation	Column Pressure, psia	Solvent Temperature, °F
1	250	30
2	250	70
3	500	30
4	500	70
5	750	30
6	750	70

3.2.2.2   ChemCAD Modeling

ChemCAD modeling was mostly performed after all AspenPlus modeling was complete, by which point it was clear that the GSAS would need a chiller to achieve acceptable CO_2 capture at high flow rates. Most of the ChemCAD modeling was performed to determine what effect the chiller would have on gas sweetening at different flow rates, gas compositions, temperatures, and pressures. Figure 4 provides a conceptual image of the ChemCAD model for SELEXOL, with unit operations in italic and major process streams labeled.

The ChemCAD model was later modified to examine the possibility of using the GSAS for Rectisol treatment using chilled methanol. The model for methanol sweetening was nearly identical to the ChemCAD model for SELEXOL sweetening except that a makeup stream was added to replace methanol lost in flash distillation. A full table of recorded ChemCAD simulations and results is given in Section 4.2.2.2.
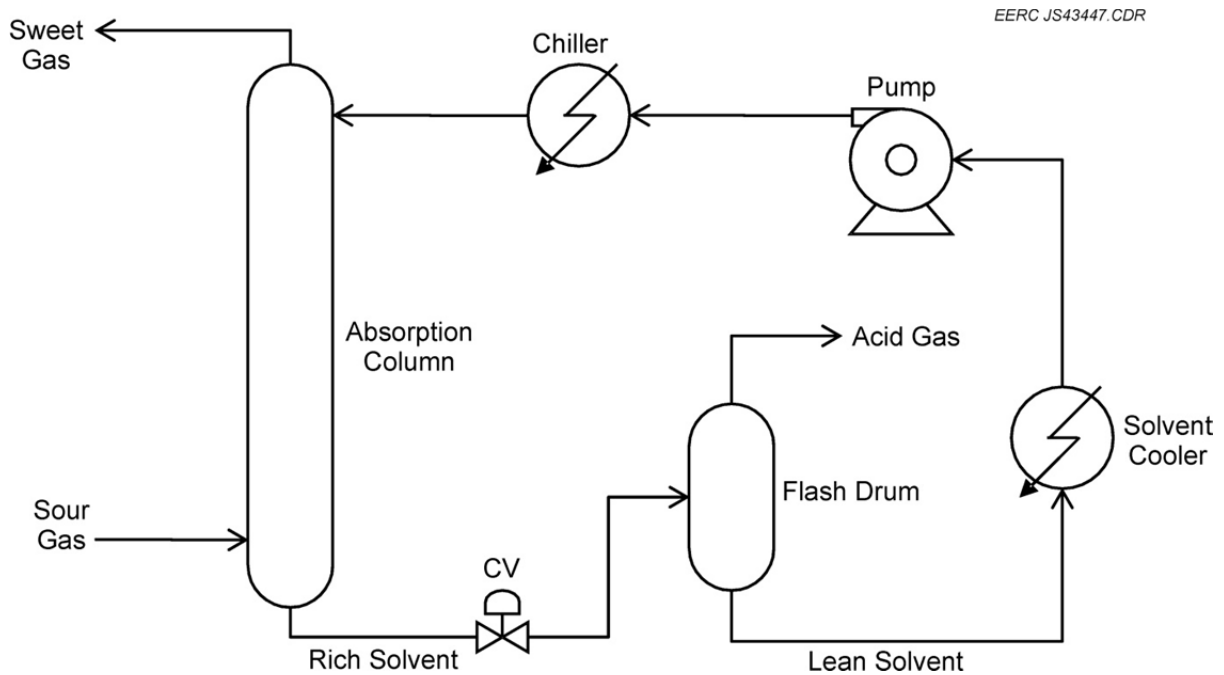
Figure 4. Unit operations and streams included in ChemCAD SELEXOL model.

3.3 Pilot-Scale FT System Testing

3.3.1 Warm-Gas Cleanup (BP1)

The pilot-scale FT system was constructed and tested for the first time in BP1. The design was based on recommendations from Calvin Bartholomew, formerly of BYU. The EERC joined the BYU FT Consortium during BP1 to obtain access to novel catalyst formulations, FT reactor designs, and a general knowledge base from a pool of researchers and industry experts. A detailed description of the FT reactor design is given in Appendix B. Appendix B also includes a detailed description of the HPFBG used to generate syngas for pilot-scale testing.

Four semicontinuous test periods were conducted on the FBG during BP1, each lasting approximately 1 work week (100 hours). During the first two test periods, a Powder River Basin (PRB) subbituminous coal was gasified. This coal was selected because it was immediately available and was likely to be a fairly benign coal in terms of gasification behavior. During the second two periods, North Dakota lignite from the Falkirk Mine was gasified. This coal was selected because the cost-share partner in BP1 had a strong interest in gasifying North Dakota resources. In each test period, several biomass samples were cofed with the coal, and at several times, the feed was switched to 100% biomass. The biomass types included switchgrass from the North Dakota State University (NDSU) Agricultural Experiment Station in Streeter, North Dakota; dried distiller's grains and solubles (DDGS) from the Archer Daniels Midland corn bioethanol plant in Walhalla, North Dakota; and olive pits from Greece.

Dolomite was added to every batch of lignite at a blend ratio of 20 grams of dolomite per pound of coal. Dolomite is reported to capture H_2S during lignite gasification as well as to help crack certain hydrocarbons into gaseous components. It was added to help improve syngas quality by reducing the production of H_2S and gasifier tar.

All of the biomass samples were pretreated by leaching to reduce the alkali, chlorine, phosphorus, and sulfur content. Leaching helps to avoid ash-related problems during the gasification process and also reduces potential catalyst poisoning during the FT process. A portion of the olive pits were torrefied to increase the heating value, and a portion of the DDGS was left untreated to examine the relative impact of gasifying treated versus untreated biomass. Table 6 provides analytical data for each of these feeds, with "TL" indicating "torrefied and leached." It should be noted that the biomass was extensively floor-dried to reduce moisture prior to feeding. Especially in the case of switchgrass, this notably changed the feed properties and probably raised the higher heating value (HHV) substantially.

During the four BP1 test periods, the HPFBG configuration was somewhat different than in BP3 (Appendix B should be referenced for details on HPFBG design and operation). The total gasifier height was only 8 ft during BP1 but was increased to approximately 21 ft prior to BP3. Solids separated by the cyclone in BP1 were collected in a pressurized pot and periodically drained, while in BP3 these solids were continuously recycled back to the gasifier bed. In BP3, an ice-cooled trap upstream of the recycle syngas compressor would capture traces of moisture and light tars escaping the quench pots. This ice-cooled trap did not yet exist in BP1.

16

Table 6. Composition of Coal and Biomass Feeds Used in Gasification Testing

	PRB Antelope Coal	ND Lignite	Treated Olive Pits	TL Olive Pits	Treated DDGS	Treated Switchgrass	DDGS
Leached?	No	No	Yes	Yes	Yes	Yes	No
Torrefied?	No	No	No	Yes	No	No	No
Proximate Analysis (all values reported as weight percent as received)							
Moisture	22.41	23.40	49.62	42.85	30.24	61.57	7.49
Volatile Matter	35.29	27.67	34.91	26.22	51.07	25.73	68.73
Fixed Carbon	36.56	37.35	13.73	28.75	16.72	6.68	19.91
Ash	5.74	11.58	1.74	2.17	1.97	6.02	3.86
Ultimate Analysis (all values reported as weight percent as received)							
H	5.90	5.89	8.63	7.58	8.22	9.23	7.16
C	69.06	47.22	27.89	40.40	38.24	17.82	48.12
N	0.98	0.74	0.89	0.87	3.34	0.49	3.65
S	0.32	1.17	0.07	0.07	0.27	0.08	0.39
O	18.00	33.40	60.78	48.92	47.97	66.36	36.79
HHV, Btu/lb	8797	7843	4605	6662	6696	2727	8498
Ash Analysis (all values reported as weight percent on an ash basis)							
SiO_2	32.6	40.5	6.6	10.1	3.0	40.4	5.2
Al_2O_3	15.0	13.8	1.5	2.6	0.8	1.5	0.0
Fe_2O_3	7.48	7.57	1.80	3.72	0.60	2.14	0.43
TiO_2	1.17	0.49	0.11	0.18	0.04	0.12	0.02
P_2O_5	1.08	0.28	2.10	3.59	43.12	1.93	39.65
CaO	21.3	16.1	51.7	54.9	23.5	40.0	1.9
MgO	5.86	5.12	0.77	3.22	6.10	2.86	13.41
Na_2O	0.84	0.89	0.03	0.91	3.95	0.23	5.26
K_2O	0.56	1.35	0.68	13.24	13.47	5.26	30.68
SO_3	13.25	13.32	1.78	4.73	4.70	1.47	2.84
Cl	0.00	0.00	0.10	0.08	0.55	0.12	0.64
Unknown	0.00	0.00	32.63	0.73	0.00	3.80	0.00

Perhaps most importantly, only warm-gas cleanup was used in BP1, while gas sweetening was used in BP3. This was critical, as one of the goals during BP1 was to assess FT performance using low-cost options that might be more suitable for distributed gasification systems. The goal in BP3 was to ascertain the relative effect of CO_2 capture on FT catalyst performance. The warm-gas cleanup train used in BP1 included a filter vessel to reduce fine particulate to very low levels, a set of regenerable fixed beds for bulk sulfur capture, a set of polishing fixed beds to

remove traces of sulfur escaping the regenerable beds, and a train of water-cooled quench pots to condense moisture and gasifier tar out of the syngas stream. The train includes six water-cooled quench pots, but syngas for the FT reactor was sampled after the third quench pot.

Syngas exiting the gasifier quench pots was continuously analyzed by Raman spectrometry using a laser gas analyzer (LGA). Syngas was also continuously analyzed using a three-column Varian gas chromatograph (GC) that includes two thermal conductivity detectors (TCDs) as well as a pulsed-flame photometric detector (PFPD) for ultralow sulfur detection (theoretically down to ppb levels). Dräger tubes were periodically used to measure H_2S at low concentrations (down to 0.2 ppm). After steady-state gasification had been achieved and the sulfur capture fixed beds brought online, H_2S in the syngas would fall exponentially to below Dräger tube or GC–PFPD detection limits over the course of several hours. Once H_2S had dropped below 1 ppmv as measured by Dräger tube, clean, dry syngas was passed to the FT system. It was necessary to wait until H_2S had dropped so low because H_2S is a strong FT catalyst poison.

Both fixed-bed FT reactors were loaded with an iron-based catalyst that was developed at the EERC under a separate project. At the start of BP1, it was anticipated that the EERC would not be able to obtain commercial FT catalysts, and so one of the activities in this subtask was catalyst development to provide catalyst for pilot-scale testing (Section 3.1.1.1). However, the catalyst developed under this activity was not ready in time for FT system testing, so a large batch of an existing EERC iron-based catalyst formulation was instead produced and used for pilot-scale testing. The catalyst performance was measured under both ideal gas and simulated syngas in a laboratory reactor to verify that it would perform adequately in the pilot-scale FT reactor (Section 3.1.1.2).

During the first two test periods of BP1 (Tests FBG002 and FBG003), only one fixed-bed FT reactor was used. This left the other loaded reactor available in the event that the first reactor was overheated or deactivated as a result of sulfur breakthrough from the upstream sorbent beds. Both reactors were kept hot so that the second would be ready to go on short notice, but the second reactor bed was kept under nitrogen. During the second two test periods of BP1 (Tests FBG004 and FBG005), both reactor beds were used in an attempt to increase the amount of FT product recovered. Product gas exiting the FT reactor was continuously monitored by a second LGA as well as a dual-column Yokogawa GC that includes two TCD detectors. Using flow rates, product collection rates, and gas compositions, the EERC could estimate catalyst productivity, CO and H_2 conversion, selectivity to light gas (STLG), and selectivity to CO_2 (STCO2).

As described in Appendix B, wax product from the pilot-scale FT reactor was collected in a heated wax trap, while liquid product was collected in a train of three water-cooled quench pots. These were periodically drained into a low-pressure pot for product recovery. During the first test period (Test FBG002), this low-pressure pot was kept on ice to minimize the amount of volatile organics that would boil out of solution on depressurization. The pot was not kept on ice in the other three test periods of BP1. At the end of each test period, a boroscope was used to examine the inside of the pots for solidified product.

Liquid drained from the FT reactor was weighed and separated into aqueous and organic fractions. The organic fraction was analyzed by GC–mass spectrometry (MS) to determine the carbon chain length distribution and the types and relative amounts of hydrocarbons present in the organic product. The aqueous fractions were combined and analyzed for total organic content (TOC) by an outside lab. The TOC measurement involves first acidifying the aqueous solution and exposing it to a vacuum, which removes dissolved CO_2 and carbonate but might also remove some volatile organic carbon. The remaining sample then goes to an ammonium persulfate oxidizer to convert all remaining carbon to CO_2, and the amount of CO_2 generated is measured indirectly by redissolving into a deionized (DI) water stream and measuring the CO_2 uptake of the DI water. TOC was fairly low in Tests FBG002 and FBG003, so the aqueous samples were disposed of without further measurement. In Tests FBG004 and FBG005, the combined aqueous samples were also measured by GC to determine the relative types and amounts of hydrocarbons present in the solution.

3.3.2   Gas Sweetening (BP3)

The goal of BP1 had been to assess FT system performance using low-cost gas cleanup options, but results suggested that the catalyst had performed suboptimally. The goal of BP3 was to install and test a gas-sweetening system so that the same FT catalyst used in BP1 could be tested with more expensive gas sweetening. Details on gas-sweetening system design are given in Appendix B.

A single 5-day test period (FBG021) was conducted with gas sweetening. The same composition of iron-based FT catalyst was used in Test FBG021 as had been used with warm-gas cleanup in BP1. Prior to loading, the activity of this catalyst was assessed as a laboratory reactor as described in Test FTR44 in Section 3.1.1.3 to determine whether it had lost activity because of long storage. The catalyst was reduced and activated in situ under CO in the pilot-scale reactor prior to exposure to syngas.

During operation, there were four gas streams to analyze: Sour gas going to the GSAS, acid gas being vented off the GSAS, sweet gas going from the GSAS to the FT reactor, and FT product gas. The same four analyzers (two GCs and two LGAs) were used in BP3 as in BP1. The Yokogawa GC and one LGA were dedicated to the sour gas stream to provide necessary readings to the process control software. Researchers put in a four-way valve so that the sample point for the Varian GC and second LGA could be switched between different gas streams. This provided intermittent analysis of the sweet gas and FT product gas streams rather than the continuous analysis used in BP1. A mass spectrometer was also installed in BP3 to periodically measure gas composition in each gas stream.

FT product was drained as in Test FBG002 into an ice-cooled pot. Wax was also drained periodically from the heated wax trap. At the end of testing, a boroscope was used to examine the inside of the pots, and the product collection pots were opened to recover solidified product. Liquid samples were weighed and separated into organic and aqueous fractions. Organic liquid product was analyzed by GC–MS. Aqueous product was analyzed using a Waters high-performance liquid chromatograph (HPLC) equipped with both a refractive index (RI) detector

and an ultraviolet (UV) detector. Water samples were also submitted to an outside laboratory for TOC analysis.

For the bulk of the test, bulk sulfur was removed from the sour gas upstream of the GSAS so that only CO_2 was removed by gas sweetening. During the final 22 hours of operation, the warm-gas capture beds were bypassed so that some H_2S would slip through the GSAS to the pilot-scale FT reactor. This was done to determine how rapidly the iron-based catalyst would deactivate under slightly elevated (25 ppm) H_2S, which might show whether the catalyst in BP1 could have deactivated because of low-level (<1 ppm) sulfur exposure.

3.3.3   FT Product Hydrotreatment

The coal-derived FT product from Test FBG002 (Section 3.3.1) was combined for upgrading to fungible fuel. This was done to determine whether the FT product generated using warm-gas cleanup would present any unique difficulties for refining that might not be present when using cold-gas sweetening. Biomass-derived FT product was kept separate and was not upgraded.

Hydrotreating serves two purposes: First, hydrotreating removes heteroatoms such as oxygen, sulfur, and nitrogen that are undesirable in a finished fuel product. Second, hydrotreating shortens and isomerizes the heavy paraffinic molecules generated by FTS. Paraffins and paraffinic olefins are the primary products of FTS but are unsuitable in jet fuel because they have high freezing points. FT product also contains an appreciable amount of oxygen, which is present mostly as alcohols. These features make hydrotreating a suitable option for upgrading raw FT product to fungible fuel.

The first step of the hydrotreating process was hydrodeoxygenation (HDO) to remove oxygenates. The HDO catalyst was a nickel–molybdenum (NiMo) catalyst powder, sieved to 50–150 μm. Given the small volume of FT liquid available, a batch reactor was selected for HDO treatment.

The 1-L batch reactor described in Appendix B was loaded with 5 g NiMo; 573 g FT liquids collected between 13:18 on August 25 and 17:30 on August 27, 2009; and 5 g FT wax collected at 15:00 on August 27, 2009. The headspace was thoroughly purged to remove air, then held at 500 psig H_2 for 15 minutes prior to running to check for leaks.

The pressure was then raised to 1000 psig H_2. Insulation was wrapped around the reactor, and the reactor began heating while stirring to keep catalyst, liquid, and gas well-mixed. During heat-up, liquid on the bottom of the reactor began to smolder and eventually ignited. The test was cut short for safety reasons. The total time from start of heating until the stirrer was stopped again and the reactor opened was 3 hours, 25 minutes. A sample was taken for GC–MS analysis to see if the first HDO treatment had been sufficient to reduce olefins and oxygenates.

A second HDO treatment was then performed. The reactor reached temperature in 1 hour and was held at temperature for 1 hour, 48 minutes before cooling. A sample was taken for GC–

MS analysis and the remainder of the product recovered and distilled into two fractions. Each fraction was analyzed, and the heavy fraction selected for further hydrotreating.

The next step of hydrotreating was isomerization. The heavy fraction of HDO product was pumped through the small continuous reactor (SCR) described in Appendix B. The purpose of this step was to achieve isomerization, olefin saturation, and mild hydrocracking. These make the liquid more suitable for use as transportation fuel by lowering its freeze point and increasing its stability.

The catalyst used for hydrotreating in the SCR was a cobalt–molybdenum (CoMo) catalyst pellet. This catalyst is particularly sensitive to oxygenates, so the SCR was disassembled and thoroughly cleaned prior to testing. Dried NORPAR-15, a mix of *n*-alkanes, was then pumped through all lines for 30 minutes to fully flush out any traces of residue from previous testing or cleaning.

The SCR was loaded with 62.8 g of CoMo catalyst and pressure-checked at 500 psig with N_2 prior to running. After thorough flushing with N_2, the reactor was heated under N_2 and H_2 to dry and activate the catalyst. Once the reactor was at condition, NORPAR-15 was run through the reactor for 3 hours to soak the catalyst surface and flush any final traces of contamination. The reactor was then depressurized to 500 psig, and a high flow rate of unmetered H_2 was blown through the reactor to flush most of the NORPAR-15 before starting HDO FT product flow.

The HDO FT product was then pumped through the SCR reactor cocurrent with H_2. The recovered product was analyzed by GC–TCD to determine degree of cracking and isomerization, then recycled through the SCR several times to improve isomerization and fuel properties. Samples containing residual NORPAR-15 as detected by GC–TCD were disposed of without recycling. After the final pass through the reactor, 1000 sccm H_2 was flushed through the reactor at atmospheric pressure to vaporize or flush out any remaining liquid. The product collected after 100 minutes of flushing was added to the isomerized product.

After isomerization, the hydrotreated FT product was distilled to recover a jet fuel cut. The freeze point and density of the jet fuel were measured to assess its suitability. The EERC has several years of experience in producing and analyzing alternative jet fuels, making this the most convenient fuel product to use for assessing the effectiveness of hydrotreatment.

3.4   Distillation Column Design and Selection

The DCL process is fundamentally different from FTS. The most important difference is that coal is not gasified in a DCL process but, instead, hydrogenated directly into a liquid. The raw liquid produced by DCL is too heavy for use as a transportation fuel and must be distilled to recover lighter fractions so that the heavy fractions can be further processed or recycled.

A distillation column purchased under Activity 10 in BP3 was intended for processing liquids from DCL. Petroleum-derived fuel contains a mix of aromatic, cycloparaffinic, and isoparaffinic compounds. DCL produces a significant amount of aromatic and cycloparaffinic compounds, whereas FTS produces almost exclusively isoparaffinic compounds. By blending the product of both processes, it may be possible to generate a fuel that is entirely coal-derived and yet indistinguishable from petroleum-derived fuel.

The dual-column semiautomatic distillation system was ordered from B/R Instrument Company, Easton, Maryland. The system is equipped with two types of distillation columns. The first is a spinning-band column for distillation to recover middle distillate, which can be catalytically upgraded for fuel production, from raw DCL liquid. The second column is a packed column for the fractional distillation of the catalytically upgraded middle distillate to separate and recover transportation fuels such as motor gasoline, aviation fuel, and diesel.

While the second column is a fairly standard distillation column for separating hydrotreated fuels, the spinning-band column is uniquely designed for handling heavy DCL liquids. The spinning-band column includes a 12-liter, stainless steel stirred pot. Above this is a 21-mm-diameter glass column with a Monel-alloy spinning band. This column provides 20 theoretical stages and includes two independent heaters, top and bottom. The distillation rate is up to 0.7 liters per hour at a 2:1 reflux ratio at atmospheric pressure, and it also includes a vacuum pump for vacuum distillation. Up to eight different distillation cuts can be automatically separated into 500-mL receivers. All features of the semiautomatic distillation system are computer-controlled, including temperature, reflux ratio, vacuum, and product collection.

4.0 RESULTS AND DISCUSSION

4.1 Catalyst Production and Laboratory Testing

All catalyst production and testing was performed in support of pilot-scale testing, either by augmenting results or by providing data on catalyst performance before catalyst was loaded into the pilot-scale reactor.

4.1.1 *Iron-Based Catalyst Production and Laboratory Testing*

While part of Activity 2 involved production and assessment of novel iron-based catalyst, a major part of the effort also focused on testing existing iron-based catalyst in support of pilot-scale work. The following sections give results on iron-based catalyst production, laboratory assessment of novel iron-based catalyst, and laboratory efforts in support of pilot-scale efforts.

4.1.1.1 *Production of Novel Iron-Based Catalyst*

4.1.1.1.1 Production Test 1

The first catalyst production test used the Fe–Cu solution precipitated with K_2CO_3. The Fe–Cu flow was initially set at a slow flow rate of approximately 50 mL/minute and the pH

adjusted to between 7 and 8 by adjusting the K_2CO_3 flow. Difficulty was encountered with controlling the pH because of the slow response of the electrode.

Severe frothing soon occurred in the reactor, with the solution overflowing several times. The condenser line also became plugged several times. The frothing, overflow, and plugging required interrupting the test until the situation was remedied. In retrospect, it was deduced that the frothing was because of generation of CO_2 from the carbonate solution when the pH dropped below 8. This was exacerbated by the 82°C solution temperature and the vigorous stirring of the solution. The use of K_2CO_3 as a base was thus found to be not ideal for the precipitation reaction. The test was terminated after approximate 45 minutes, with 525 mL of Fe–Cu solution and 485 mL of K_2CO_3 fed.

Vacuum filtering of the precipitate was done with a Buchner funnel holding 24-cm-diameter FPR 240 paper filters. Initially, the precipitate was collected in the funnel directly from the condenser. This proved to be impractical since the filtering proceeded very slowly. After the funnel was filled to capacity, additional precipitate was collected in a separate container for later filtering.

The collected product was filtered the next day and rinsed with three 1-liter batches of DI water. Again, the filtering process was extremely slow, although allowing the precipitate to settle and decanting the clear liquid portion to filter first was of some benefit. A total of 501.9 grams of wet product was obtained. Drying of a small (3.1-gram) sample indicated that the product contained approximately 77% water. The dry product obtained was thus approximately 113 grams. The wet product was found to be quite sticky and difficult to handle and transfer.

4.1.1.1.2 Production Test 2

The second catalyst production test used the Fe–Cu solution precipitated with KOH. The Fe–Cu flow was initially set at a slow flow rate of approximately 50 mL/minute and the pH adjusted to between 7 and 8 by adjusting the KOH flow. Again, difficulty was encountered with controlling the pH because of the slow response of the electrode. No frothing occurred during the test. The second test ran until the supply of KOH was depleted. Approximately 4500 mL of the Fe–Cu solution and 8600 mL of KOH were fed. The precipitated product was collected in 1-gallon (4-liter) plastic buckets for subsequent filtering after settling. The solution pH of each was tested, and additional KOH added until basic (pH = 8). After allowing time for settling, the filtration and washing were performed.

The precipitate was filtered out of solution using a Buchner funnel, as in Test 1. The filtered "mud" was then slurried with approximately 3 times its weight in water. This slurry was then filtered again using the Buchner funnel.

4.1.1.1.3 Silica and Potassium Impregnation

After filtration, CAB-O-SIL® (a fumed silica product made by the Cabot Corporation) and potassium hydrogen carbonate were added to the precipitate. 10 grams of CAB-O-SIL and 7 grams of $KHCO_3$ were added for every 96 grams of precipitate. The first batch of catalyst that

was made using potassium carbonate had to be disposed of because of contamination by other chemicals.

To prepare the second batch of catalyst, 960 grams of precipitate was mixed with 100 grams of CAB-O-SIL and 70 grams of $KHCO_3$. This mixture was slurried with water in a large beaker. The beaker was placed in an oven at 50°C for several hours so that excess moisture would evaporate until the catalyst mixture had the consistency of mud.

4.1.1.1.4 Pelletizing

Several different techniques were tried for pelletizing the catalyst. One technique involved using a household cookie press with a custom-made 2-mm quadrate end. This technique did not produce a product with a consistent shape. A second technique involved using a syringe with a small opening in the tip. The catalyst was extruded into lines on a cookie sheet, and these lines were scored to the desired length. This process was not consistent enough, as the lines varied greatly in width.

The third and most successful technique involved spreading the catalyst onto perforated metal plates. The plates were 1/8 in. (3.2 mm) thick, and the holes had a diameter of 3/16 in. (4.76 mm). The plates were filled by spreading the catalyst on with a spatula to ensure that all holes were filled. Excess catalyst was scraped off, and the plates were placed on trays and left to dry at 50°C in an oven for several hours. As the excess moisture in the pellets evaporated, the pellets shrank and fell out onto the tray below. This process produced a consistently shaped product and was easily repeatable. The pellets were approximately 3 mm thick with a diameter of 4.7 mm. After the pellets had air-dried for several hours, they were sifted to remove fine particles. The pellets were then dried in an oven at 120°C for 16 hours.

4.1.1.1.5 Calcination

The catalyst was cooled and then placed in a Pyrex pan. It was heated at 60°C for 1 hour, 190°C for 1 hour, and finally 270°C for 8 hours. The catalyst did not crack or visibly change appearance during the calcination process. The finished catalyst product had a diameter of 3 mm and a thickness of 2 mm when the calcination process was completed.

4.1.1.2 *Testing of Novel Iron-Based Catalyst*

After production, the catalyst was loaded in the laboratory reactor described in Appendix B, activated, and tested under bottled gas, as described in Section 3.1.1.2. The catalyst appeared to undergo an induction phase early in Test FTR43 as productivity increased to a peak by the third day. Table 7 provides peak and average catalyst performance for run Test FTR43. Catalyst performance was relatively poor even at its peak on Day 3. By this point, powdery black residue was observed in the liquid drained from the cold trap. The powder tended to float between the aqueous and organic material and did not mix with either layer. More of the black material continued to appear in the liquid samples as the run continued, and the catalyst began to

Table 7. Laboratory Performance of Novel Iron-Based Catalyst in Test FTR43

Catalyst Condition	Peak	Average
Aqueous Productivity, $g \cdot kg\text{-}cat^{-1} \cdot hr^{-1}$	210	50
Liquid Hydrocarbon Productivity, $g \cdot kg\text{-}cat^{-1} \cdot hr^{-1}$	60	40
Wax Productivity, $g \cdot kg\text{-}cat^{-1} \cdot hr^{-1}$	20	10

quickly deactivate. Pressure control also became difficult because the back-pressure control valve would become plugged shut or stuck open.

After 189 hours, the reactor was opened, and the catalyst was found to have broken into small pieces or powder. The black material in the liquid was most likely fine catalyst powder, which also may have gotten to the control valve and caused it to plug and stick. The catalyst had been pelletized at atmospheric pressure (Section 4.1.1.1). It is assumed that the weak pressure during pelletization led to poor mechanical strength and high friability, even in a laboratory reactor under low gas flow rates. This catalyst was never loaded into the pilot-scale FT reactor because of concerns that the longer reactor tubes might completely plug with broken catalyst or that downstream control valves might become damaged because of abrasion from catalyst powder.

4.1.1.3 Testing Iron-Based Catalyst in Support of Pilot-Scale Work

4.1.1.3.1 Performance under Bottled Gas

The iron-based catalyst that was ultimately used in the pilot-scale reactor showed much poorer performance with simulated syngas compared to an ideal ratio of bottled gases. The activity was also substantially lower after more than 2 years of aging prior to BP3. Table 8 gives the productivities for wax, liquid hydrocarbons, and aqueous product at the various conditions tested. The catalyst tested in Test FTR40 (simulated syngas) was from a different batch than that used in Tests FTR32 and FTR44, and it did show lower inherent activity. However, the general observation that use of simulated syngas had a strong negative impact on catalyst performance remains valid even when accounting for the lower inherent activity. It should be noted that higher flow rates in Test FTR32 did have some effect on FT catalyst performance, and the overall flow rate in Test FTR40 was fairly high. However, the decreased productivity in FTR40 seems too drastic to explain as a flow rate effect. It is most likely the result of the gas composition.

Other researchers have reported that CO_2 has much less effect on iron-based FT catalyst except at very high concentrations (15–18, 21, 22). However, these researchers generally studied the effect of CO_2 by replacing some CO with CO_2 to maintain a sufficiently high H_2 concentration. H_2 concentration cannot be increased in actual coal-derived syngas without either a WGS reactor or a gas-sweetening column (preferably both). The gas composition in Test FTR40 is fairly close to the actual gas composition in syngas generated by the EERC's HPFBG. The results of Test FTR40 demonstrate that CO_2 negatively impacts iron-based FT

Table 8. Laboratory Test Conditions and Results for Iron-Based Catalyst Used in Pilot Reactor

Test ID	FTR32	FTR32	FTR40	FTR44
Catalyst Condition	Fresh	Fresh	Fresh	Aged
H_2 Flow Rate, slpm	0.15	0.22	0.12	0.15
CO Flow Rate, slpm	0.20	0.30	0.11	0.20
CO_2 Flow Rate, slpm			0.29	
N_2 Flow Rate, slpm			0.13	
Run Duration, hours	168	48	71	278
Aqueous Productivity, $g \cdot kg\text{-}Fe^{-1} \cdot hr^{-1}$	880	1350	270	360
Liquid Hydrocarbon Productivity, $g \cdot kg\text{-}Fe^{-1} \cdot hr^{-1}$	350	480	60	160
Wax Productivity, $g \cdot kg\text{-}Fe^{-1} \cdot hr^{-1}$	120	70	20	50

catalyst performance if the H_2 concentration is reduced as CO_2 concentration increases. H_2 could be increased by using WGS to shift all CO to CO_2, but the cited researchers reported that replacing all CO with CO_2 has a strong negative impact on FT catalyst performance. The authors conclude from this that some gas sweetening is inevitable if a fluidized-bed gaifier is used to feed a FT reactor using iron-based catalyst. The same may not be true of high-temperature entrained-flow gasifiers, which tend to generate more H_2.

While CO_2 negatively impacted steady-state catalyst performance in Test FTR40, it did not cause rapid deactivation. The catalyst was run for 71 hours under simulated syngas following 148 hours of operation at more ideal conditions. During the 71 hours of CO_2 exposure, catalyst activity seemed fairly stable. This suggests that high concentrations of CO_2 in simulated syngas suppress catalyst activity but do not cause rapid deactivation.

4.1.1.3.2 Performance under Actual Syngas

As a new batch of catalyst was used in Test FTR45, the performance had to first be verified under a variety of bottled-gas conditions (this batch of catalyst will also be used in the pilot-scale FT reactor in the near future, so there was an incentive for the EERC to establish baseline performance in support of upcoming tests). Table 9 gives catalyst performance metrics under bottled gas, biomass-derived syngas, and again bottled gas following exposure to syngas (Test 7). As can be seen, the catalyst performance suffered greatly when exposed to unsweetened syngas, as both the wax productivity and liquid hydrocarbon productivity dropped off significantly. The aqueous productivity did not drop nearly as drastically as the hydrocarbon productivity. Combined with the wax productivity of zero, this indicates that the catalyst was generating more light gas, which is undesirable for processing to liquid fuels. After 68 hours of syngas exposure, the catalyst was reexposed to bottled gas. The performance did not recover. This indicates that the catalyst had been deactivated by exposure to unsweetened syngas.

Table 9. Catalyst Performance in Test FTR45

Test	1	2	3	4	5	6	7
H$_2$ Flow Rate, slpm	0.22	0.15	0.15	0.17	0.19	–	0.19
CO Flow Rate, slpm	0.30	0.20	0.20	0.23	0.25	–	0.25
Syngas Flow Rate, slpm	–	–	–	–	–	0.35	–
Temperature, °C	250	250	260	260	260	260	260
Pressure, psig	250	250	250	250	250	445	250
Run Duration, hours	24	48	20	25	120	68	72
Aqueous Productivity, g·kg-Fe^{-1}·hr^{-1}	740	370	480	520	570	190	220
Liquid Hydrocarbon Productivity, g·kg-Fe^{-1}·hr^{-1}	230	150	190	220	250	20	60
Wax Productivity, g·kg-Fe^{-1}·hr^{-1}	30	50	90	100	100	0	0

During and after exposure to syngas, the FT product had an unusual odor as well as a darker color than usual. The odor and discoloration may have been indicative of organic acids and/or aromatics. The catalyst surface was very coked when the reactor was opened after testing. The reason for excessive coking is not certain, but similar coking was observed on catalyst recovered from the pilot-scale FT reactor at the end of BP1 (Section 4.5.1). The FT product from BP1 also contained a significant fraction of aromatics that appeared to be derived from light gasifier tars. It seems reasonable that FT catalyst would be more prone to coking when exposed to aromatic or polyaromatic compounds, as these are known coke precursors in petroleum refining. The excessive coking strongly suggests that warm-gas treatment is not sufficient for any syngas stream containing volatile organics.

4.1.2   Cobalt-Based Catalyst Production and Laboratory Testing

The catalysts produced with only cobalt and lanthanum showed very little FT activity and no wax productivity, as seen from Tests FTR46 and FTR47 in Table 10. It should be noted that because cobalt-based FT catalysts do not catalyze the WGS reaction, every molecule of water generated corresponds to an atom of carbon converted to hydrocarbon. The ratio of organic to aqueous productivities is thus a very good indicator of C_{5+} selectivity for cobalt-based catalysts,

Table 10. Cobalt-Based Catalyst Performance

Catalyst Test:	FTR46	FTR47		FTR48	
Run Duration, hours	40.3	21.8	25.5	103.9	6.8
Temperature, °C	220	220	240	210	210
Pressure, psig	250	250	250	250	250
H$_2$ Flow Rate, slpm	0.21	0.21	0.21	0.21	0.15
CO Flow Rate, slpm	0.10	0.10	0.10	0.10	0.10
N$_2$ Flow Rate, slpm	–	–	–	–	0.40
Aqueous Productivity, g·kg-Co^{-1}·hr^{-1}	340	190	430	630	430
Liquid Hydrocarbon Productivity, g·kg-Co^{-1}·hr^{-1}	10	3	50	160	50
Wax Productivity, g·kg-Co^{-1}·hr^{-1}	0	0	0	20	10

because only C_{5+} hydrocarbons tend to condense with the water. The low ratio of organic to aqueous productivities in Tests FTR46 and FTR47 mean that most of the hydrocarbon formed was light gas which, in turn, means that C_{5+} selectivity was very low.

In Test FTR47, the temperature was raised from 220° to 240°C on the second day of testing in an effort to boost catalyst activity. The liquid hydrocarbon productivity improved, but the C_{5+} selectivity was still quite poor.

The addition of ruthenium to catalyst in Test FTR48 had a dramatic effect on catalyst performance. This was the only test with cobalt catalyst in which any wax was collected, and the ratio of organic to aqueous productivity suggests that C_{5+} selectivity was much better than in Tests FTR46 or FTR47. Total organic productivity (liquid plus wax) was still somewhat low compared to the iron-based FT catalyst described in Section 4.1.1.3 but was not unacceptable.

Productivity in Test FTR48 slowly decreased over time, and small bits of black solid collected in the liquid product. This probably indicates that the catalyst was physically breaking. As described in Section 3.1.2, the as-received catalyst support spheres would not fit into the laboratory reactor and had to be broken into thirds or quarters. This process left sharp edges on the catalyst support and also likely introduced small stress fractures near the sheared faces. The sharp edges probably broke off during the run and appeared in the product as small bits of particulate.

When the feed gas in Test FTR48 was diluted with nitrogen near the end of testing, the catalyst productivity decreased as expected. However, the effect did not appear to be as drastic as when iron-based catalyst had been exposed to CO_2-rich gas in Test FTR40 (Table 8). This suggests that the loss of activity in Test FTR40 was caused not only by dilution but also by an inhibiting effect of CO_2 over iron. The amount of N_2 added in Test FTR48 is nearly equal to the sum of N_2 and CO_2 added in Test FTR40. CO_2 is reported to act as an inert over cobalt-based catalysts (16, 17, 19) and should affect cobalt-based catalyst similarly to N_2. Since cobalt did not suffer as badly under N_2 in Test FTR48 as iron did in Test FTR40, cobalt-based catalysts might be more tolerant of syngas dilution by CO_2 than iron-based catalysts. However, given the short run duration with N_2 in Test FTR48 and the fact that the blend of bottled gas was different than in Test FTR40, the test results are inconclusive. The relative performance of cobalt versus iron with simulated warm-gas cleanup remains uncertain.

4.2 Process Modeling

4.2.1 HPFBG and FT Process Modeling

Empirical inputs for the AspenPlus-based HPFBG model were selected using data from Test FBG002 (Section 4.3.1). Table 11 compares the gas concentration as measured by LGA to the concentration as predicted by the model. It should be noted that measured syngas concentrations are as-reported in this table and do not total 100%. The components in the gas stream were predicted reasonably well by the model. Some discrepancies arise where the

Table 11. Exit Gas Concentrations: Gasifier Data vs. Model Predictions

Component (dry basis)	Syngas Concentration, mol%	Model Prediction, mol%
H_2	28.3	29.6
CO	15.9	15.5
CO_2	33.0	36.6
CH_4	5.2	4.16
HC	0.00	0.00
H_2O	0.13	0.13
N_2	12.7	14.0
H_2S	<1 ppm	0.30 ppm

Note: H_2S is postcapture as measured by Dräger tube.

equilibrium predictions from the model do not match with the experimental data, but overall, the syngas predictions are fairly close.

The FT reactor model predictions were much less accurate than the gasifier predictions, as seen in Table 12. The HPFBG model did a reasonable job at predicting the amount of syngas generated per pound of coal fed, but the FT model grossly overestimated the amount of liquid hydrocarbon produced per standard cubic foot of syngas.

The model not only overpredicted the amount of liquid hydrocarbon generated in the FT reactor, it also did a poor job of predicting the liquid properties. Figure 5 shows the liquid hydrocarbon distribution as measured from the FT reactor in Test FBG002 and compares it to the model predictions. The GC–MS data shown in Figure 5 are from 22:45 on August 26 and were carefully scrutinized to give a more accurate product distribution than those shown in Section 4.5.1.1. This level of scrutiny was not applied to all samples because of the significant amount of time required to manually identify all GC–MS peaks in a given chromatogram. Although the model predicts the approximate shapes of the normal and olefin distributions reasonably well, the relative ratios of normal paraffins to olefins are incorrect, particularly for molecules with 10 or fewer carbon atoms. Also, no alcohols could be positively identified in the organic phase of the FT product.

Table 12. Comparison of Model FT Reactor Results to Actual Performance

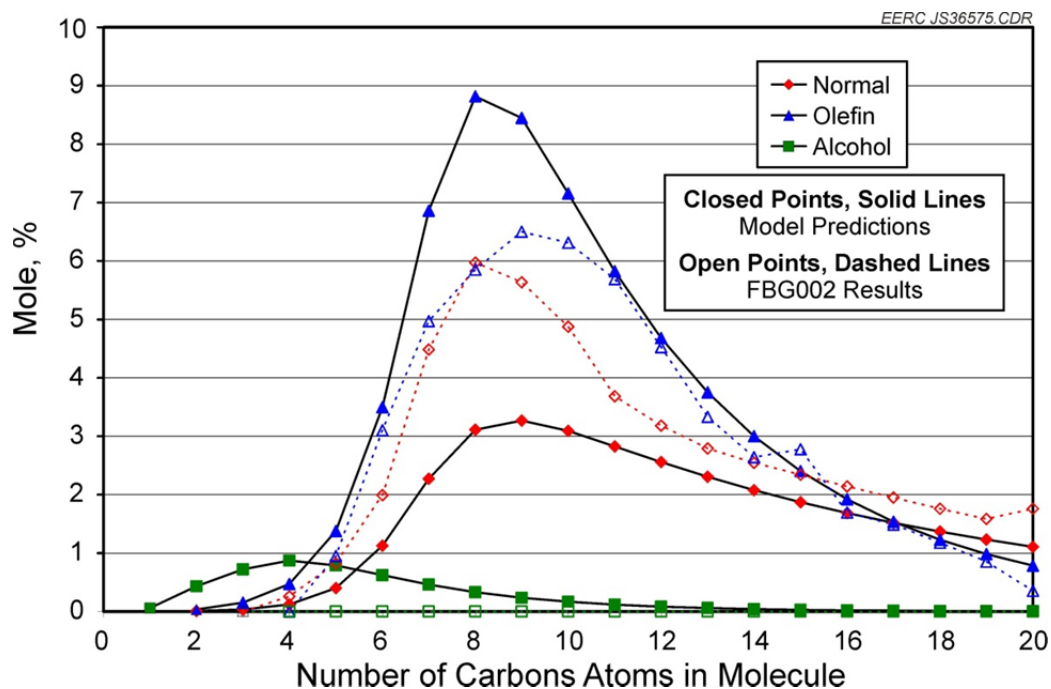|	Model	Actual, Test FBG002
Syngas Generated, scf/lb-coal	29.8	25.7
FT Water Generated, g/scf-syngas	1.78	2.2
Liquid Hydrocarbon Generated, g/scf-syngas	1.13	0.39

Figure 5. Liquid hydrocarbon distribution: reactor data vs. model predictions.

The most likely cause for the discrepancies between model and pilot-scale results is that the syngas fed to the FT reactor had a substantially different composition than the gas used in laboratory tests to generate the model equations. The α-values for the ASF model were based on laboratory data generated from bottled gas with a H_2-to-CO ratio of 0.85:1, while the pilot-scale data were generated from syngas with a H_2/CO ratio of 1.8:1. The syngas also contained significant amounts of CO_2, N_2, and other gas components not present in the laboratory tests. As described in Section 4.1.1.3, adding CO_2 to the laboratory reactor badly impacted FT catalyst performance, and actual syngas affected catalyst even worse.

The model was developed under Activity 3 in BP1. Because Activity 3 did not exist in BP3, the model was never used to predict system performance with cold-gas sweetening, which removes CO_2 and other gas contaminants that negatively impacted catalyst performance. As will be described in Section 4.5.2, the use of gas sweetening greatly improved FT catalyst performance and generated a product much more similar to what was produced in the laboratory. The model as it currently stands does not accurately predict FT system performance with warm-gas cleanup, but it may be sufficient for predicting performance with gas sweetening.

4.2.2 GSAS Process Modeling

The column design underwent several changes as model results became available. Initially, the column was to sample sour gas from the HPFBG quench pots, which typically operate below 300 psig. Lean solvent was originally going to be cooled using a water-cooled heat exchanger. The first design of the flash drum would have operated at room temperature. None of the

components would have been compatible with methanol or with low temperatures. These features were all changed based on model results.

4.2.2.1 AspenPlus Model Results

4.2.2.1.1 Number of Equilibrium Stages

Varying the number of stages had little effect on the performance of the column. The number of stages was increased from 12 to 18 and the CO_2 capture increased from 90.6% to only 91%. Decreasing the number of stages from 12 to 6 had a slightly greater impact as the CO_2 capture efficiency decreased to 86.4%.

4.2.2.1.2 Solvent Temperature

Solvent temperature had a significant effect on the rate of CO_2 absorption in the equilibrium AspenPlus GSAS model. For a constant DEPG solvent flow rate (green triangles in Figure 6), the CO_2 capture efficiency decreased from 93.7% to 57.6% when the temperature was increased from 30° to 70°F. However, the DEPG density also decreased as solvent temperature increased. A lower solvent density meant that more solvent could be pushed through the column without causing the model to predict column flooding (blue squares in Figure 6). Using the maximum flow rates, the CO_2 capture at 70°F could be increased from 57.6% to 86.3%, and in general, the effect of solvent temperature on CO_2 capture could be minimized.
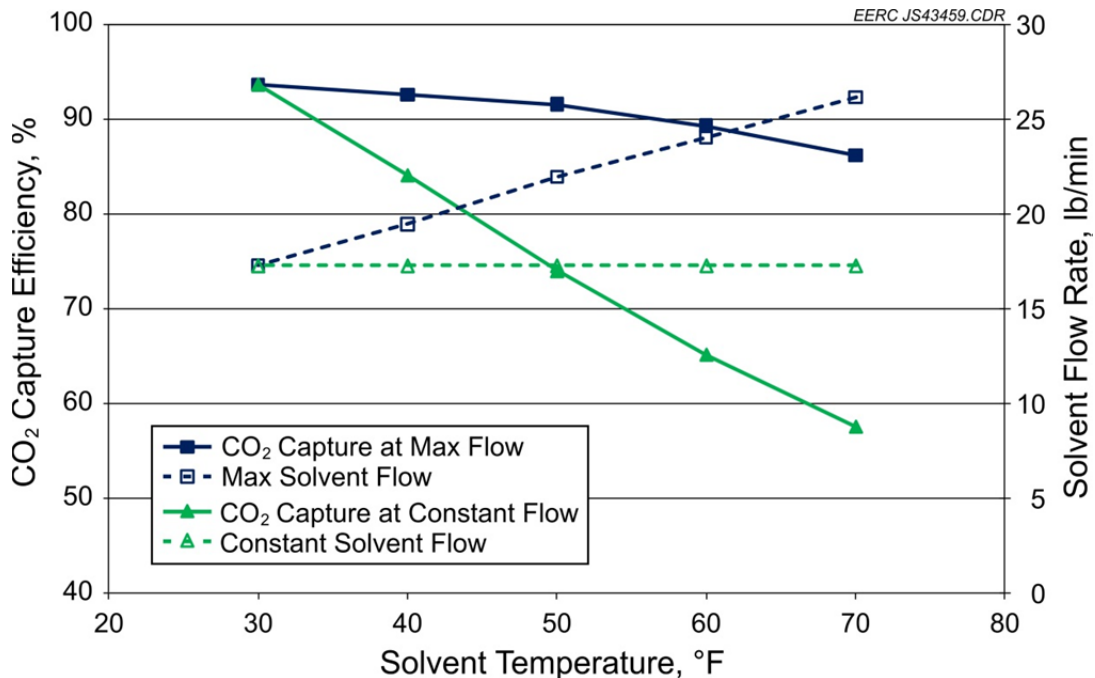

Figure 6. Predicted effect of solvent temperature and flow rate on CO_2 capture efficiency.

4.2.2.1.3 Flash Drum Pressure

Flash drum pressure can have an effect on CO_2 capture because lower flash drum pressure allows more CO_2 to be separated from rich solvent, which means that leaner solvent is returned to the absorption column and can absorb more CO_2. Decreasing the flash drum pressure from 16 to 2 psia had an appreciable effect on CO_2 capture and solvent regeneration in the equilibrium AspenPlus GSAS model. Figure 7 depicts the model predictions at various flash drum pressures with flash drum temperature held at 70°F. This figure also shows the relative effect of flash drum pressure at two lean solvent inlet temperatures, 30° and 70°F (it should be noted that these are solvent temperatures at the inlet to the absorption column, not to the flash drum).

In Figure 7, solvent regeneration efficiency is defined as the fraction of CO_2 entering the flash drum that is removed from the rich solvent stream. Solvent regeneration increases with decreasing pressure in the flash drum. This provides a leaner solvent to the absorption column and increases CO_2 capture, since leaner solvent is able to absorb more CO_2. However, the predicted benefit levels off below around 4 psia. It should be noted that column temperature has an effect on regeneration because lower column temperatures allow better CO_2 capture, which means the solvent entering the flash drum is richer.
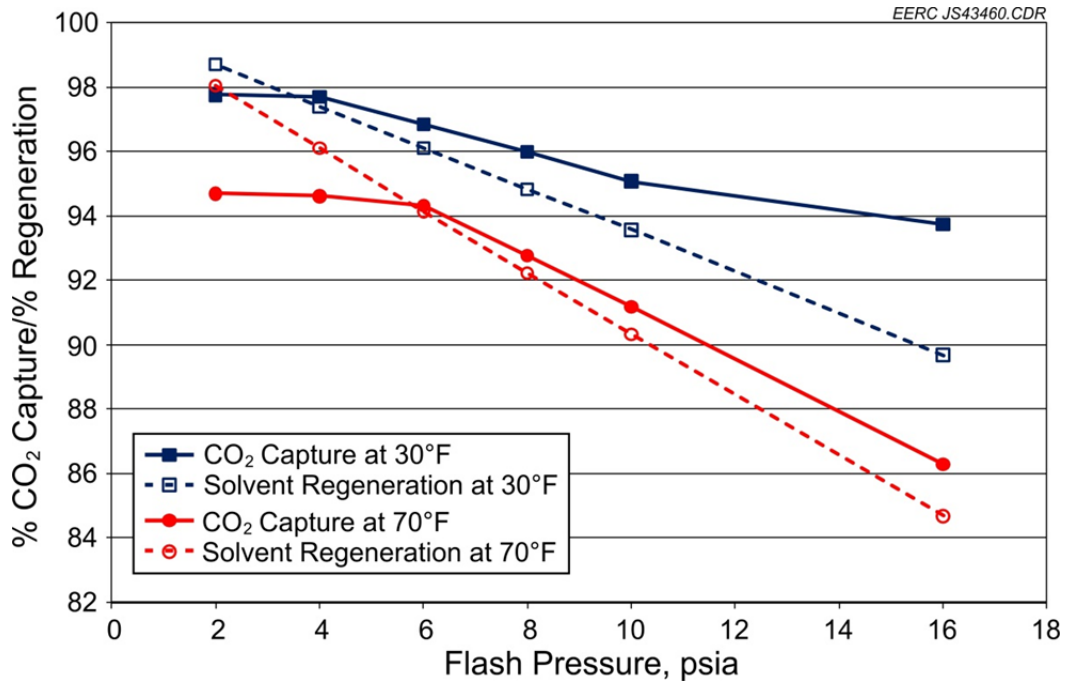

Figure 7. Predicted effect of flash drum pressure on CO_2 capture and solvent regeneration with flash drum at 70°F.

4.2.2.1.4 Flash Drum Temperature

For modeling the effect of flash drum temperature on CO_2 capture and recovery, pressure in the flash drum was held constant at 16 psia. Increasing the flash drum pressure had much the same effect as decreasing the flash drum pressure: CO_2 recovery improved at higher temperatures, which provided leaner solvent to the absorption column and improved CO_2 capture. The effect on CO_2 capture was strongest at low temperatures, while increasing the flash drum temperature much above 130°F had much less impact on CO_2 capture. Figure 8 depicts the model CO_2 capture and solvent regeneration efficiencies at various flash drum temperatures.

4.2.2.1.5 Rate-Based Modeling

Equilibrium modeling can provide a minimum number of theoretical stages required for CO_2 capture, but it cannot give the height or diameter of these stages. Rate-based modeling was used to determine an acceptable column diameter and height. Because the equilibrium AspenPlus GSAS model had suggested that column operation at 250 psia with flash drum pressure above atmospheric would give less than desirable performance, column pressure was varied between 250 and 750 psia in rate-based modeling (Table 5 shows specific conditions examined with the rate-based model).
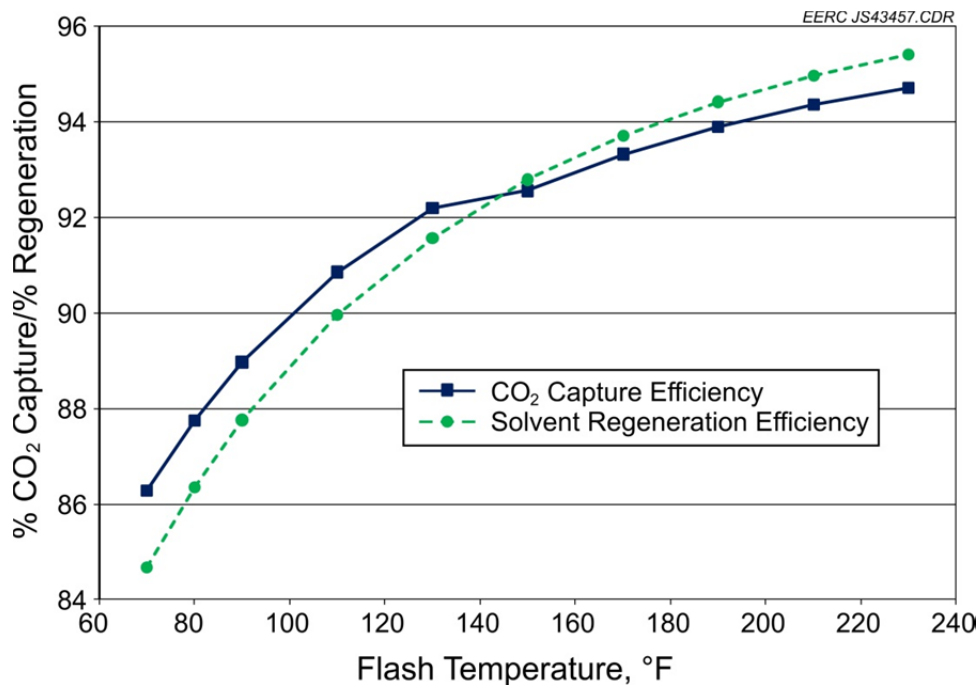

Figure 8. Predicted effect of flash drum temperature on CO_2 capture and solvent regeneration at 16 psia.

Figure 9 shows the predicted rate-based effects of column pressure and solvent inlet temperature on CO_2 capture and maximum solvent flow rate. The maximum solvent flow rate is the highest flow rate possible before the column is predicted to flood, and the CO_2 capture is the amount captured at the maximum solvent flow rate. CO_2 capture increased with increasing pressure. Temperature also had an effect on the rate-based capture efficiency, most notably at low column pressures. At the same time, maximum solvent flow rate decreased dramatically with increasing pressure. The maximum flow rate was cut by one-third when the column pressure increased from 250 to 750 psia. Temperature alleviated some of this effect because solvent has a lower density at higher temperatures which, in turn, allows more solvent to flow through the column before it floods.

The column diameter calculated by AspenPlus for each scenario is given in Figure 10. The maximum solvent flow rate decreases with increasing pressure, as does the actual flow rate of gas. The reduced gas volume and liquid flow rate mean that the required column diameter also decreases. At no set of conditions was the required column diameter much greater than 3 in. This led the EERC to select 3-in. Schedule 80 pipe for the column body.

4.2.2.1.6 Discussion of AspenPlus Model Results

Although high pressure and low temperature limited the amount of solvent that could flow through the model column without flooding, the opposing effect of temperature and pressure on
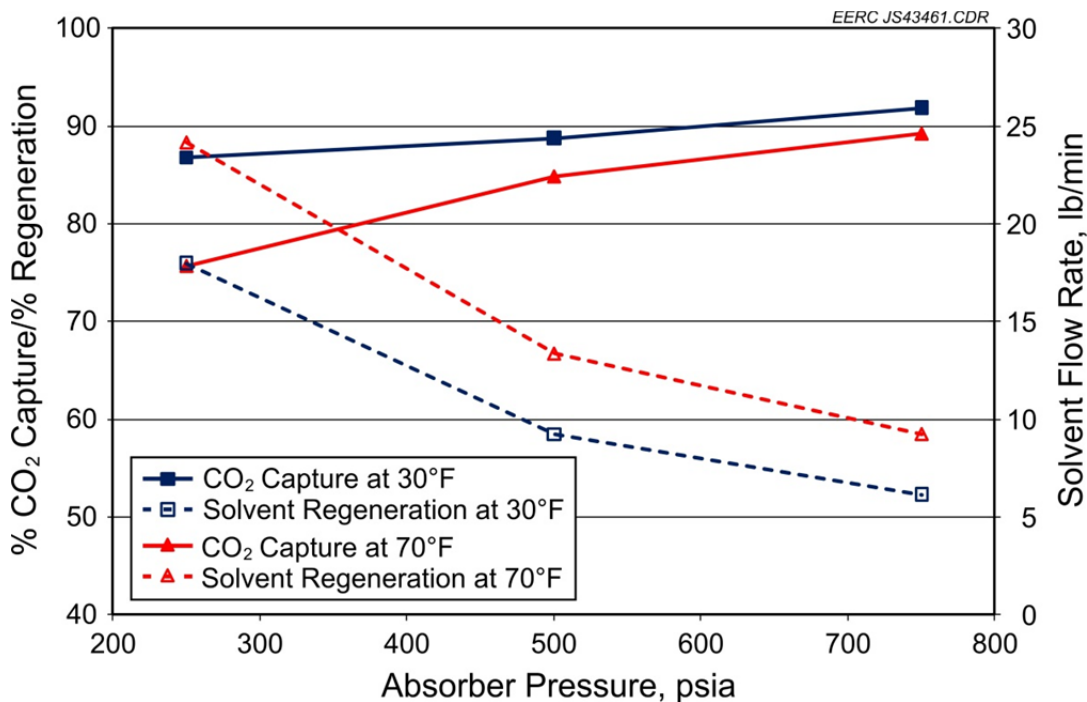

Figure 9. Predicted effect of column pressure and temperature on CO_2 capture and maximum solvent flow rate.
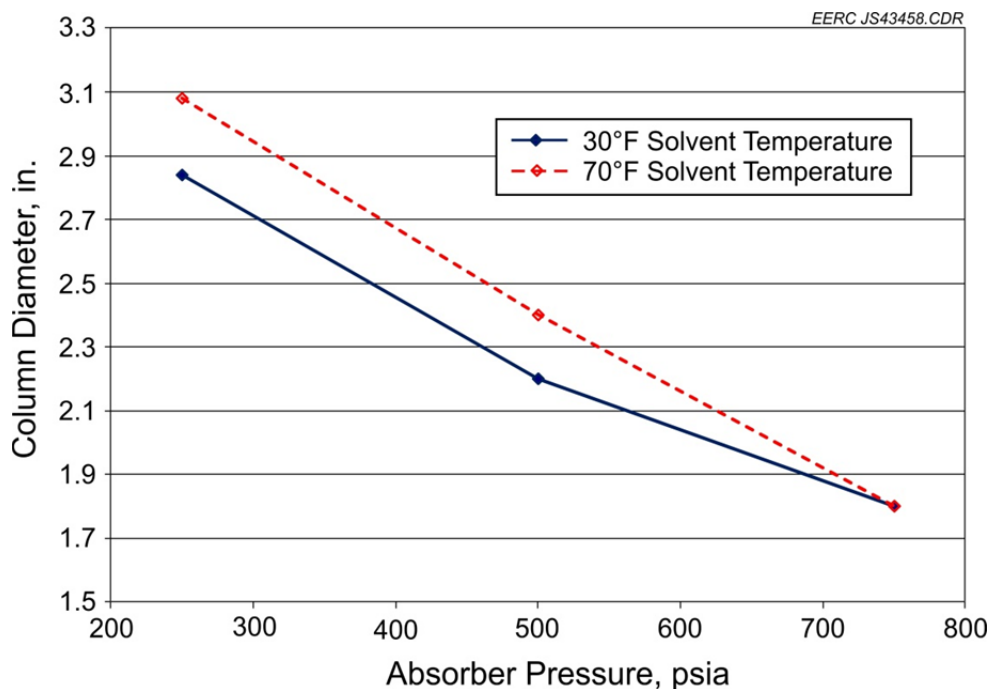
Figure 10. Predicted effect of column pressure and solvent inlet temperature on column diameter.

CO_2 solubility is so strong that CO_2 capture was highest at the conditions that gave the lowest solvent flow rate. Both equilibrium and rate-based modeling gave this result, as seen in Figures 6 and 9.

The predicted effect of high solvent temperature on CO_2 capture could be partially offset by increasing flow through the column, as seen in Figure 6, but the necessary solvent flow rates were quite high given the total amount of solvent in the GSAS reservoir. Moreover, the flash drum only contains about 8 lb of liquid at steady state, depending on the solvent. Flowing solvent at 26 lb/hr to maximize capture at 70°F would limit the residence time through the flash drum to about 20 seconds. Such a short residence time might prevent the flash drum from reaching equilibrium and would reduce solvent regeneration efficiency.

Based on both the reduced CO_2 capture and the high flow rates needed for high-temperature operation, it would probably be preferable to run at cold temperatures even if this made the column more prone to flooding. These model results led the EERC to make several changes to the original GSAS design. Gas was supplied to the GSAS from the HPFBG recycle compressor instead of the gasifier quench pots, as the pressure of the recycle syngas stream is much higher than the pressure at the quench pots (Figure B-6 in Appendix B shows the HPFBG process layout). Originally, the GSAS design included only water cooling. Because AspenPlus modeling suggested that capture efficiency would be less than acceptable unless solvent was cooled below 32°F, the equipment budget was modified to include a glycol chiller.

4.2.2.2 ChemCAD Model Results

Most of the ChemCAD modeling was conducted after all ApsenPlus modeling was complete, by which point it was clear that the GSAS would include a chiller. As such, the ChemCAD results include various test cases to determine the effect of chilling on CO_2 capture at various flow rates, gas compositions, temperatures, and pressures. The full table of recorded ChemCAD simulations is given in Table 13. In general, the model predicted that the gas-sweetening system would perform well using SELEXOL at temperatures below 32°F (0°C) and pressures above 290 psig (21 bar). Methanol also performed well in the model when the lean solvent temperature was kept at or below −20°F (−29°C) and the column pressure kept around 750 psig.

With the exception of water, most model components readily flashed out of rich solvent by simply reducing pressure and raising temperature in a single-stage flash drum vessel. By contrast, the ChemCAD model predicted that only 72%–92% of the water entering the flash drum would escape with the acid gas. The remaining 8%–28% of entering moisture was predicted to remain dissolved in SELEXOL. Effectively no water slipped through the absorption column under any condition modeled. No model predictions were possible for water capture in methanol because the ChemCAD model would not converge when moisture was included with other soluble gas components. The strong absorption and weak desorption potential for moisture made clear that the sour gas entering the column would need to be as dry as possible. Along with the need for higher pressure, this observation reinforced the decision to take sour gas from the HPFBG recycle compressor surge tank rather than from one of the quench pots.

The EERC did not originally intend to use the GSAS for Rectisol (i.e., methanol) treatment. However, because ChemCAD model results suggested that Rectisol treatment at low sour gas flow rates might be possible at temperatures as high as −20°F, the EERC modified the GSAS design to make it suitable for operation as a Rectisol unit. Extended bonnets were purchased for all control valves on the GSAS that would be exposed to cold solvent or gas. All components were selected with an eye toward chemical compatibility with methanol. Flow rate calibration data for methanol in the solvent flowmeter were obtained from the flowmeter vendor. The temperature-limiting features of the chiller were also identified based on conversations with the chiller vendor. These features allow GSAS operation at much colder temperatures than originally intended and also permit the use of methanol as a solvent for short-duration tests (less than 100 hours). A makeup pump or vapor recovery system would be required for stable operation beyond about 100 hours because ChemCAD modeling predicts significant methanol loss to the acid gas stream.

4.3   Gasifier Performance

Tests FBG002 through FBG005 examined the potential for warm-gas cleanup on FTS during BP1. These were the first four tests ever conducted on the HPFBG. Because these were the first gasification tests ever performed on the unit, the system faced a number of operational difficulties that were resolved before Test FBG021 in BP3. Similarly, the GSAS was operated

Table 13. ChemCAD Predictions for SELEXOL and Rectisol Model Systems at Varying Conditions

	1	2	3	4	5	6	7	8	9
Solvent Properties									
Solvent Type, S/R[1]	S	S	S	S	R	R	R	R	R
Flow Rate, gal/hr	21	42	42	42	50	30	30	42	20
Temperature, °F	15	5	5	32	−90	−50	−50	−20	−20
System Properties									
Column Press, psig	285	785	785	285	785	750	750	750	750
Flash Temp., °F	90	110	110	110	50	40	50	50	50
Sour Gas Properties									
Flow Rate, scfh	300	1000	300	300	1000	1000	1000	300	300
Temperature, °F	60	60	60	60	70	60	60	50	50
Composition, mol%									
CO	28.4	27.4	27.4	27.4	30.0	30.0	30.0	30.0	30.0
H_2	28.4	27.4	27.4	27.4	30.0	30.0	30.0	30.0	30.0
CO_2	37.9	36.5	36.5	36.5	40.0	40.0	40.0	40.0	40.0
CH_4	–	3.6	3.7	3.6	–	–	–	–	–
H_2O	0.5	0.5	0.5	0.5	–	–	–	–	–
H_2S	0.1	0.1	–	0.1	–	–	0.1	0.1	0.1
N_2	4.7	4.6	4.6	4.6	–	–	–	–	–
Sweet Gas Properties									
Sweet Gas Flow, scfh	187	595	156	181	530	564	564	129	156
Capture, mol%									
CO_2	93.8	98.8	99.5	96.9	99.8	99.1	99.0	99.2	98.9
H_2S	96.5	99.3	–	97.3	–	–	98.9	96.8	97.2
H_2O	99.3	99.8	99.9	99.5	–	–	–	–	–
Total Gas Volume[2]	62	60	52	60	53	56	56	43	52
Acid Gas Properties									
Acid Gas Flow, scfh	113	404	144	118	503	458	468	183	155
Solvent Loss, % feed	–	–	–	–	0.85	0.92	1.32	0.37	0.65

[1] S = SELEXOL, R = Rectisol (methanol).
[2] This value is the total reduction in gas flow across the column. This does not correlate to acid gas removal, as some amount of desirable sweet gas species such as CO and H_2 are inevitably removed along with CO_2 and H_2S.

for the first time in BP3, and a few operational issues with the sweetening column affected HPFBG operation during Test FBG021. The following sections provide details on gasifier operation, which gives some insight into the FT reactor and GSAS performance discussed in later sections.

4.3.1   Test FBG002

Table 14 provides average run conditions for Test FBG002. As can be seen, operating conditions were similar for all of the feeds. Feed rate was lower with the 30% switchgrass blend

Table 14. Average HPFBG Run Conditions During Test FBG002

Feed:	PRB	30% Leached Olive Pits	30% TL Olive Pits	30% Leached DDGS	30% Switchgrass	30% DDGS
Bed Temperature, °F	1510	1505	1528	1522	1526	1500
Freeboard Temperature, °F	1542	1552	1564	1563	1561	1557
Feed Rate, lb/hr	7.0	6.8	7.1	7.4	5.0	5.6
Gas Flow, scfh						
Recycle	403	427	418	409	410	424
Steam	334	409	409	407	407	408
Nitrogen	16	0	0	0	0	0
Oxygen	55	58	58	58	58	58
Purge	321	377	346	349	350	346
Outlet	134	78	57	50	54	112
Bed dP, in. H_2O	31	25	23	22	25	20
Freeboard dP, in. H_2O	11	7	5	7	8	10
Bed Pressure, psig	305	309	308	309	309	309
Start of Test, d/m/y hh:mm	8/24/09 10:58	8/27/09 17:00	8/27/09 23:49	8/28/09 3:19	8/28/09 10:02	8/28/09 14:28
Test Duration, hh:mm	73:11	6:49	3:30	6:43	4:26	2:29

because the fuel has a lower density, and feed rate was not corrected. This did not greatly affect bed temperatures despite the low HHV of leached switchgass shown in Table 6 (Section 3.3.1). The temperatures were probably not affected because the switchgrass was floor-dried to much lower moisture content before use, which likely raised its HHV substantially.

Figure 11 shows the bed temperature distribution during testing. As can be seen, temperatures dropped and spiked several times during the week. This was primarily because of brief losses in coal feed. Most of the coal feed losses were the result of cyclone plugging: Bed velocity was too high, and large solids carried up into the line going to the cyclone caused plugging. Despite these numerous upsets, temperatures were fairly stable for most of the run, including when treated biomass was added to the feed. Bed temperatures actually improved when 30% TL olive pits were added, which is only somewhat surprising given the HHV of torrefied pits. Analysis of air-dried TL olive pits showed that the HHV may have been higher than for PRB coal.

The temperatures began to diverge late on the final day of testing, when 30% untreated DDGS was added to the feed. This temperature divergence indicated that the bed was not fluidizing well, which implied that it was beginning to agglomerate. When the reactor was taken off-line, the bed material was found to contain many large chunks indicative of agglomeration.
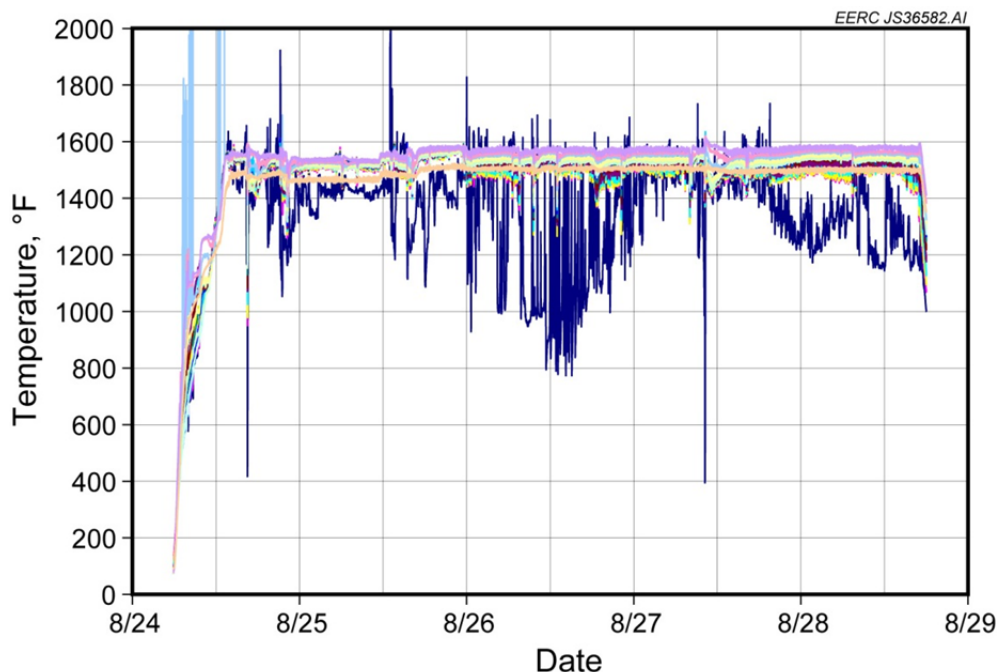
Figure 11. Bed temperature distribution during Test FBG002.

These results demonstrate that untreated DDGS led to agglomeration after only 2.5 hours of operation, while no signs of agglomeration were present when biomass was pretreated by leaching. The leaching process was apparently sufficient to allow 30% biomass to be gasified with PRB coal for at least a short duration.

4.3.2 Test FBG003

Because of anticipated budget and scheduling constraints, two projects shared the gasifier during Test FBG003 so that each project could be completed on time and within budget. As a result, only a portion of the syngas was sent to the FT reactor, with the remainder being sent to a thermal oxidizer for unrelated testing. Similarly, process conditions were selected to produce enough syngas of sufficient quality to feed both the FT reactor and the thermal oxidizer, which is the reason for the elevated feed rates and system pressures in Table 15.

PRB coal was again used as the gasifier feedstock in Test FBG003 and was run for the majority of the test duration to ensure stable gasifier operation and steady flow to both the FT reactor and the thermal oxidizer. After the thermal oxidizer was taken off-line, feed was switched to 100% treated DDGS for 4 hours, then to 100% treated olive pits.

The results shown in Table 15 may be somewhat misleading, as they imply that the pressure drops across the bed and freeboard rose significantly when the feed was switched from PRB coal to treated DDGS. In fact, the gasifier suffered a major upset 1.5 hours before the DDGS feed was started, and it had to be taken off-line for 1 hour and 15 minutes to clear a plug

39

Table 15. Average HPFBG Run Conditions During Test FBG003

Feed:	100% PRB	100% DDGS	100% Olive Pits
Bed Temperature, °F	1539	1461	1537
Freeboard Temperature, °F	1552	1565	1555
Feed Rate, lb/hr	11.4	12.4	21
Gas Flow, scfh			
Recycle	542	468	363
Steam	387	389	378
Nitrogen	26	23	45
Oxygen	81	78	73
Purge	227	269	285
Outlet	243	382	354
Bed dP, in. H_2O	28	53	63
Freeboard dP, in. H_2O	7	24	37
Bed Pressure, psig	493	470	486
Start of Test	9/8/2009	9/11/2009	9/11/2009
dd/mm hh:mm	11:00	9:10	13:18
Test Duration, hh:mm	68:32	4:08	0:58

in the cyclone. This can be seen in Figure 12 at 7:40 on September 11 as a sudden drop in bed temperatures as well as in various figures in Appendix A. As a result of the loss in fluidization during this upset, the bed had already begun to agglomerate when DDGS feed was started. As such, it is difficult to say for certain what effect the 100% DDGS feed had on system performance in Test FBG003. The situation is exacerbated for the 100% olive pit feed, as the bed fully agglomerated after less than an hour of run time. Whether either biomass contributed to rapid agglomeration is uncertain, as the cyclone plug that occurred prior to the start of biomass feed was quite severe. However, the HPFBG recovered from other cyclone plugs during BP1. It seems probable that the DDGS and olive pits contributed to more rapid agglomeration and shutdown than would otherwise have been the case.

4.3.3 Test FBG004

During Test FBG004, the gasifier performed much more poorly than in previous tests. In particular, the recycle syngas flow rate was highly erratic, and the back-pressure control valve did a poor job at controlling system pressure. As will be discussed in Section 4.5.1.3, flow to the FT reactor was also erratic. The primary reason for this decrease in performance appears to have been a drop in outside air temperatures compared to previous tests, as shown in Figure 13. Center lines represent weighted average temperatures for the week, while the boxes above and below extend to maximum and minimum temperatures, respectively. As can be seen, the maximum air temperature (52°F) in Test FBG004 was almost lower than the lowest temperature observed previously (50°F); the average temperature was more than 20°F lower (43°F in Test FBG004 as compared to 66°F in both Tests FBG002 and FBG003); and the minimum temperature was below freezing.
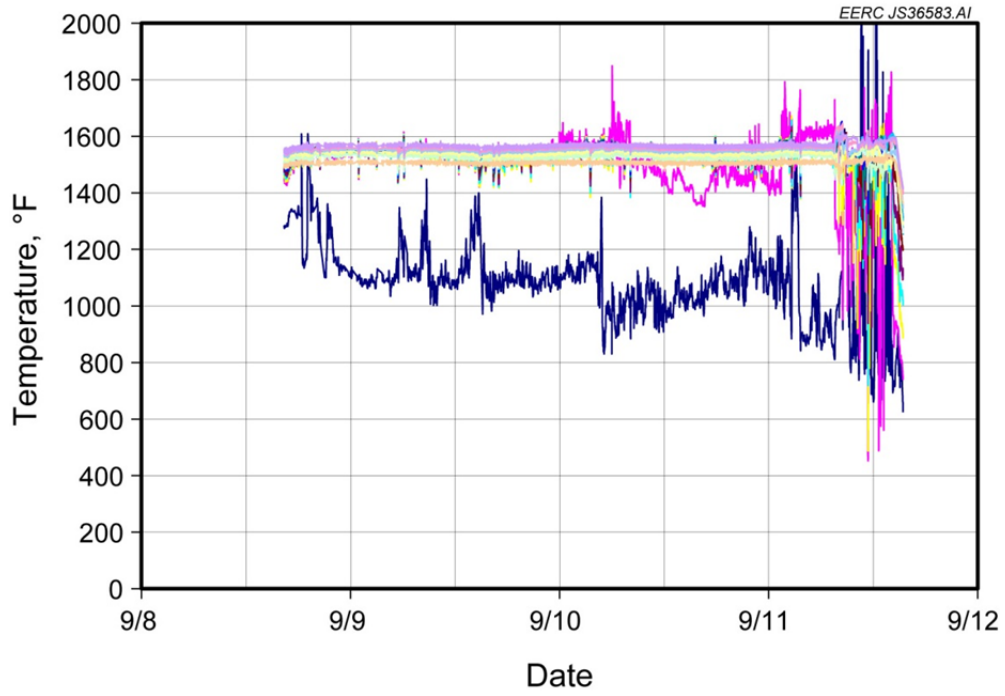
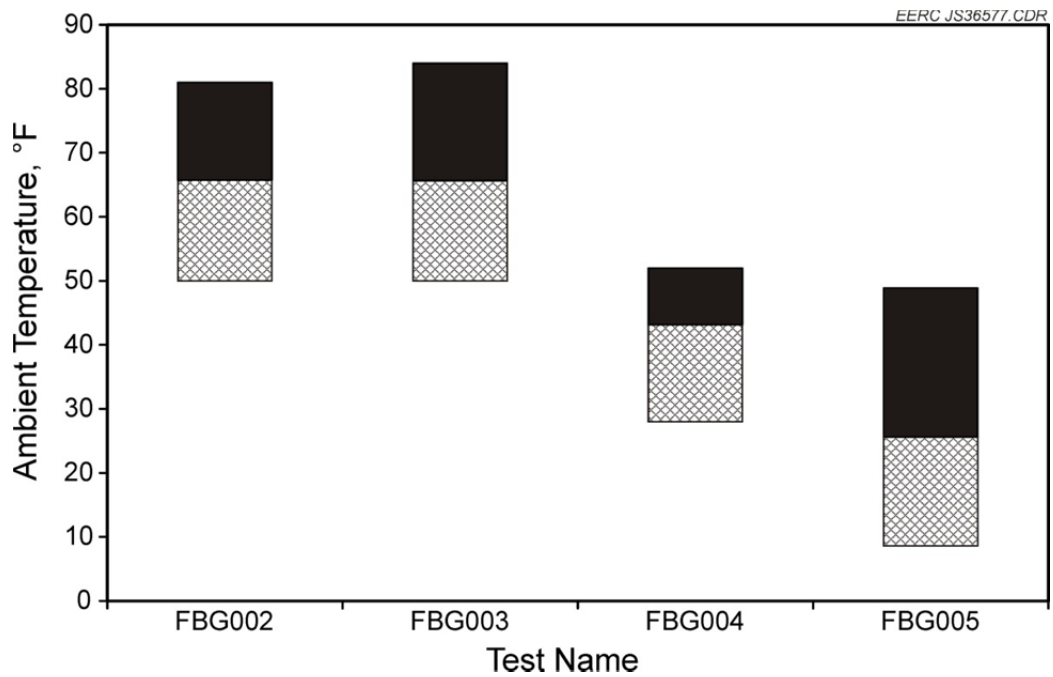Figure 12. Bed temperature distribution during Test FBG003.

Figure 13. Ambient air temperature during each week of testing.

41

As a result of the lower ambient air temperatures, water and tars tended to condense in cooled, exposed lines, particularly those downstream of the gasifier's water-cooled quench pots. The gasifier is housed inside of a building, but the temperature in some areas of the pilot plant area is often close to outdoor temperatures. Although the bulk of the water and tars was captured in the quench pots, the small amount that was able to slip through uncondensed would slowly deposit and build up in cold fittings until they were blocked off completely. This was especially an issue in valves and regulators with large pressure drops, as the Joule–Thompson cooling effect of adiabatic expansion would bring the syngas temperature to below freezing. Volatile gasifier tars like naphthalene would then form solid deposits on the control valve stems, causing the valves to stick open or shut. These problems were remedied after several days when all problem areas had been identified and wrapped in heat tape, and tar condensation was not as severe a problem at the end of Test FBG004 or during Test FBG005. The frequent plugging by heavy tar accumulation shows that dolomite addition at 20 g/lb coal was not sufficient to crack significant gasifier tar when using lignite or blends of lignite and biomass.

Although the HPFBG suffered several system upsets as a result of plugged lines, the addition of treated biomass to the lignite did not seem to have any adverse effect on operating conditions. Based on the temperature distribution in Figure 14, adding 30% treated switchgrass and treated DDGS to the feed actually seemed to help system performance. Signs of agglomeration were corrected, and as can be seen in Table 16, the temperatures rose when biomass was added to the coal. When switchgrass was mixed with the coal, the coal feed rate set point had to be raised by 75% to account for the lower density and energy content of the switchgrass. The rate was then lowered back to its normal set point when the feed was switched to 30% DDGS and was kept the same when feed was switched to 30% olive pits.

The reactor was eventually taken off-line because of agglomeration. However, because each fuel was run for several hours, it is clear from Test FBG004 that leached biomass can be cogasified with lignite coal without causing significant short-term operational issues. The agglomeration that ultimately stopped the test was the result of a loss in coal feed, which allowed the bed to burn out and become hot enough for ash to flux and form an agglomerate. Prior to this loss in coal feed, the temperature distribution in the bed was fairly steady, even after the gasifier had been brought back online following a complete shutdown on the night of October 8.

4.3.4   Test FBG005

Most of the trouble areas identified in Test FBG004 were heated in Test FBG005 to avoid problems with tar condensation. However, in some cases, this only created new problems. For instance, the line exiting the recycle syngas surge tank was heated because the large pressure drop out of this tank caused adiabatic expansion and cooling, leading to rapid plugging in Test FBG004. In Test FBG005, the gasifier was taken off-line for several hours in the afternoon of December 1 to repair an auger. Only 13 minutes after the gasifier was restarted, all of the fittings downstream of the surge tank quickly plugged and led to a complete loss in recycle syngas and purge flow. It appears that the gas in the surge tank and exit lines became warm enough to vaporize any condensed tars when gas flow stopped, and these tars were then carried
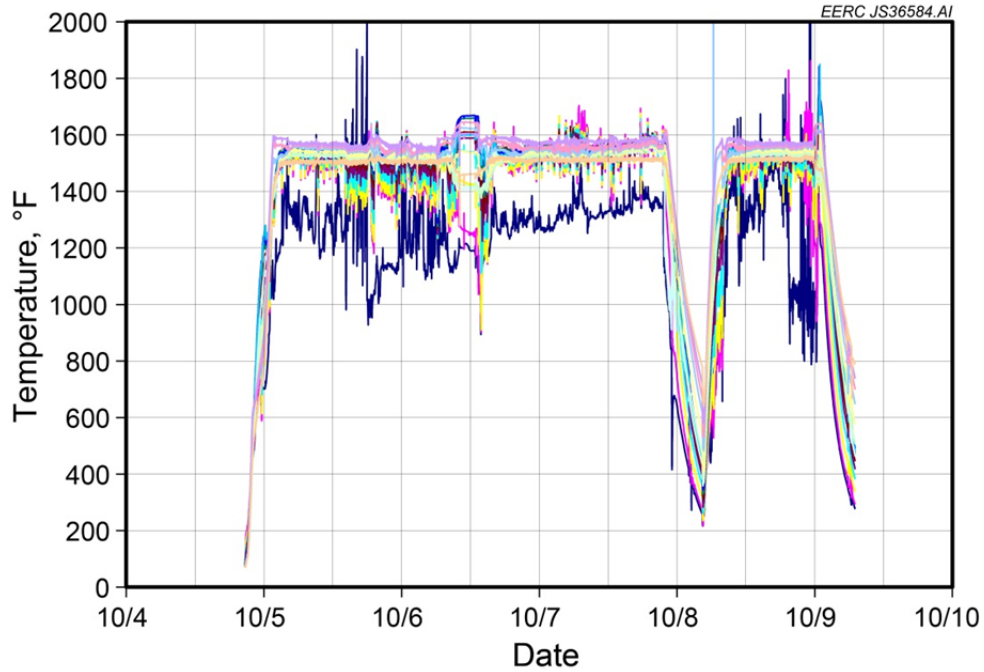
Figure 14. Bed temperature distribution during Test FBG004.

Table 16. Average HPFBG Run Conditions During Test FBG004

Feed:	100% Lignite	30% Switchgrass 70% Lignite	30% DDGS 70% Lignite	30% Olive Pits 70% Lignite
Bed Temperature, °F	1513	1550	1533	1527
Freeboard Temperature, °F	1547	1558	1555	1557
Feed Rate, lb/hr	8.8	8.4	8.1	8.8
Gas, scfh				
Recycle	581	558	568	584
Steam	365	374	372	397
Nitrogen	27	57	52	0
Oxygen	90	84	84	85
Purge	172	160	150	156
Outlet	136	154	417	72
Bed dP, in. H_2O	29	27	31	31
Freeboard dP, in. H_2O	6.9	10.5	11.7	15.3
Bed Pressure, psig	428	394	396	422
Start of Test, dd/mm	10/5/2009	10/7/2009	10/7/2009	10/8/2009
hh:mm	0:58	10:50	16:48	16:37
Test Duration, hh:mm	48:03[1]	5:58	9:39	7:04

[1] An additional 3:49 of lignite run time was conducted following an upset during the 30% DDGS test, but this was not counted as it did not approach steady state.

43

downstream en masse and redeposited on cooler valve stems when flow resumed. The FT reactor suffered from a similar issue, with vaporized tars passing uncondensed through heated lines, as will be shown in Section 4.5.1.4.

Table 17 provides average run conditions for Test FBG005. In contrast to the results of Test FBG004, Test FBG005 suggests that the addition of 30% DDGS to lignite had a detrimental effect on gasifier operation. This is probably not a valid result, as the loss of recycle and purge gas described above occurred only 13 minutes after DDGS was added to the coal, and the system had to be taken off-line for over an hour and a half to clear out the lines. This is seen as a bump in temperatures just after midnight on December 2 in Figure 15. When the gasifier was restarted, bed temperatures were steady but not as high as they had been before the shutdown, indicating that some agglomeration may have occurred when the system was down.

When feed was switched to 100% DDGS, problems arose quickly. A primary cause of these problems was that the lower density of the DDGS relative to lignite resulted in a lower flow rate, and the high HHV led to high bed temperatures. By the time operators noticed that the flow rate had decreased, the bed temperatures and CO_2 concentration had risen noticeably. After the feed rate was corrected, the temperature distribution became erratic, indicating that agglomeration had begun to form at the higher O_2/feed ratio and operating temperatures. This agglomeration remained for the duration of the test, mostly obscuring any temperature trends when feeding 30% olive pits in lignite during Test FBG005.

Table 17. Average HPFBG Run Conditions During Test FBG005

Feed:	Lignite	30% DDGS 70% Lignite	100% DDGS	30% Olive Pits 70% Lignite
Bed Temperature, °F	1490	1459	1457	1459
Freeboard Temperature,°F	1542	1547	1556	1552
Feed Rate, lb/hr	8.7	9.1	7.5	N/A
Gas, scfh				
Recycle	467	375	422	413
Steam	365	408	419	418
Nitrogen	8	4	8	0
Oxygen	52	52	52	55
Purge	179	192	161	236
Outlet	141	135	103	138
Bed dP, in. H_2O	36	62	59	62
Freeboard dP, in. H_2O	13.7	16.6	26.1	22.4
Bed Pressure, psig	337	350	342	350
Start of Test, dd/mm	11/30/2009	12/1/2009	12/2/2009	12/2/2009
hh:mm	11:58	22:05	10:30	22:50
Test Duration, hh:mm	25:57	10:58	6:42	2:04
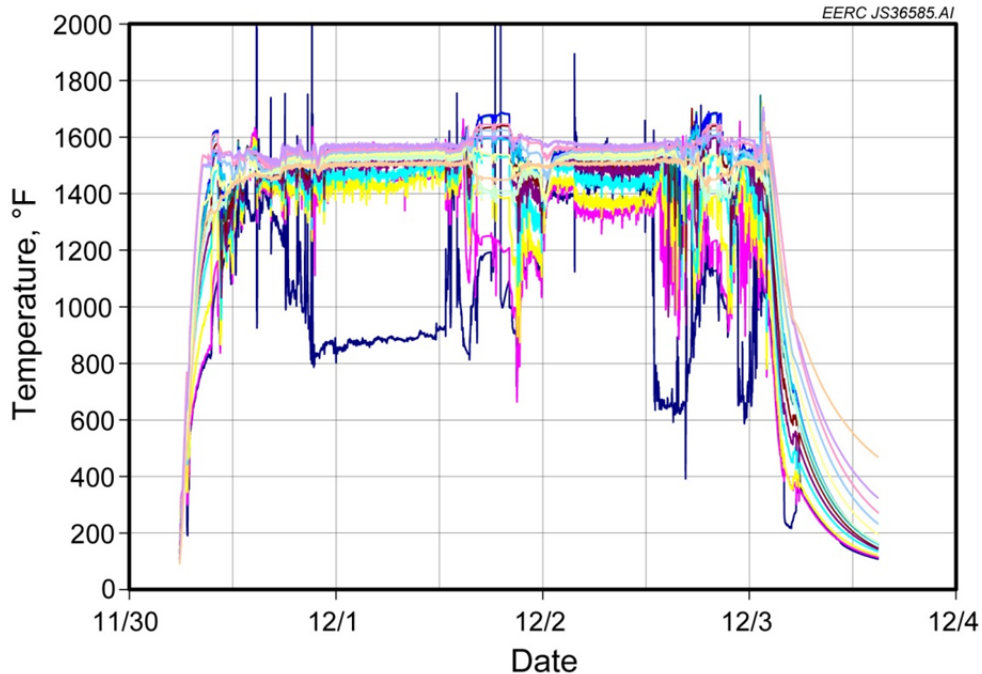
Figure 15. Bed temperature distribution during Test FBG005.

4.3.5 Test FBG021

Test FBG021 occurred almost 2 years after Test FBG005, by which point the HPFBG design had undergone a number of changes. A new distributor plate provided better gas and solids mixing in the bottom of the bed, which reduced localized combustion and helped prevent agglomeration. A refractory lining had been added to the original freeboard to give it the same inner diameter as the bed, and a new 316 stainless steel, 15-ft freeboard section had been added above. This gave longer solids residence times and helped carbon conversion but reduced maximum operating temperature and pressure. A recycle auger returned solids collected by the cyclone back to the bed, which helped keep the cyclone clear of plugging and also converted some of the solids into syngas. An ice-cooled knockout pot between the quench pots and the recycle compressor helped capture light gasifier tars, and permanent heaters on all recycle regulators and control valves prevented the condensation and plugging that had plagued Test FBG004. N_2 purges for the coal hopper had been reconfigured to minimize N_2 dilution (not counted as part of the purge flow in Table 18).

The design changes improved overall performance and allowed the EERC to operate at steady state for several days without incident. However, when the GSAS was brought online in the first day of operation, it permitted too much gas flow and caused HPFBG pressure to quickly drop. Each time the GSAS was shut off, pressure would quickly recover, then fall again when the GSAS was brought online. Coal and oxygen feed were increased to raise the gasifier pressure and provide more syngas flow to the GSAS. However, the bed had already begun to agglomerate

45

Table 18. Average HPFBG Run Conditions During Test FBG021

Feed:	100% PRB
Bed Temperature, °F	1518
Freeboard Temperature, °F	1393
Feed Rate, lb/hr	8.2
Gas, scfh	
Recycle	338
Steam	359
Nitrogen	0
Oxygen	75
Purge	107
Outlet	152
Bed dP, in. H_2O	37
Freeboard dP, in. H_2O	2.1
Bed Pressure, psig	299
Start of Test, m/d/y	11/14/2011
hh:mm	0:33
Test Duration, hh:mm	98:13

because of sudden surges and drop-offs in gas flow, as indicated by the large temperature spike just after midnight on November 15 in Figure 16. The HPFBG was shut down early on November 15, 2011, and large chunks of agglomerate were drained from the bed. The gasifier was restarted and reached steady state by 22:00 on November 15. After this initial upset, the unit ran smoothly until the end of the test on November 18. Table 18 gives average operating conditions during the steady-state period November 15–18.

4.4 Gas-Sweetening Absorption System Performance

The GSAS performed well at steady state during Test FBG021. As with any initial start-up, several design issues were identified that should be corrected for future operation.

The GSAS was to be operated for an hour or more on 100 scfh of sour gas before bringing the FT reactor online. This would have established steady-state operation and ensured adequate gas sweetening before exposing FT catalyst to syngas. During this time, sweet gas from the 600-psig GSAS column was to be vented to a thermal oxidizer operating at approximately atmospheric pressure. However, the back-pressure control valve on the GSAS column had been sized to operate with a pressure drop of less than 100 psid and a flow rate of up to 1000 scfh. The high pressure drop to the thermal oxidizer permitted too much gas flow during start-up and caused the HPFBG to depressurize, as described in Section 4.3.5. Even when the control valve was set to 99% closed, the flow rate could not be kept below 150 scfh. After several attempts to start the GSAS caused excessive flow and depressurization, it was decided to bring the GSAS and FT reactor online as a single unit. The much smaller pressure difference between the GSAS column and the FT reactor inlet allowed better flow control and prevented gasifier depressurization.
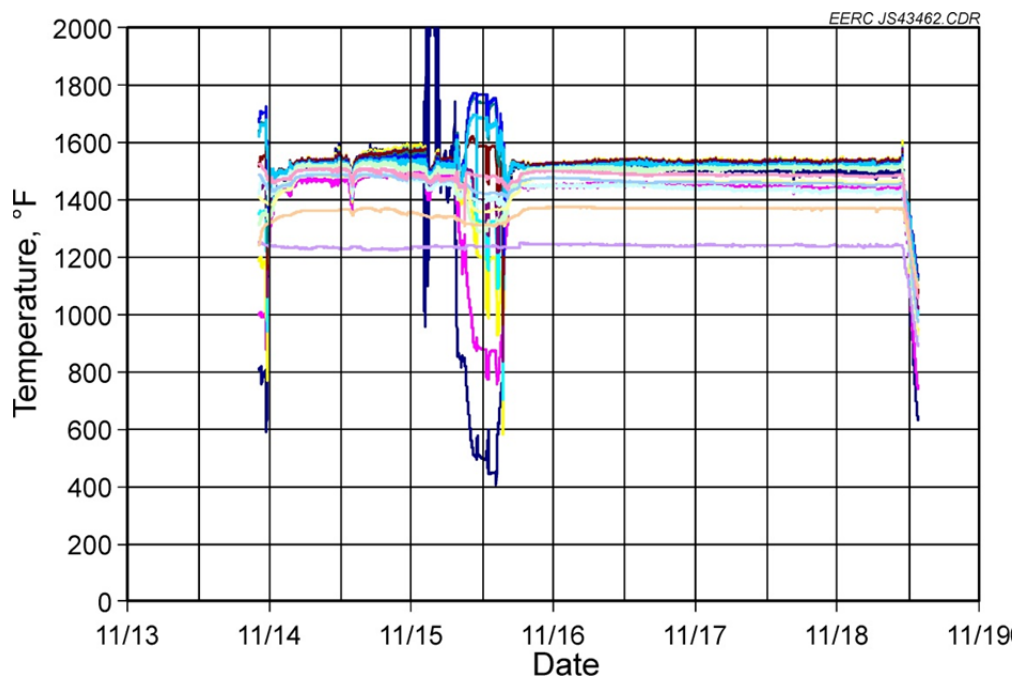
Figure 16. Bed temperature distribution during Test FBG021.

During the depressurization cycles, the coal feed rate to the HPFBG had been raised from 8 to 10 lb/hr to provide more syngas to the GSAS. The GSAS ran smoothly for 10 hours and 37 minutes at the higher feed rate with the FT reactor online. The differential pressure across the column then began to rise. The column was quickly taken offline and drained, but the pressure at the top of the column would not decrease, and no liquid was draining from the column.

All indications were that the bottom of the column was plugged. The most likely explanation is that the high coal feed rate generated extra volatile matter, and the depressurization cycles caused much of this material to surge through the gasifier quench pots uncondensed. As seen in Figure 17, the gasifier quench pots were quite laden with solidified gasifier tar at the end of testing. It should be noted that the quench pot baffles are constructed of flat plate metal, and the thick bulges consist of a solid mass of condensed tar. Some of the more volatile tar may have reached the lower plate of the GSAS during periods of high flow rate and low gasifier pressure. The GSAS operated at a much colder temperature than any of the gasifier quench pots, so this volatile matter would have condensed and solidified at the bottom of the column, causing flow restriction and eventual plugging. This is similar to the situation described in Section 4.3.3, when volatile matter plugged several lines on the gasifier itself.

Because the column could not be drained while it was plugged, the insulation was pulled away from the column so that it could be wrapped in copper tubing. Hot water was flushed through this tubing until the plug cleared and the column could be drained. A boroscope was then inserted into the bottom disengager to examine tar deposits. No trace of tar was observed

Figure 17. Internal baffles of gasifier quench pot No. 5 coated in tar.

anywhere in the bottom disengager. Because only the most volatile organics likely reached the GSAS, any condensate probably melted away or vaporized when heated solvent finally drained out of the column.

After this upset, the target coal feed rate to the HPFBG was kept at 8 lb/hr, and the GSAS was operated at higher temperatures. Heat trace was also wrapped around the sour gas inlet line to minimize condensation at the gas inlet. These changes permitted stable operation throughout the week. However, two of the flowmeters failed during operation. The mass flowmeter for measuring inlet sour gas flow rate did not read correctly and will either need to be recalibrated or replaced. The acid gas flowmeter proved to be oversized and could not measure the low flow rate of acid gas generated during Test FBG021. This flowmeter will also likely need to be replaced. The only gas flow rate that could be reliably measured was the sweet gas flow rate. All other flow rates could only be calculated using gas analysis and stoichiometry.

The GSAS was operated for most of the week with warm-gas bulk sulfur removal upstream so that only CO_2 and volatile matter were captured by gas sweetening. On the second-to-last day of operation, the sulfur capture beds were bypassed. The sulfur content of the sour gas stream rose several orders of magnitude. The solvent temperature was greatly reduced at this time and the heat trace to the inlet line was shut off. This was done to ensure adequate gas sweetening as well as to cause the column to plug again so that the condensation could be examined.

The GSAS performed as expected when exposed to sulfur-laden gas. The CO_2 capture efficiency was not affected by sulfur capture, and the H_2S capture efficiency reached steady state shortly after high levels of sulfur were introduced to the column.

The column never plugged during the final 22 hours of operation at reduced temperature. After shutdown, the column was drained and depressurized fairly quickly so that the bottom disengager could be examined by boroscope while it was still cold. However, no trace of tar or other condensate was observed. This suggests that the plugging observed in the first day of testing was the result of upsets in gasifier operation causing an unusual amount of volatile matter to escape the quench pots and reach the GSAS. Nevertheless, a glycol-chilled knockout pot has since been fabricated to condense volatile matter from sour gas upstream of the GSAS inlet.

4.5   Pilot-Scale FT System Testing

4.5.1   Warm-Gas Cleanup (BP1)

As expected, the FT process appeared to be mostly feedstock-agnostic, with almost no change observed in product quality when the gasifier was switched from one fuel to another. However, significant changes in catalyst behavior were observed over time, indicating that the catalyst was beginning to deactivate. Table 19 summarizes the run conditions and primary results for each test. The syngas and recycle product gas flow rates appear to be inaccurate in several tests, and corrected values based on N_2 balance were used for calculating CO conversion and STLG. As will be described later, significant gasifier tar accumulated in the FT inlet lines, and this tar probably affected the rotameters used for measuring flow.

4.5.1.1   Test FBG002

FT reactor operation was somewhat intermittent during Test FBG002, as this was the first time that the reactor had been operated using online syngas and the HPFBG itself was also operating intermittently (Section 4.3.1). The FT reactor was taken off-line for several hours and was restarted three times during the test period, and the pressure, temperature, and gas flow rates were adjusted several times as operators learned how to achieve the desired conditions. Despite the intermittent and variable operation, the catalyst performed relatively well, achieving the lowest STLG and highest conversion of any test conducted during BP1.

Table 19. Average FT Reactor Run Conditions and Product Properties with Warm-Gas Cleanup

Test ID:	FBG002		FBG003		FBG004		FBG005	
	Bed 1		Bed 1		Bed 1	Bed 2	Bed 1	Bed 2
Pressure, psig	260		411		328	328	300	299
Inlet Temperature, °F	387		348		322	331	342	350
Average Bed Temperature, °F	511		504		501	499	499	499
Syngas Flow Rate, scfm	0.87		2.18		0.59	0.57	0.46	0.44
Recycle Product Gas, scfm	4.8		6.3		3.8	3.8	3.2	3.0
Outlet Gas, scfm	0.55		1.52		1.03		0.83	
Run Time, hh:mm	53:07		65:42		37:52		28:45	
	Syngas In, FT Product Gas Out							
Composition, mol%	In	Out	In	Out	In	Out	In	Out
H_2	28.3	13.3	13.8	7.1	14.2	7.4	23.4	13.1
CO	15.9	8.3	8.6	4.3	13.1	9.5	14.5	9.8
CO_2	33.0	45.1	20.5	23.2	42.6	43.7	37.5	42.2
CH_4	5.2	8.8	2.1	3.0	1.2	2.7	3.1	4.9
HC	0	1.0	0	0.42	0.35	0.52	0.77	2.1
H_2O	0.13	0.37	0.06	0.30	0.09	0.20	0.15	0.21
N_2	12.7	17.6	53.9	57.7	27.2	32.3	14.9	21.8
Max. H_2S, ppm[1]	0.4	N/A	< 1[2]	N/A	0.9	N/A	0.5	N/A
	CO	H_2	CO	H_2	CO	H_2	CO	H_2
Conversion, %	61	65	54	52	24	50	49	58
STLG	17.5		23.7		31.6		28.3	
CO Conversion, mol·kg-cat^{-1}·hr^{-1}	3.8		3.8		1.5		14.4	
Aqueous Product, g·kg-cat^{-1}·hr^{-1}	72		42		14		24	
Organic Liquid Product, g·kg-cat^{-1}·hr^{-1}	13		4.1		0.86		1.6	
Organic/Aqueous Ratio, g/g	0.18		0.097		0.062		0.066	
Aqueous TOC, mg/L	7880		7950		16,100		25,500	

[1] H_2S as measured by Dräger tube when FT reactor first brought online.
[2] Exact Dräger tube value not recorded at time reactor brought online.

Figure 18 shows GC–MS results for the FT liquids collected in Test FBG002, organized chronologically from top to bottom. Normal paraffin peaks were identified, and all GC peaks between *n*-paraffins were simply grouped by the next-largest *n*-paraffin peak to give an approximate product distribution by chain length. This method is not particularly accurate because many compounds have GC retention times greater than an *n*-paraffin with the same number of carbon atoms, but the method does give consistent relative results and requires significantly less time than manually identifying each GC–MS peak. It should be noted that the peak heights correspond to MS signal strength and do not represent actual concentrations.

One of the more notable features of Figure 18 is the kink on August 27 between 15:00 and 19:30. This kink is the result of a gasifier upset that caused a large amount of N_2 to be introduced to the syngas, and the change in syngas composition had a clear effect on product distribution until the nitrogen was bled out of the recycled syngas. A similar effect on product distribution can be seen in the first and last samples analyzed, when neither the gasifier nor the FT reactor were operating at steady state. As was observed in laboratory testing described in Section 4.1.1.3, syngas dilution did not permanently affect the catalyst activity.

Ignoring the first and last sample analyzed and also the kink on August 27 between 15:00 and 19:30, there are three main features to note in Figure 18. First, the product distribution becomes slightly lighter with time. The peak around *n*-nonane (9 carbons) grows higher as the test progresses, while the heavier peaks grow slightly smaller. Second, this trend is more or less gradual with time, indicating that it is not the result of a sudden change in feed (This is clearer if
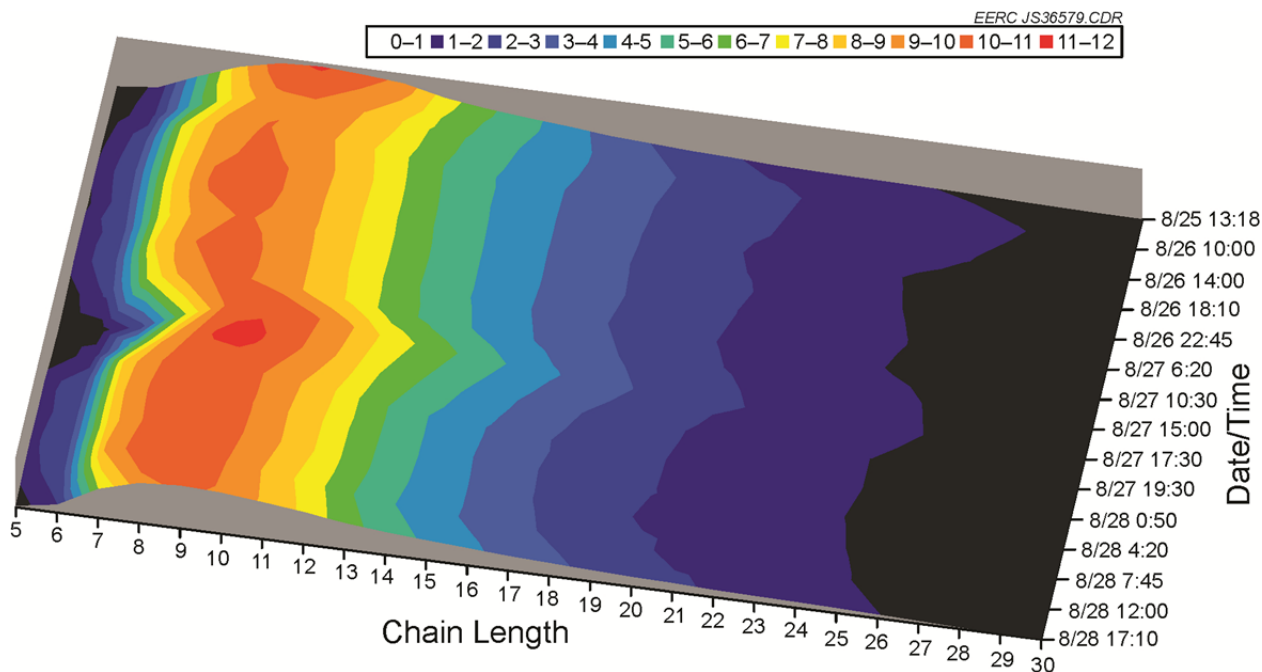
Figure 18. GC–MS analysis of FT product with time for Test FBG002.

the kink on August 27 is removed from the graph, but the revised graph is not shown here in the interest of brevity). These results show that the catalyst was slowly deactivating (producing less wax and more light products) during Test FBG002. They also show that, although the catalyst was deactivating throughout the week, adding 30% biomass to the gasifier feed did not have any significant impact on FT catalyst behavior or product quality.

An initial change in catalyst activity because of induction is common and has been observed with this catalyst in laboratory-scale testing. The slow deactivation observed in Test FBG002 was originally attributed to this induction effect, and at the end of BP1, the deactivation seen in Figure 18 was dismissed as both insignificant and unavoidable. However, as shown in Section 4.1.1.3, this catalyst quickly and permanently deactivated in a laboratory reactor when exposed to unsweetened syngas during BP3. The results of pilot-scale testing with gas sweetening (Section 4.5.2) further suggest that the catalyst deactivation observed in Test FBG002 was significant and was the result of using unsweetened syngas. Based on the catalyst appearance when it was removed from the bed, the most likely cause of deactivation was coking. As seen in Figure 19, gasifier tars (aromatics) were present in the organic liquid product, even fairly early in Test FBG002. These were the suspected cause of coking in laboratory testing. Further discussion and evidence of coking by gasifier tar are provided in sections describing later pilot-scale tests with warm-gas cleanup.

Figure 20 depicts productivities of condensed products with time for Test FBG002. The water productivity decreased slightly over the course of the test, while the productivity of liquid
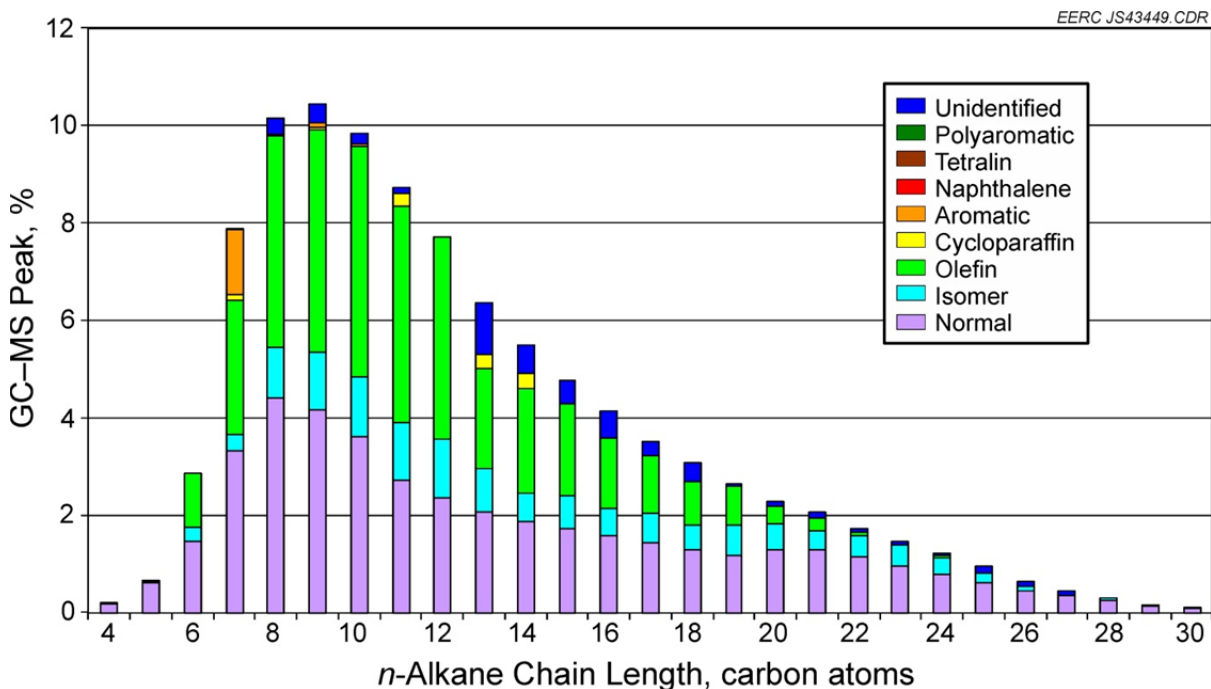
Figure 19. GC–MS peak breakdown for August 26 22:45 FT sample.

hydrocarbons increased slightly. Only a single point is available for wax, as the wax level in the heated wax trap never rose high enough to be drained online. Only 10 g of wax was recovered from the wax trap posttest.

4.5.1.2 Test FBG003

In terms of FT reactor operation, the system performed fairly well during Test FBG003, especially considering that the syngas supply rate was restricted by parallel operation of a thermal oxidizer. Initially, syngas flow to the FT reactor was intermittent and low (similar to operation throughout most of Test FBG002), but flow was successfully increased from an average of less than 1 scfm to a stable flow rate of more than 2 scfm after 13 hours of run time. Conversion of CO and H_2 was initially high at 70% prior to this change but dropped to 50% and remained quite stable thereafter. The reason for the sudden drop in conversion when flow rate was increased was probably that syngas had less residence time on the catalyst surface and thus underwent less reaction per mole of feed. Indeed, although the percent conversion of CO and H_2 dropped when the flow rate increased, the organic liquid production rate more than doubled from 2.1 to 4.8 g·kg-cat^{-1}·hr^{-1} and remained fairly steady until near the end of Test FBG003 (Figure 21).

The FT liquid samples from Test FBG003 were lost before they could be analyzed. Likewise, all water samples were combined and destroyed after TOC analysis, so no further analysis of the FT water by-product could be made. As a result, it is impossible to know for certain what effect the increase in flow rate after 13 hours had on product quality. However, the
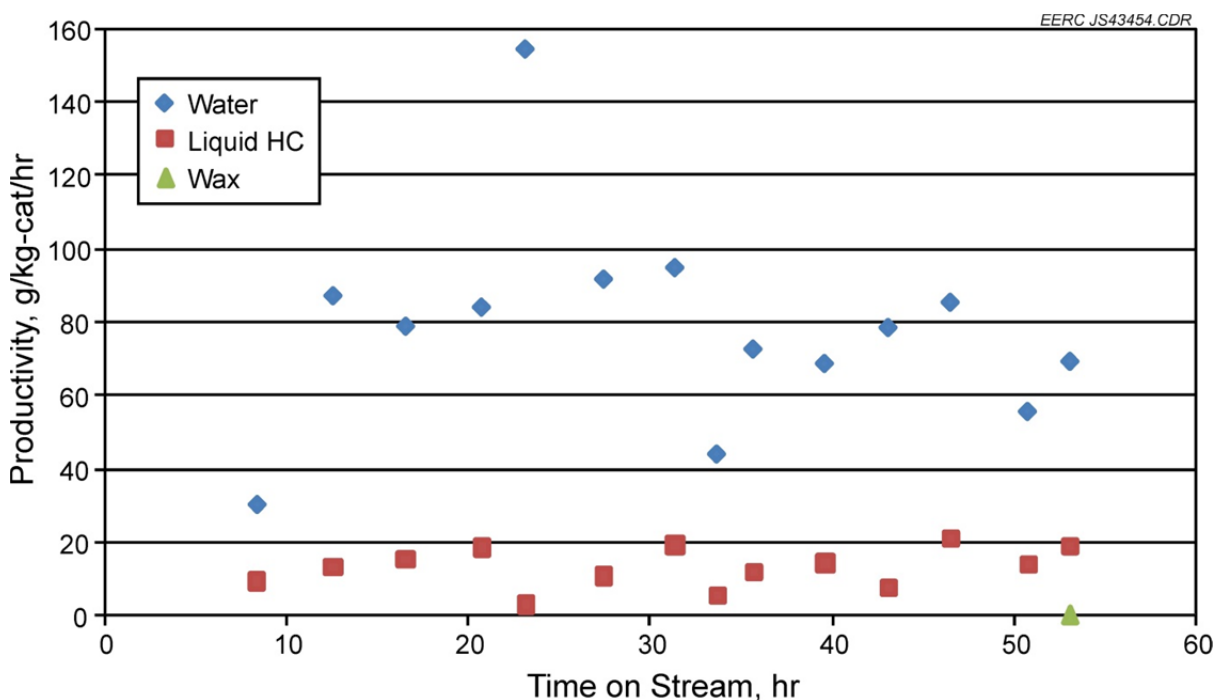
Figure 20. Aqueous, organic liquid, and wax productivities with time for Test FBG002.
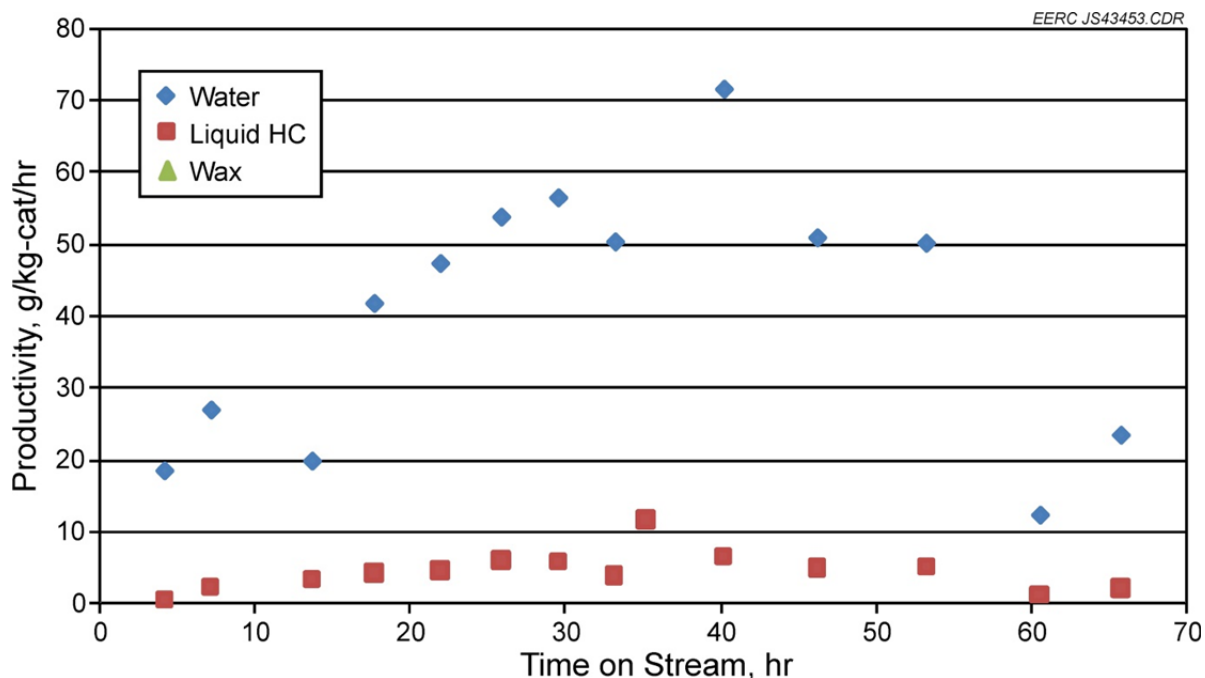
Figure 21. Aqueous, organic liquid, and wax productivities with time for Test FBG003.

STLG appears to have increased slightly after the change, and the ratio of organic to aqueous productivity dropped to less than 0.10 and then held steady. Thus it appears that the higher flow rate resulted in more light gas and lower C_{5+} selectivity. This finding is reasonable, as FT synthesis is based on chain propagation, and pushing product through the reactor at a faster rate offers less time for hydrocarbon chains to grow and results in poorer selectivity (24).

The much lower organic/aqueous product ratio in Test FBG003 as compared to Test FBG002 was probably partially real but also somewhat artificial. Based on long-term trends that will be shown in later sections, the catalyst was probably continuing to deactivate throughout Test FBG003, and this would cause poorer C_{5+} selectivity and a lower organic/aqueous product ratio. However, in Test FBG002, all product was collected into an ice-cooled pot to minimize evaporative losses. This pot was not put on ice in any later tests, so more of the light organic material escaped during product collection. This negatively impacted the organic/aqueous ratio. The loss of light organic product is especially evident from the GC–MS results given in the next two sections.

4.5.1.3 Test FBG004

FT reactor operation was extremely erratic during Test FBG004 because of the lower ambient air temperature, as discussed in Section 4.3.3. Tars from the gasifier condensed not only in the exposed syngas lines but also in the FT reactor inlet regulator and flowmeters, forcing operators to shut down the FT system several times during the week so that these instruments could be removed and cleaned with acetone. The FT system was intentionally taken off-line and restarted five times during 4 days of operation, not including numerous times during which inlet

54

flow was lost because of plugging. Heat trace was successfully applied to the FT inlet lines and instruments after 24 hours (only 15 hours of syngas exposure to the FT catalyst), but continued problems with the gasifier itself prevented stable operation until after 28 hours of syngas exposure. The gasifier was shut down on the same day, after only 38 hours of total syngas exposure, because a cyclone plug stopped gas flow out of the gasifier. While the total actual time elapsed between the start of testing and shutdown was 64 hours, very little FT steady-state data are available for Test FBG004, and the information in Table 19 represents the weighted average of a wide range of non-steady-state values.

During the brief 10-hour period of stable operation on the final day of testing, STLG averaged 30%–40% and appeared to be increasing toward 50% before the system was finally shut down. CO and H_2 conversion were both trending downward during this 10-hour period. In previous tests, STLG had not averaged much more than 20%, and CO conversion had more closely matched H_2 conversion and averaged 50% or more. Moreover, STLG and conversion were fairly stable over the course of an entire week in previous tests, so it is remarkable to see both values degrading in a 10-hour period in Test FBG004.

In addition to the indications of very rapid catalyst deactivation given by STLG and conversion, it is also remarkable that the aqueous production rate trended strongly upward with time on stream from 17 to 67 g/hr in Test FBG004, as seen in Figure 22. By contrast, the liquid organic production rate remained fairly constant during most of Test FBG004 but did improve during the 10-hour window of steady operation prior to shutdown. In no other tests did water or liquid production rates trend upward over the course of the week.

One major difference between Test FBG004 and previous tests was that both FT beds were utilized with the expectation that the fresh catalyst in the second bed would give better conversion. Assuming that the catalyst in the second bed was no less active than the catalyst in the first bed at the start of Test FBG002, the FT catalyst must have undergone significant deactivation during Test FBG004. As will be shown in the discussion on Test FBG005, long-term GC–MS trends suggest that the fresh catalyst was initially more active but then rapidly deactivated during Test FBG004. During the 10-hour steady-state period near the end of testing, temperature, pressure, and flow rates were similar to those in Test FBG002 (when CO conversion was over 60% and STLG was around 18%), and yet the catalyst performance did not recover.

Other than the use of the second reactor bed and the intermittent operation, the next major difference between Tests FBG002 and FBG004 was the syngas quality. H_2 and CO both held fairly constant at 15%–18% during the 10 hours of steady-state operation on October 8. CO_2 in the syngas reached 47% during this period, and CO_2 in the recycled product gas increased to more than 53%. As is clear from Table 19, average syngas CO_2 was higher in Test FBG004 than in any other test. High partial pressure of CO_2 was shown to have a detrimental effect on iron-based FT catalysts in laboratory testing (Section 4.1.1.3) and is the most reasonable explanation for poor catalyst performance observed in Test FBG004. The high and increasing level of CO_2 also partly explains why water production increased over time. CO_2 inhibits the WGS reaction, which means less FT product water can be converted to H_2.
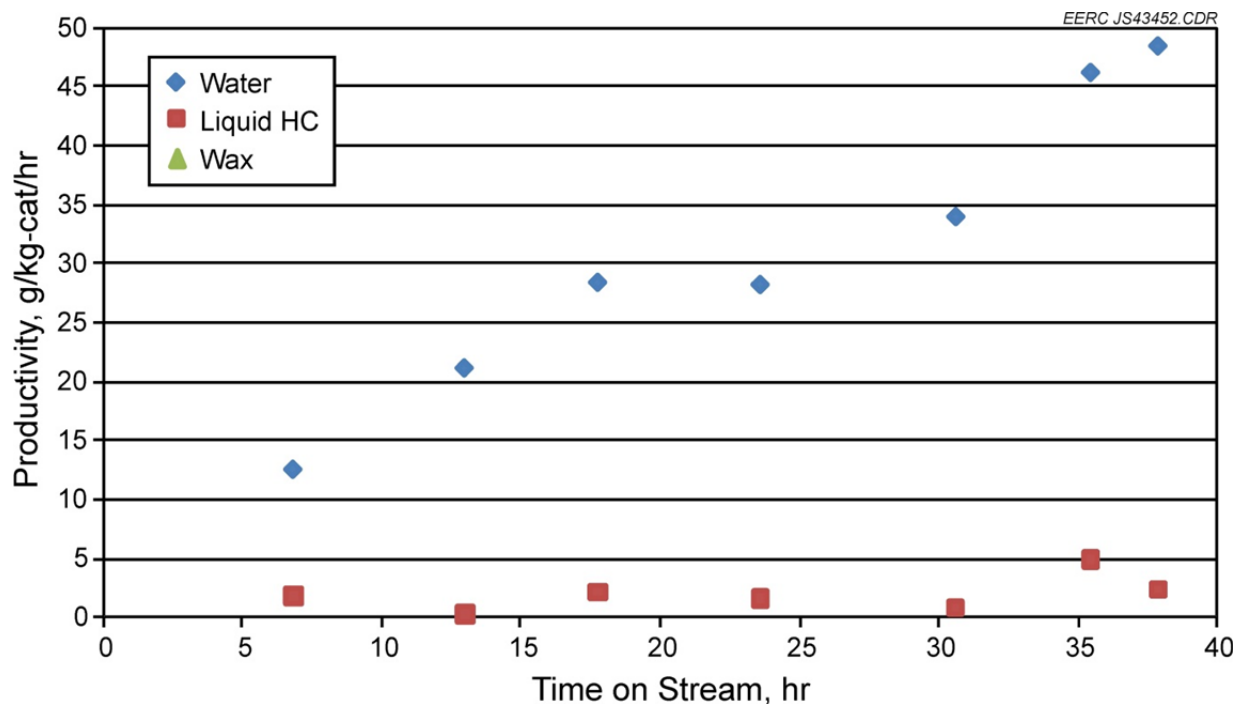
Figure 22. Aqueous, organic liquid, and wax productivities with time for Test FBG004.

Another major difference between FBG004 and earlier tests is that more gasifier tars seem to have been generated from lignite than from PRB. These may have also contributed to catalyst deactivation. As discussed in Section 4.1.1.3, high CO_2 concentrations in simulated syngas had a negative impact on iron-based FT catalyst in the laboratory but did not seem to cause rapid deactivation. Use of actual syngas, however, did rapidly and permanently deactivate FT catalyst in the laboratory reactor, most likely by coking.

Figure 23 gives GC–MS analysis results with time for the FT product collected during Test FBG004. One odd feature that is immediately apparent when comparing Figures 18 and 23 is the loss of most of the product lighter than *n*-nonane (C9), causing the main peak to shift toward the heavier range in Test FBG004. This observation completely contradicts every other trend discussed so far, as it would suggest that STLG was lower and that C_{5+} selectivity was higher in Test FBG004 than in Test FBG002. The most likely explanation for the loss of light material is that product was collected into an ice-cooled pot during Test FBG002 but was collected at room temperature thereafter. The higher temperature in the collection pot, which is held at a slight vacuum, probably allowed more of the light product to vaporize before it could be recovered as liquid. For this reason, the organic/aqueous product ratio for Test FBG002, shown in Table 19 and Figure 20, cannot be compared to the organic/aqueous ratio for any later tests, as more of the organic liquid was almost certainly lost.
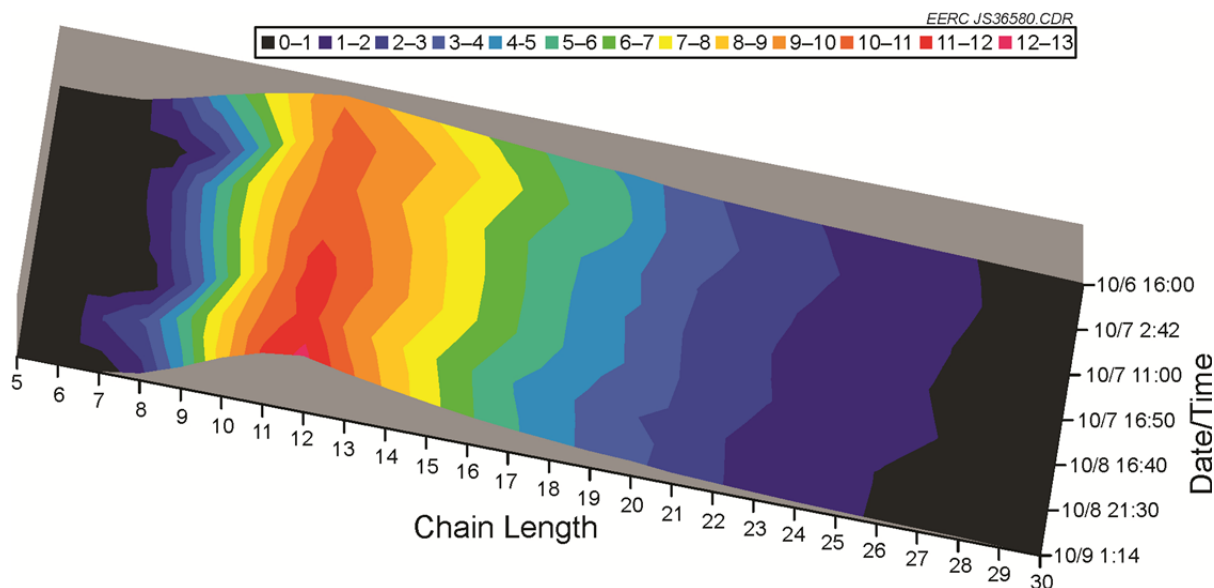
Figure 23. GC–MS analysis of FT product with time for Test FBG004.

Ignoring the loss of material lighter than nonane, the GC–MS trend for Test FBG004 shows a distinct change in product quality over time, with less wax formation and more light product formation. The trend is fairly continuous over time and does not occur in a discrete step, indicating that it is a result of general process conditions rather than of changing gasifier feed from coal to biomass. Although a gradual increase in light product formation was observed in Test FBG002, the rate of change is much more pronounced in Test FBG004, indicating a greater degree of catalyst deactivation over time than observed in earlier testing. The likely reason is poor syngas quality, as discussed previously. Not only was the syngas quality generally poor, but prior to the steady-state period on October 8, the FT reactor itself was often idling hot with only product gas recycling through the reactor because of intermittent losses in fresh syngas flow. Recycling the product gas without introducing fresh syngas caused CO_2, light gasifier tar, FT product water, and other undesirable components to concentrate in the FT product gas, and this probably caused the catalyst to deactivate at an advanced rate.

Figure 24 is a GC–MS analysis of FT product drained before the 10-hour steady-state period. Unlike the Test FBG002 sample shown in Figure 19, the sample from Test FBG004 contained detectable naphthalene, tetralin, and cycloparaffin but comparatively little benzene or other single-ring aromatic compounds. This suggests that lignite generated more naphthalene than did PRB coal when gasified in the HPFBG. The percentage of GC–MS peak area that could not be identified was also higher in the sample from Test FBG004 than in the one from Test FBG002. While these compounds could not be positively identified, their RIs do not suggest that they are typical FT products.

57
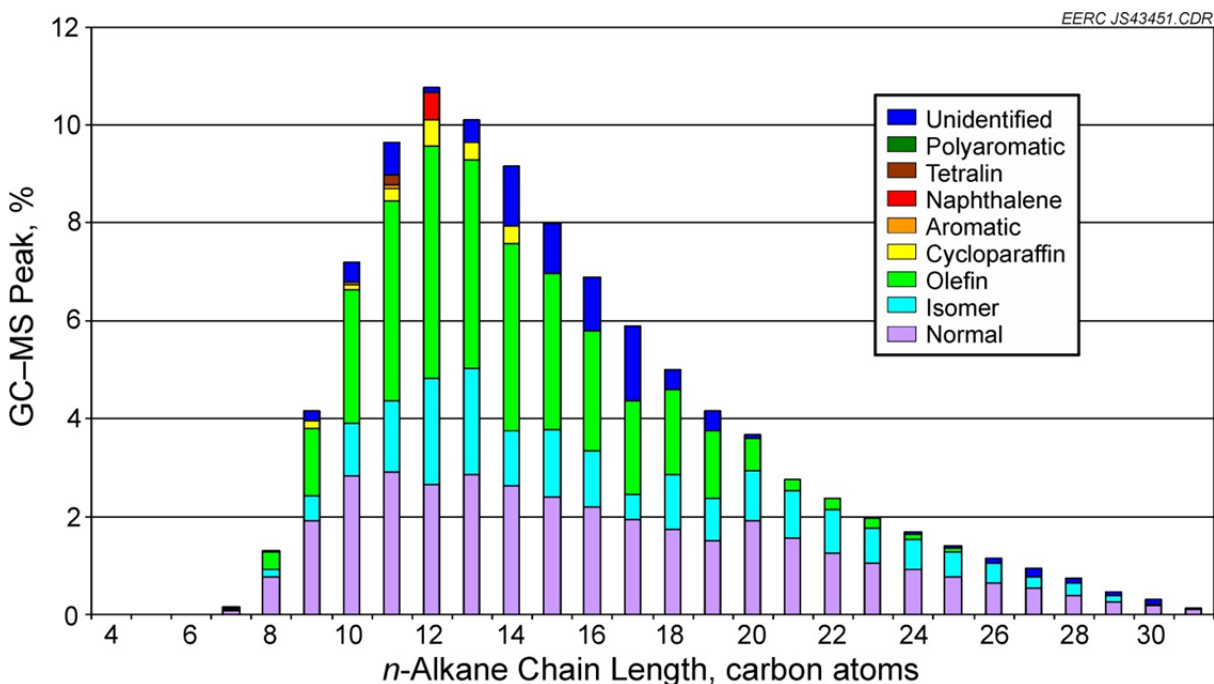
Figure 24. GC–MS peak breakdown for October 7, 16:40 FT sample.

4.5.1.4   Test FBG005

Prior to Test FBG005, it was not yet suspected that the catalyst had coked. The deactivation observed in FBG004 was thought to be oxidation caused by high levels of CO_2 and FT product water. CO was passed over both FT catalyst beds in the hope of regenerating oxidized catalyst, as this was the method used to dry and calcine the catalyst when it was first loaded prior to Test FBG002. As had been observed in the initial activation, CO_2 evolved as oxygen from the catalyst surface reacted with CO in the feed. CO flow was maintained as before until the CO_2 concentration dropped to around 1%, indicating that most of the moisture and oxygen had been removed from the catalyst surface.

Although the FT reactor was taken off-line for around 13 hours during Test FBG005 because of a gasifier upset, the system was much more stable than in Test FBG004, as heat trace was used to prevent tar and water condensation in exposed lines and fittings. Flow was still somewhat intermittent because of the cold weather (Figure 13), but overall, operation was fairly stable.

As shown in Table 19, syngas and recycle flow rates were kept lower during Test FBG005 than in any earlier test. The syngas composition was relatively similar to that of Test FBG002, with less than 40% CO_2 during most of the test and a H_2/CO ratio of 1.6:1. The syngas quality was substantially better than in Test FBG003, when the syngas had more than 50% nitrogen dilution, H_2 exceeded 15% for only 2 hours, and CO never exceeded 10%. All of these factors suggested that catalyst performance should have been better than in Test FBG003 and nearly as good as in Test FBG002.

However, CO conversion averaged only 49% and H_2 conversion 58%, which was similar to Test FBG003 despite the higher concentration of reactants and the longer residence times. STLG was nearly as bad as in Test FBG004, and the organic/aqueous ratio was not significantly different than in Test FBG004. CO conversion per unit catalyst was also not much better than in Test FBG004 at 2.3 mol·kg-cat^{-1}·hr^{-1}.

The concentration of *n*-alkane may also be taken as an indicator of catalyst activity, since more active catalysts may tend to saturate olefins and oxygenates. As shown in Figure 25, the trend for *n*-alkane content organic liquid product in Test FBG005 appears to be a continuation of Test FBG004 (recall that no GC–MS data were available for Test FBG003, which explains the wide gap, and that a new catalyst bed was brought online in Test FBG004, which explains why *n*-alkane content was initially higher than at the end of FBG002). These facts all demonstrate that the attempt to regenerate catalyst under CO between Tests FBG004 and FBG005 was largely unsuccessful.

Figure 26 further confirms that the FT product was not greatly improved by catalyst reduction under CO. As with Tests FBG003 and FBG004, product was collected at room temperature in Test FBG005, so most light product was lost during product collection. The product from Test FBG005 does not appear to be as consistent with the product from previous tests. Much of this is caused by the presence of aromatics in the FT liquids, as seen in Figure 27 for the December 2 16:00 sample. The benzene peak at C_7 is minor or nonexistent in most other samples analyzed, and benzene is not a typical FT product, indicating that it is probably
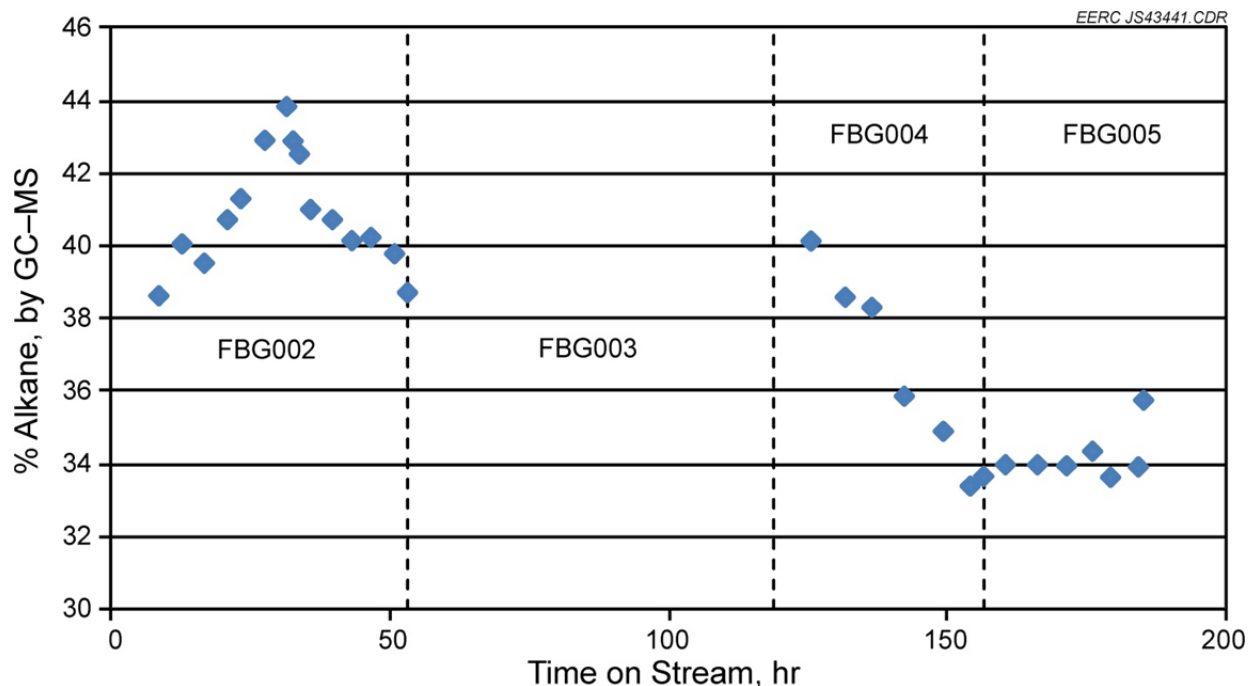
Figure 25. Alkane content of organic FT liquid with total time on stream.
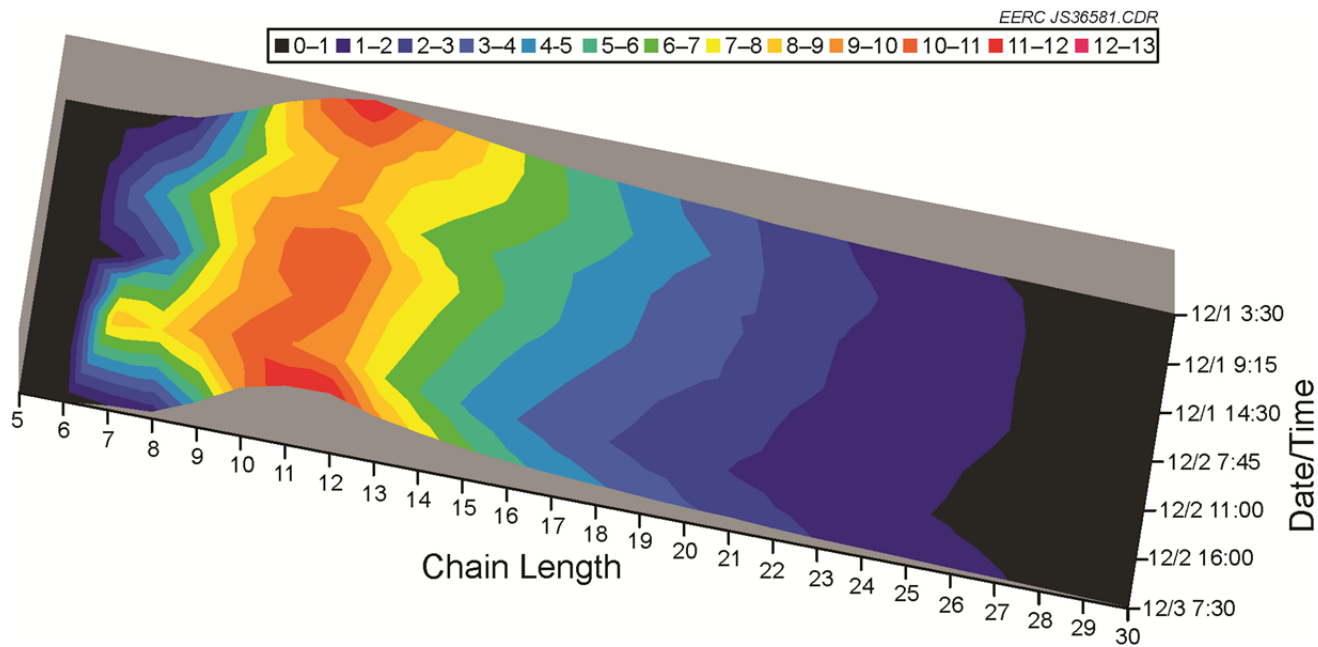
Figure 26. GC–MS analysis of FT product with time for Test FBG005.
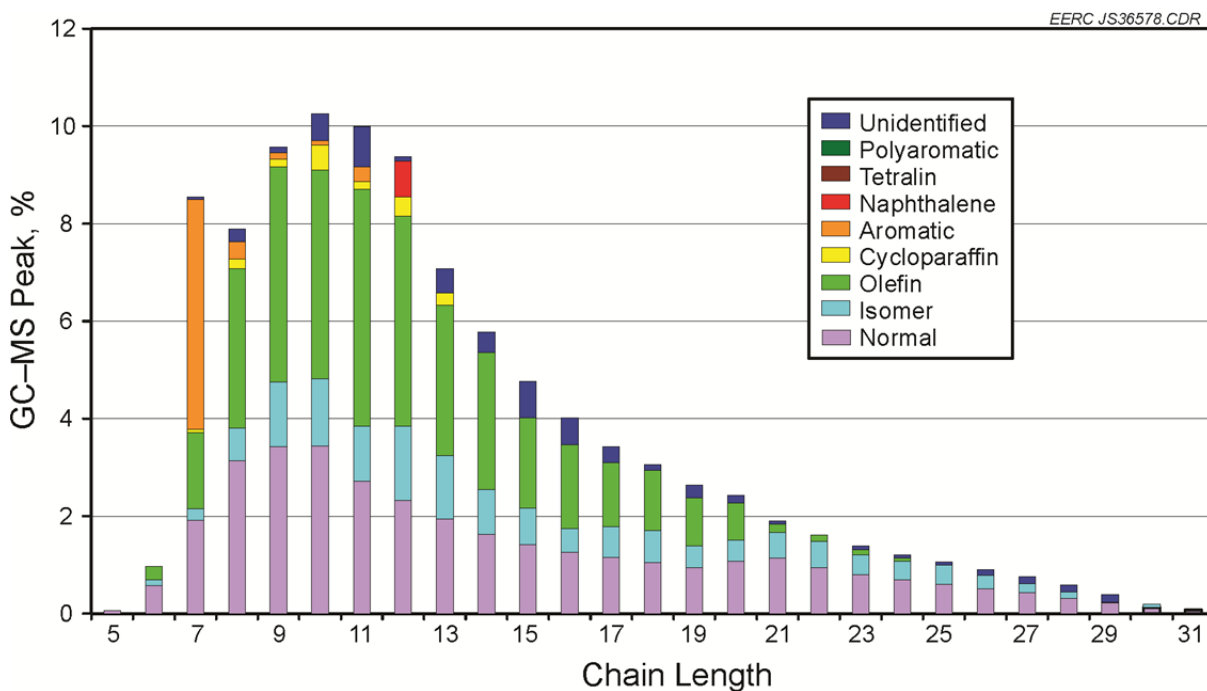
Figure 27. GC–MS peak breakdown for December 2 16:00 FT sample.

contamination from the gasifier. (It should be noted that benzene is a C_6 molecule, not a C_7 molecule. As explained in Section 4.5.1.1, all GC–MS peaks except *n*-paraffins were grouped with the next largest *n*-paraffin peak in the GC–MS response. Benzene appears between hexane and heptanes in the GC–MS, so it is counted as a C_7 molecule.) The high benzene content in this sample is responsible for the odd kink in Figure 26. Interestingly, this sample was the steady-state product drained after feeding 100% DDGS to the gasifier. This is the one indication during BP1 that biomass had any impact on FT catalyst performance.

The reason so much tar reached the FT product when feeding 100% DDGS during Test FBG005 is likely that the sample lines were heated. In earlier tests, the lines to the FT reactor were not heated, and any aromatic-rich tars that escaped from the gasifier quench pots were condensed before reaching the FT system. After the poor system operation observed in Test FBG004 as a result of cold weather and higher tar content in lignite-derived syngas, the inlet lines were wrapped in heat tape. Heating prevented the inlet regulator and rotameters from becoming plugged, but it also allowed tars escaping from the gasifier quench system to remain in a vapor state and reach the FT reactor with the syngas.

Except for samples contaminated with high levels of gasification tar, the general product distribution in Figure 26 shows a fairly strong similarity to that shown in Figure 23. It should be noted that the naphthalene peak observed in Figure 24 is still present in Figure 27. The TOC of the aqueous phase was relatively large at 25,500 mg/L, continuing the trend of increasing TOC observed in FBG004. Davis and coworkers have reported that alcohol production over iron-based catalysts increases with aging and loss of CO conversion (22). Figure 28 gives the trends in productivity with time, showing that organic productivity was never much better than in Test FBG004, while aqueous productivity was somewhat higher. The high aqueous productivity suggests that the catalyst's WGS activity did not improve in Test FBG005 despite the better quality of syngas compared with Test FBG004. Along with the conversion, STLG, and organic/aqueous ratio, these similarities in the liquid products further indicate that the attempt to regenerate catalyst between tests was unsuccessful. Because CO_2 was evolved during the regeneration attempt, it is clear that passing hot CO over the catalyst helped to remove oxygen from the catalyst surface. Since the catalyst activity did not recover, it is probable that catalyst deactivation was caused by more than simple oxidation.

The most probable explanation is coking caused by exposure to high levels of gasifier tar. The rate of deactivation by coking seems somewhat high, but given how quickly the gasifier and FT reactor lines tended to plug with tar, it is obvious that there was significant tar present in the syngas. Light tar from the gasifier was dramatically present in the product from Test FBG005, but lower concentrations of aromatic and cycloparaffinic compounds were also observed in the FT product from earlier tests. Syngas containing an appreciable aromatic content could lead to deactivation by coking. Laboratory tests in BP3 showed that unsweetened syngas caused rapid catalyst deactivation and extensive coking (Section 4.1.1.3). When the pilot-scale reactor beds were opened and drained after BP1, the catalyst appeared to have a fair amount of coke present. Catalyst in the first bed (which had seen the most syngas) would not drain from the reactor under gravity and had to be broken free by prodding with a rod while banging on the reactor wall. The
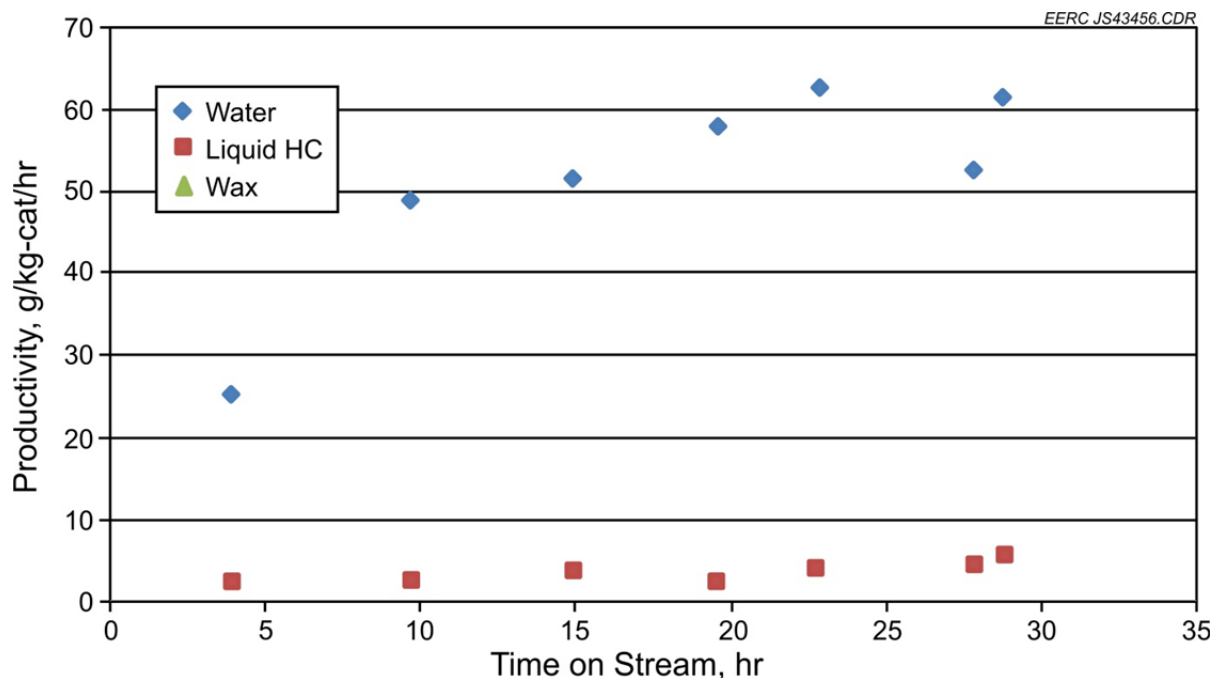
Figure 28. Aqueous, organic liquid, and wax productivities with time for Test FBG005.

catalyst particles were likely stuck together with coke or other residue. Coking might have been partially undone had the catalyst been fully oxidized under dilute air before being reduced under CO. However, given how rapidly the deactivation occurred both in the laboratory and in the pilot-scale reactor, the preferable solution would be to minimize the tar content of the syngas by using either gas sweetening or a high-temperature gasifier.

Aside from coking, one other possible candidate for catalyst deactivation is sulfur poisoning. Sulfur poisoning is known to deactivate iron-based FT catalysts, but there is good reason to believe that sulfur poisoning was not significant in BP1. The FT reactor uses a packed-bed design, so sulfur would tend to be captured in the top of the beds and would not have a noticeable impact on catalyst performance until the bed inlet was so saturated that sulfur could penetrate deep into the catalyst bed. Because H_2S was kept to less than 1 ppmv (being detected only at the ppb range by GC–PFPD) during all testing, it does not seem likely that sulfidation should have penetrated deep into the beds by the third week of testing, especially given that the second bed contained fresh catalyst at this point. Later, in BP3, catalyst would be intentionally exposed to high levels of H_2S without any immediate impact on catalyst performance. This observation further suggests that sulfur poisoning was not the major cause of catalyst deactivation during BP1.

4.5.2   Gas Sweetening (BP3)

In the laboratory-scale reactor used for catalyst testing, catalyst always had to be diluted with glass beads to control heat release (Section 3.1.1). Experience with warm-gas cleanup had shown that Dowtherm could easily remove all process heat from the pilot-scale FT reactor

without diluting catalyst. Laboratory testing of the aged batch of catalyst used in BP3 had shown that this catalyst was less active than fresh catalyst (Test FTR44 in Section 4.1.1.3), meaning that less heat would be generated and temperature control would be less of an issue at similar operating conditions. The aged catalyst was thus loaded into the pilot-scale FT reactor undiluted as had been done in BP1 with warm-gas cleanup.

Despite the lower inherent activity of the aged batch of catalyst, temperature control in the pilot-scale FT reactor was much more of an issue in BP3 than in BP1. Figure 29 superimposes the temperature profiles through the catalyst bed in each of the pilot-scale tests. The temperature profile was quite flat in all of the tests using warm-gas cleanup. In Test FBG021, the temperature peaked notably at the half-way point of the bed, and the inlet temperature had to be kept low to prevent exothermal runaway. Dowtherm heat removal was clearly insufficient to adequately control temperature with gas sweetening.

The catalyst not only reacted more exothermally in Test FBG021, but it also generated more and better product than in any of the pilot-scale tests using only warm-gas cleanup. Table 20 compares catalyst performance in Test FBG021 to performance in earlier tests. As can be seen, the CO conversion was higher than in any pilot-scale test using warm-gas cleanup, both on an absolute basis and on a per-unit-catalyst basis. The productivity of condensable organics was also significantly higher with gas sweetening in Test FBG021, as was the ratio of condensed organics to condensed water. Net water production is reduced by the WGS reaction over iron-
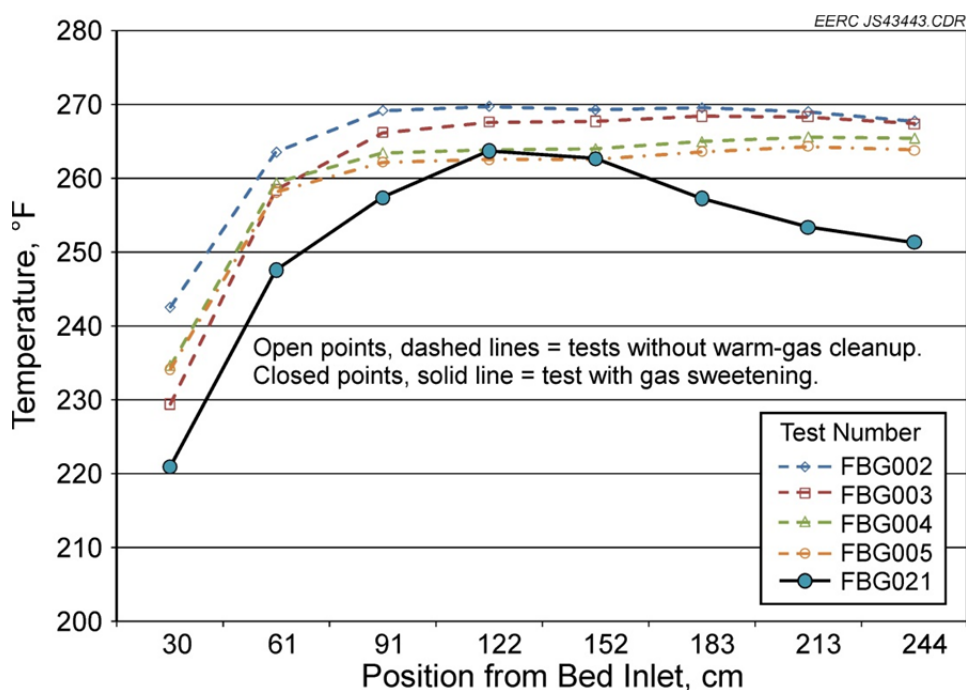
Figure 29. Temperature profile through FT catalyst bed in each of the pilot-scale tests.

Table 20. FT Catalyst Performance in Each of the Pilot-Scale Tests

Test ID:	FBG002	FBG003	FBG004	FBG005	FBG021
Cumulative Hours of Exposure	53	118	156	185	74
CO Feed, $mol \cdot kg\text{-}cat^{-1} \cdot hr^{-1}$	6.2	7.1	3.9	4.3	17.7
Recycle/Syngas Ratio, scc/scc	6.3	3.9	6.2	5.1	3.9
GHSV, $sL \cdot kg\text{-}cat^{-1} \cdot hr^{-1}$	6.3	9.0	4.8	4.1	5.9
Average Bed Temp., °C	266	262	260	259	252
Pressure, bar	18.9	29.4	23.6	21.7	21.7
CO in Fresh Feed, mol%	15.9	8.6	13.1	14.5	32.7
H_2 in Fresh Feed, mol%	28.3	13.8	14.2	23.4	50.1
CO_2 in Fresh Feed, mol%	33.0	20.5	42.6	37.5	1.7
CO Conversion, %	62	53	39	54	82
CO Conversion, $mol \cdot kg\text{-}cat^{-1} \cdot hr^{-1}$	3.8	3.8	1.5	2.3	14.4
Aqueous Productivity, $g \cdot kg\text{-}cat^{-1} \cdot hr^{-1}$	72	42	14	24	104
Liquid Organic Productivity, $g \cdot kg\text{-}cat^{-1} \cdot hr^{-1}$	13	4.1	0.86	1.6	35
Wax Productivity, $g \cdot kg\text{-}cat^{-1} \cdot hr^{-1}$	0.07	0	0	0	9.4
Organic Fraction, g/g water + organic	15%	9%	6%	6%	34%

based catalysts, so the higher organic/aqueous ratio suggests that WGS activity was higher with gas sweetening than without. The higher organic/aqueous ratio may also result from better C_{5+} selectivity, since only C_{5+} hydrocarbons will tend to condense with water in the quench pots. High C_{5+} selectivity is reflected by the high wax productivity in test Test FBG021 compared to other pilot-scale FT tests.

Figure 30 shows the Test FBG021 organic product distribution with time as determined by GC–MS. The product distribution was much more consistent than in any of the previous pilot-scale tests, indicating a much lower rate of catalyst deactivation. The product is lighter on average than the product collected in Test FBG004 or FBG005, which is to be expected because those products were collected at room temperature while this was collected into an ice-cooled pot to minimize evaporation. The product also appears somewhat lighter on average than the product from Test FBG002, when product was also collected on ice (Figure 18). The reason for the lighter product distribution compared to Test FBG002 is not clear, especially since the higher wax productivity and organic/aqueous ratio suggested that product should be heavier in Test FBG021. One possible explanation is that the ambient temperature was colder in Test FBG021 than in Test FBG002. This might have prevented light organics from vaporizing after collection. Another possible explanation is that the GC–MS instrument and its method were modified in the 2 years between these tests, allowing better resolution of light hydrocarbons.
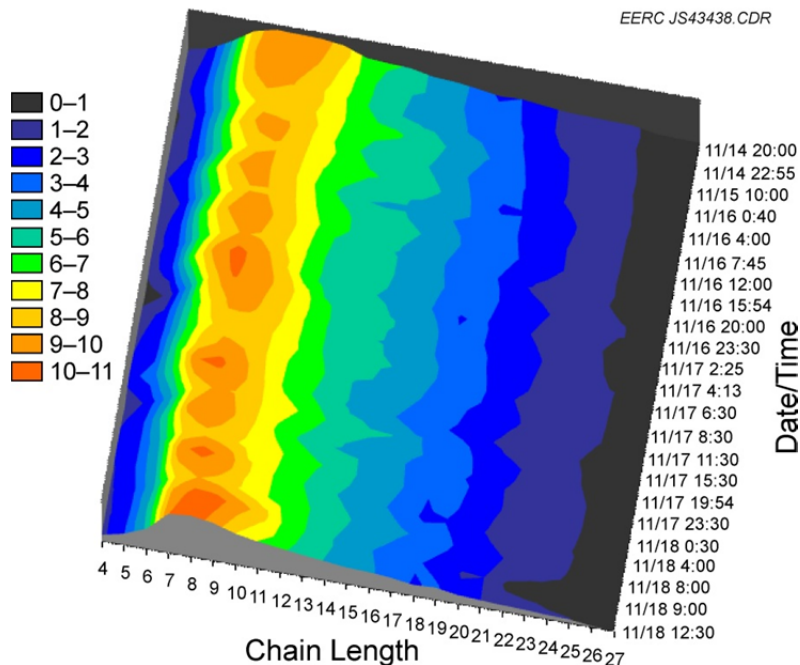
Figure 30. GC–MS analysis of FT product with time for Test FBG021.

Another notable difference between Test FBG021 and previous tests is that there is no material heavier than heptacosadecane (C_{27+}) in the liquid product of Test FBG021. This is probably because of the higher wax productivity. Wax that was collected from the quench pots partially melted at room temperature. At colder temperatures in the quench pots, the wax likely coprecipitated some C_{27+} hydrocarbons that would otherwise have remained in a liquid state. The difference may also be simply that the GC–MS instrument was modified in the 2-year period between Tests FBG005 and FBG021, perhaps giving poorer resolution of heavy hydrocarbons.

Figure 31 depicts productivity with time for all of the condensed phases. The aqueous productivity decreased over time, while the hydrocarbon productivity increased. This is similar to the trends observed with warm-gas cleanup in Test FBG002 (Figure 20), when catalyst was first exposed to syngas, except that the productivities of liquid hydrocarbon and wax were much higher. The fact that both sets of data show the same trend suggests that this may be the result of catalyst induction. Figure 32 gives the same trends for all tests superimposed, with the results from each warm-gas test in BP1 combined to give long-term noncontinuous trends in catalyst productivity. The water productivity clearly continued to decline with time with warm-gas cleanup, but the liquid hydrocarbon productivity also declined substantially with time.

Figure 33 gives the breakdown of individual GC–MS signal peaks for a representative sample from Test FBG021. There is almost no aromatic material present in the sample from Test FBG021. Also, more of the product is saturated *n*-paraffins. Higher saturation probably results from higher H_2 concentration, while the lower aromatic content results from less tar carryover from the gasifier. There are still some GC–MS peaks identified as cycloparaffins, and

65
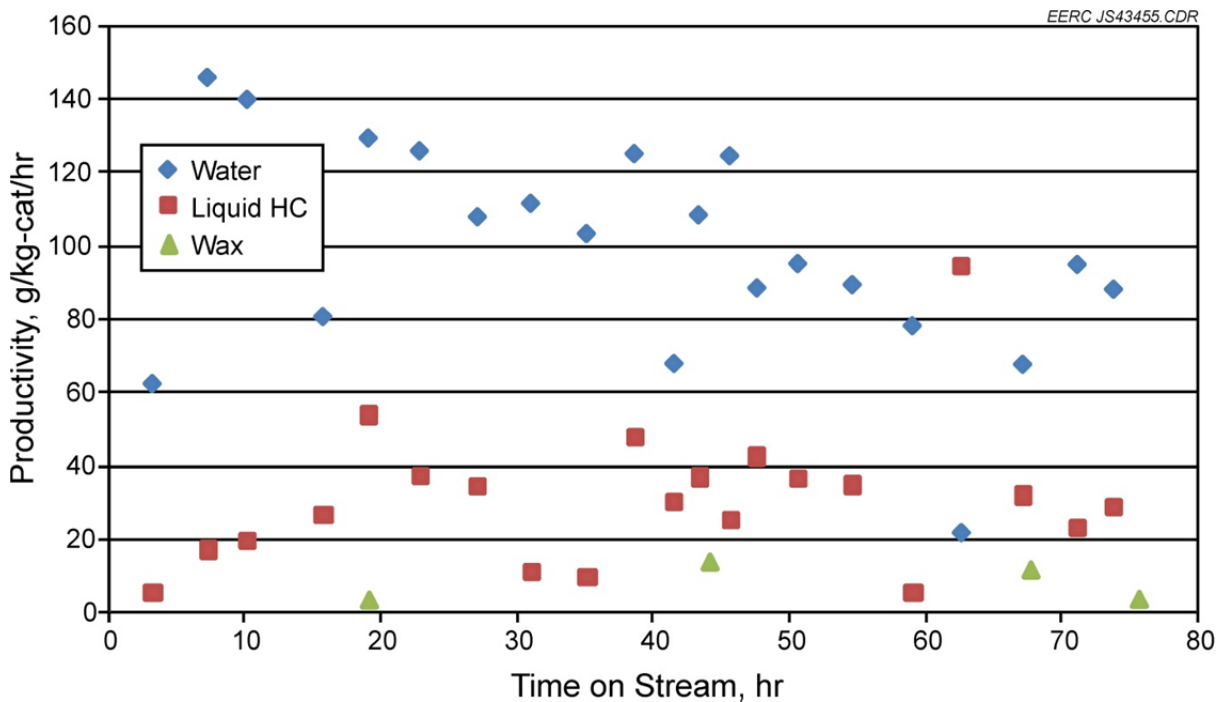
Figure 31. Aqueous, organic liquid, and wax productivities with time for Test FBG021.
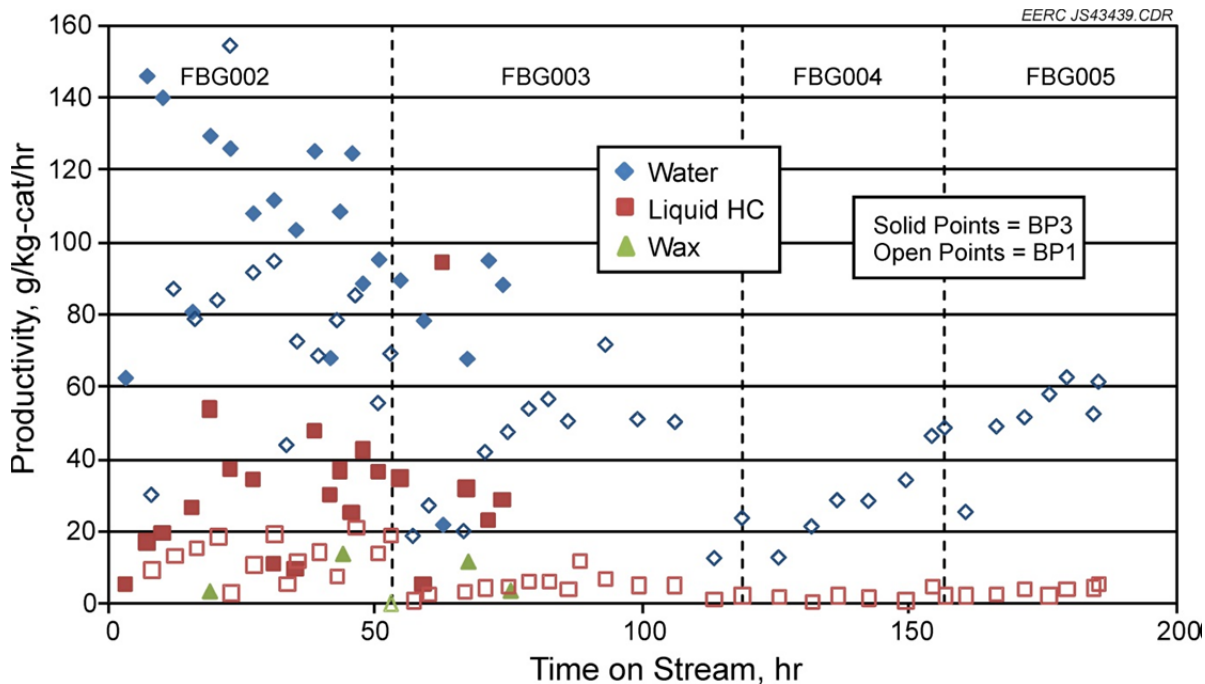
Figure 32. Aqueous, organic liquid, and wax productivities with time for all tests.

EERC JS43450.CDR
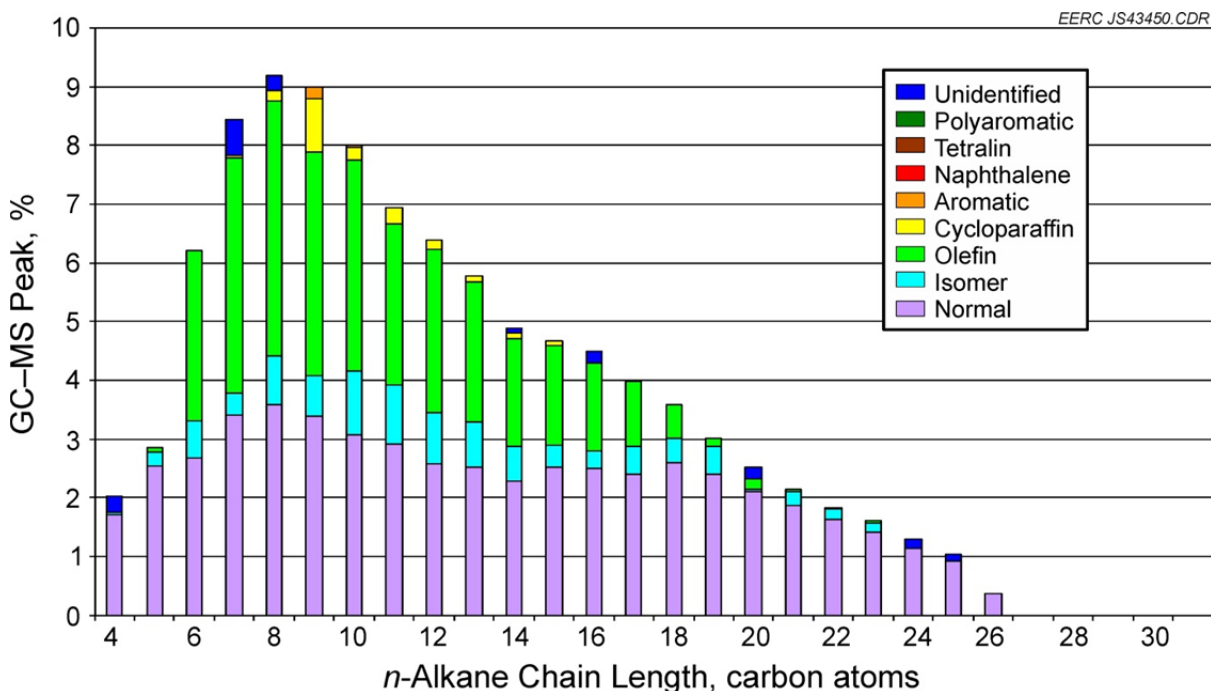
Figure 33. GC–MS peak breakdown for November 17 11:30 FT sample.

there is also some material that was not identified by the GC–MS as belonging to one of the class of compounds in the legend. However, the Kovats RI for some of the unknown peaks suggested that they were alcohols, which are a normal FT by-product (Equation 3, Section 1.0). Further examination of the unknown peaks verified that some of them were, in fact, alcohols and other oxygenates.

The TOC of the aqueous fraction in Test FBG021 was substantially higher than in any test with warm-gas cleanup, so several water samples were further analyzed by HPLC to determine the relative amounts of different oxygenates present in the aqueous phase as well as to see if the distribution changed much over time. Table 21 compares average alcohol concentrations from the various pilot-scale tests. As explained in Section 3.3.1, TOC measurements were low because

Table 21. Comparison of Alcohol Content and Aqueous TOC in Pilot-Scale FT Tests

Test ID	FBG002	FBG003	FBG004	FBG005	FBG021
Cumulative Hours of Syngas Exposure	53	118	156	185	74
Aqueous Concentration, wt%					
Methanol	NA[1]	NA	0.8	1.8	2.2
Ethanol	NA	NA	1.5	3.0	2.5
1-Propanol	NA	NA	0.4	1.1	0.8
1-Butanol	NA	NA	0.1	0.3	0.6
TOC, mg/L	7880	7950	16,100	25,500	32,900

[1] Not analyzed.

67

light organics were vaporized in a vacuum before analysis. As can be seen, the relative distribution of aqueous alcohols was not much different with gas sweetening than with only warm-gas cleanup, but cleanup did affect the total amount of alcohol generated. TOC and total aqueous alcohol content increased with time on stream in Tests FBG002 through FBG005, which has been reported to be associated with catalyst deactivation (22). TOC and alcohol content held fairly steady in Test FBG021, as seen in Figure 34, with only slight decrease over time.

While appreciable alcohol began to appear in the aqueous phase in Tests FBG004 and FBG005, no alcohols were ever positively identified in the organic phase with warm-gas cleanup. Alcohols were readily identified by GC–MS in the organic liquid product from Test FBG021. While the alcohol content and TOC held fairly steady over time in the aqueous phase of Test FBG021, the total alcohol content identified in the organic phase decreased substantially (Figure 35). The distribution of alcohols also changed slightly, with the GC–MS peak for 1-pentanol replacing 1-propanol as the predominant organic-phase alcohol over time.

Note that as the alcohol content of the organic phase dropped off, the aqueous productivity also dropped, and the organic productivity trended upward (Figures 31 and 35). Although the shape of the organic liquid FT product distribution in Figure 30 did not change, the product composition did become more saturated (Figure 36). These observations all suggest that WGS activity increased with time. Early in Test FBG021, selectivity to CO_2 was negligible at about 7%–10%, as seen in Figure 37. Over time, the CO_2 selectivity rose to almost 20%. CO_2 is
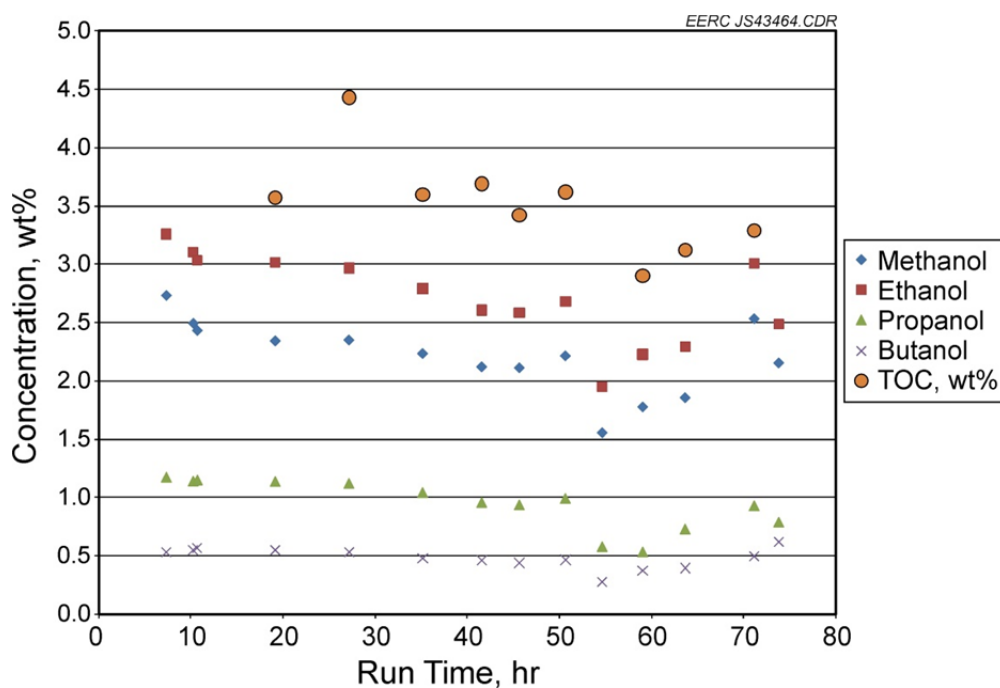
Figure 34. Alcohol concentration and TOC of FT aqueous phase with time for Test FBG021.
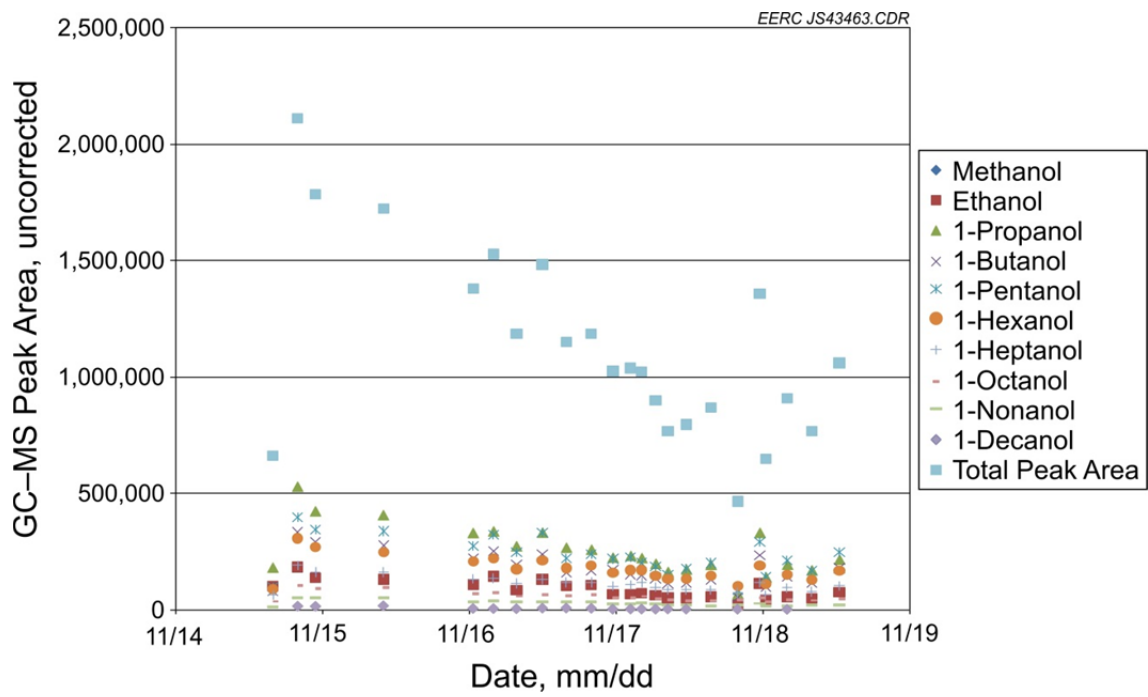
Figure 35. Uncorrected GC–MS peak areas for primary alcohols in organic phase for Test FBG021.
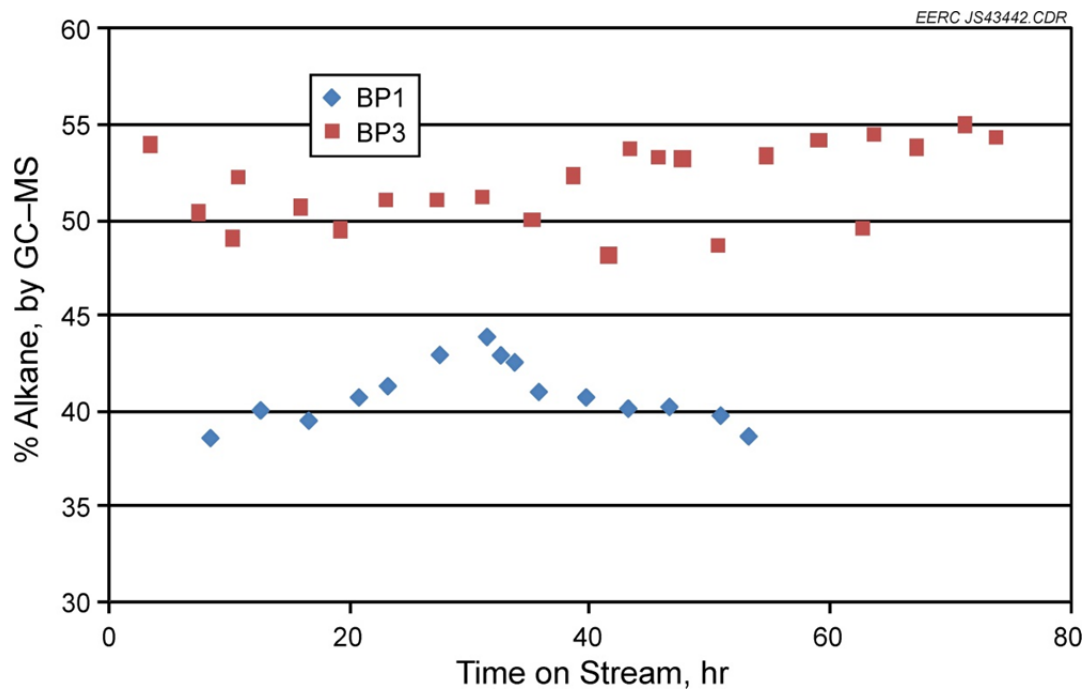
Figure 36. Alkane content of FT organic liquids in Tests FBG002 (BP1) and FBG021 (BP3).

produced by the WGS reaction, and a higher CO_2 selectivity indicates that more FT product water is being converted to H_2 and CO_2. This would leave less water in the condensed product and would generate more H_2 to saturate olefins and alcohols.

4.5.3   FT Product Hydrotreatment

4.5.3.1   HDO

While heating the batch reactor for the initial HDO step, the reactor pressure began to climb more rapidly than expected. This is unusual for HDO, but it probably indicated that some of the light organics in the FT product were vaporizing to boost pressure. Typical HDO feeds contain much less light organic material. When the reactor was cooled to room temperature, pressure dropped rapidly to 845 psig, which would be expected as vaporized material condensed and caused the pressure to drop.

The product after the initial HDO treatment was clear and light yellow with a gasoline-like odor. GC–MS analysis showed no change from the starting material, so the HDO treatment was repeated.
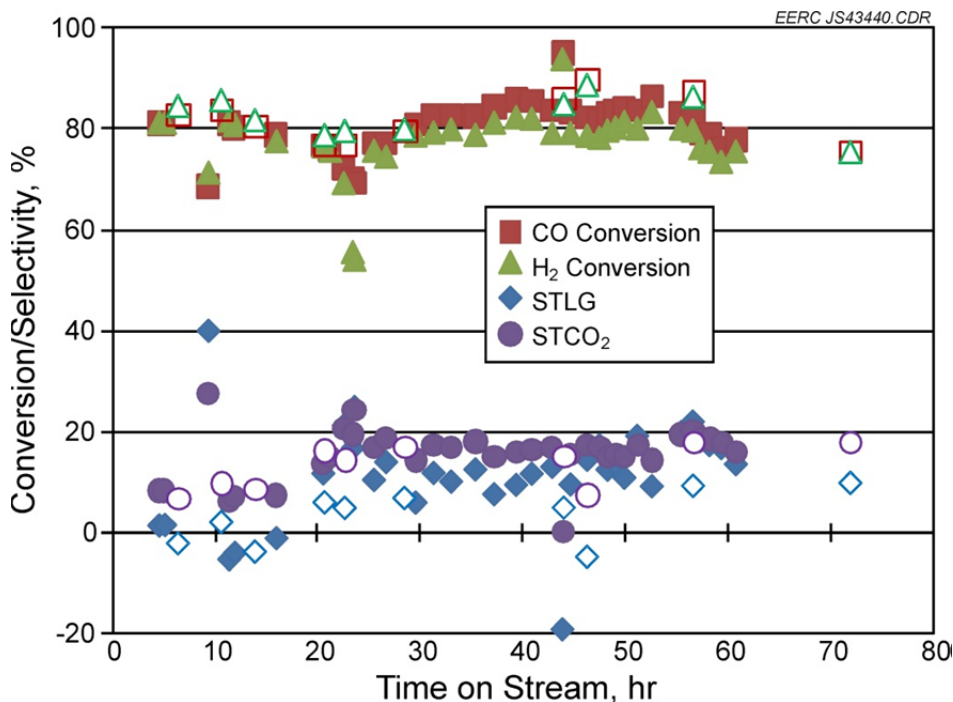
Figure 37. Molar H_2 and CO conversion, STLG, and $STCO_2$ in Test FBG021. Solid points are calculated from Varian data, while open shapes are from steady-state LGA averages.

70

During the second HDO treatment, the pressure again rose rapidly during heat-up. Once up to temperature, the reactor slowly lost pressure, indicating either a leak or H_2 consumption. Liquid material began to drip out of the bottom drain valve over the course of the test, suggesting part of the pressure drop was caused by leaking. This liquid was probably what ignited during the first HDO treatment. The valve was kept uninsulated in the second HDO treatment, preventing liquids from becoming hot enough to ignite. After HDO, the pressure dropped rapidly while the reactor was cooled.

Comparing starting and ending temperature and pressure as in Equation 5, the reaction may have consumed 0.209 mol of H_2 during the second HDO treatment and about 0.09 mol during the first. The 578 g of starting FT product corresponds to about 3.0 mol of hydrocarbon. Thus the calculated H_2 consumption per mole of organic liquid was around 10%. As the reactor appeared to be leaking through the bottom drain valve, the actual H_2 consumption was probably much smaller because some of the pressure drop was caused by leaking rather than gas consumption.

$$\Delta n = n_2 - n_1 = \frac{P_2 V_2}{R \cdot T_2} - \frac{P_1 V_1}{R \cdot T_1} = V/R \left(\frac{P_2}{T_2} - \frac{P_1}{T_1} \right)$$ [Eq. 5]

The HDO product GC–MS looked unchanged from the feed, with no detectable peaks having been removed or generated. The researchers examined the product for water, which would indicate that some oxygenate had been hydrogenated and removed from the FT product as H_2O. No water was observed in the HDO FT product, and no obvious oxygenates could be detected in either the untreated FT product or the HDO product by GC–MS. It was concluded that no reaction was occurring in the HDO batch reactor. Pressure drop was probably caused mostly by leaking rather than by H_2 consumption.

The HDO product was next filtered and distilled into 138 g of clear, colorless light organics and 332 g of cloudy, yellow, waxy heavier organics. Figure 38 gives GC–TCD chromatograms of both fractions. Removing light material tends to raise the cloud and freezing points of hydrocarbon blends, which is why the liquid HDO product became waxy after distillation.

4.5.3.2 Isomerization

When the heavy distillation cut of the HDO product was pumped through the SCR for hydrotreating, the sample became clear, colorless, and less waxy, indicating that most olefins had been saturated and that waxy molecules were being hydrocracked into fuel-range products. However, isomerization was quite poor.

The product was recycled through the SCR four times in an attempt to improve product isomerization. Isomerization was still relatively poor at only 68% after five passes through the SCR, as seen in Table 22. Normally, HDO product is recycled only 2–3 times over CoMo to yield a product with closer to 80% isomerization. It should be noted that isomerization as reported in Table 22 is the sum of GC–TCD peaks and does not necessarily represent the actual molar concentration of isomers.
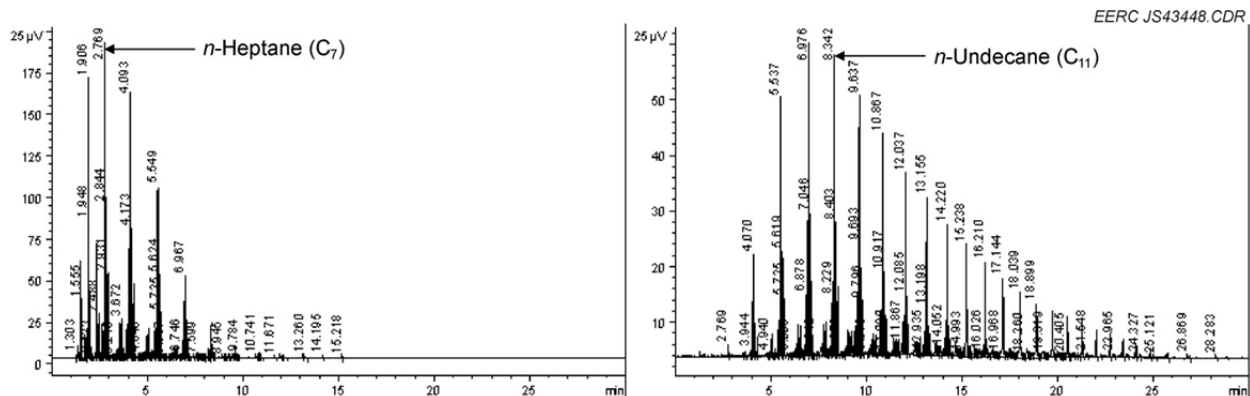
Figure 38. GC–TCD analysis of distilled HDO product light (left) and heavy (right) fractions.

Table 22. Product Isomerization FT Product Hydrotreating

Pass	Isomerization, %
1	40.4
2	39.9
3	50.1
4	55.9
5	68.2

The total mass recovery after five passes through the SCR was 83%, but much of the product was contaminated with NORPAR-15 and was not usable. Distillation of the 150 g of usable product yielded a jet fuel cut with 60.1% isomerization and a freeze point of −45°C. The specification for military JP-8 is −47°C. The density was also somewhat low, but this is typical of synthetic FT fuels and can be corrected by blending with petroleum-derived jet fuel.

CoMo is usually an effective catalyst for isomerizing oxygen-free hydrocarbons. In hydrotreatment tests using FT product generated in the laboratory, the same catalysts and procedures had produced a jet fuel cut that met several key JP-8 criteria, despite having been recycled through the SCR only three times. The flash point had been 53°C, the freeze point was −49.4°C, and the product was 61.6% isomerized. The FT product generated from clean, bottled gas was clearly more readily hydrotreated than the FT product generated using warm-gas cleanup of actual syngas. The most likely explanation for poor performance with FT product from warm-gas cleanup is that oxygen was still present in the isomerization feed to the SCR.

There are two obvious sources of oxygen in the isomerization feed. The first is HDO product water. Normally, HDO product is passed over a molecular sieve to remove traces of water generated by deoxygenation. Molecular sieve treatment was not used in this test because the HDO reaction did not appear to have any effect, and since the HDO feed did not contain any obvious oxygenates such as primary alcohols, it was thought that no reaction had occurred and, therefore, no water would have been generated. The HDO product had also been distilled, and it was thought that any moisture would be distilled off with the light organics.

The other potential source of oxygen in the isomerization feed is phenols and other gasifier tars. Phenols contain oxygen, but they are more difficult to reduce than the paraffinic oxygenates typically found in FT liquids. HDO treatment of tar-laden FT product may require higher pressures and/or longer residence times to completely deoxygenate phenols and other tar compounds.

4.6 Distillation Column Installation

The twin distillation column system was received on May 5, 2012, and installed on May 22 and 23. Figure 39 provides an image of the columns as installed.

After installation, column performance was tested using surrogate materials. The columns appear to be in good working order and should be able to provide the performance needed for processing DCL liquids into fuel blendstock.

Figure 39. Distillation columns installed for DCL liquids separation.

4.7   Reporting and Travel

Various presentations were given by Mr. Josh Strege over the course of the project as described in quarterly reports. These presentations were intended to stimulate further research and collaboration by sharing the EERC's findings with other researchers and industry representatives. In BP1, early laboratory results were shared in an oral presentation at the 2009 Clearwater Clean Coal Conference (25). Pilot-scale results from Tests FBG002 and FBG003 were presented at the 2009 International Conference on Coal Science and Technology in Cape Town, South Africa (26). These results were also published in *Fuel Processing Technology* (27). A further discussion of catalyst preparation and performance was also published in *Fuel Processing Technology* (28). Comprehensive results from BP1 were presented by Mr. Jason Laumb at the 2010 International Freiberg Conference on integrated gasification combine cycle (IGCC) and XtL Technologies (29) (which was not funded through Subtask 3.4) and at the 2011 Clearwater Clean Coal Conference (30). The final report to the North Dakota Industrial Commission (NDIC), the cost-share partner during BP1, included a more comprehensive overview of the approach and findings in BP1 (31). A copy of this report was forwarded to DOE NETL at the time of its completion.

Mr. Strege shared results summarizing all of Subtask 3.4 findings at the 2012 International Freiberg Conference on IGCC and XtL Technologies in Leipzig, Germany, on May 22, 2012. An accompanying article was submitted to the conference committee for consideration in a special issue of the journal *Fuel*. Dr. Michael Swanson of the EERC also presented summary findings at the 37th International Technical Conference on Clean Coal & Fuel Systems in Clearwater, Florida, on June 7, 2012, along with a conference paper detailing specific findings.

5.0   CONCLUSIONS

Overall, Subtask 3.4 demonstrated the continued hurdles facing small-scale FT synthesis. Work by a number of researchers has shown that CO_2 can be incorporated into FT product using an iron-based catalyst (15–18, 22), but the catalyst tested by the EERC showed low productivity and rapid deactivation both in a pilot-scale reactor and in a more controlled laboratory-scale reactor when exposed to unsweetened syngas. High CO_2 concentration in bottled gas also had a negative impact on catalyst performance at low H_2 concentrations, but rapid catalyst deactivation was not apparent. The loss of activity under CO_2 with low H_2 was more pronounced for iron-based catalyst than for cobalt-based catalyst, suggesting that it was caused by iron's ability to incorporate CO_2 into FT product. Rapid deactivation under real syngas was most likely caused by light gasifier tars that could not be captured or suitably cracked using warm-gas cleanup.

The FT product generated by warm-gas cleanup was not as readily hydrotreated as FT product generated from an ideal blend of bottled gases. HDO treatment seemed to have little effect, and subsequent hydrotreatment fared poorly. Part of the issue could be that the distilled HDO product was not treated with a molecular sieve to remove traces of moisture before further hydrotreatment. Given the significant presence of gasifier tar in the FT product generated using warm-gas cleanup, HDO may also have required more severe conditions to remove all oxygen from the FT product.

74

Despite advances in hot- and warm-gas cleanup, the results imply that gas sweetening using refrigerated solvents will continue to be necessary for FT synthesis from low- to moderate-temperature gasifiers, as these gasifiers generate significant CO_2 and gasifier tar. Unfortunately, low- and moderate-temperature gasifiers are generally the only gasifiers that are feasible at a small scale or when cofeeding biomass. This means that coal-based FT plants must either use gas sweetening, which has such high installation and operating costs that it can only be justified at a very large scale, or high-temperature gasification, which generally only operates efficiently at a large scale using high-energy feeds. The prohibitive costs of large-scale oxygen-blown gasification and gas sweetening thus remain limiting factors in encouraging widespread use of domestic coal and biomass reserves for fuel production.

Cofeeding treated biomass with coal did not have any immediate impact on catalyst performance, nor did feeding 100% biomass. This suggests that deactivation caused by any contaminants unique to the biomass was minimal compared to baseline deactivation (probably by coking) using warm-gas cleanup. However, when lignite was gasified, naphthalene appeared in the FT product, and when 100% DDGS was gasified, very high levels of benzene were detected. Neither naphthalene nor unusual levels of benzene were detected when gasifying PRB coal or 30% blends of biomass with PRB coal. These results demonstrate that, while FTS may be feedstock-agnostic, gasifier tars that are not captured or destroyed upstream of the FT reactor do appear in the organic FT product and will impact product quality.

Feeding high levels of biomass also tended to be associated with rapid agglomeration and other gasifier issues. Both biomass and lignite generated sufficient tar to cause plugging and other operational issues at cool ambient temperatures. Adding 20 g of dolomite to every 1 lb of lignite did not reduce gasifier tar significantly for sustainable FTS using warm-gas cleanup.

If biomass can be better pretreated to limit tar formation and agglomeration potential, or if a warm-gas cleanup method can be developed that reliably cracks or captures tars, then biomass may be a suitable feed for FTS using warm-gas cleanup on the small scale. This would be a great benefit to reducing the CO_2 emissions from FTS while also permitting the use of small-scale distributed FTS reactors with reduced capital costs. However, with the sorbents, FT catalysts, gasifier, and pretreatment options examined in this study, it is clear that warm-gas cleanup leads to rapid catalyst deactivation, poor FT product, significant tar content in the FT product, difficulty with predictive modeling, and issues with hydrotreating to refined fuel. This is true regardless of whether coal or biomass is used, but the high levels of tar formed from lignite and biomass may have contributed to the rapid deactivation observed in Test FBG004 compared to slow deactivation observed in Test FBG002.

Attempts to generate a large batch of iron-based catalyst using a novel production technique were successful, but the catalyst showed little initial activity in pelletized form and degraded quickly because of poor mechanical strength. The formulation was recommended by Calvin Bartholomew and his colleagues at BYU, who have decades of experience in FT catalyst development and testing. Despite their support, the EERC was unable to produce a working iron-based catalyst in a short time using the novel production technique. The alternative iron-based catalyst that was instead used for pilot-scale testing took several years to develop and required testing dozens of various formulations in a laboratory reactor before it achieved suitable

conversion. This observation suggests that future efforts by the EERC and other research teams to scale up production of novel FT catalysts should proceed slowly and methodically, as attempts at rapid scale-up have not yielded good results, even with support from a team of knowledgeable experts. The poor results also demonstrate that catalyst that works well in a powdered form for slurry reactors may perform very poorly when pelletized and used in a fixed-bed reactor.

6.0   REFERENCES

1. Fischer, F. Über die Synthese der Petroleumkohlenwasserstoffe. *Brennstoff-Chemie* **1927**, *8*, 1–5.

2. Fischer, F.; Pichler, H.; Kölbel, H. Über die Herstellung von Mischgas für die Benzinsynthese durch gleichzeitige Umsetzung von Kokereigas und Koks mit Wasserdampf im Generator. *Brennstoff-Chemie* **1935**, *16*, 401–404.

3. Fischer, F.; Pichler, H.; Kölbel, H. Über halbtechnische Versuche zur Herstellung von Synthese-Mischgas durch gleichzeitige Umsetzung von Kokereigas und Wasserdampf über Koks im Generator. *Brennstoff-Chemie* **1935**, *16*, 331–333.

4. Fischer, F. Die Synthese der Treibstoffe (Kogasin) und Schmieröle aus Kohlenoxyd und Wasserstoff bei gewöhnlichem Druck. *Brennstoff-Chemie* **1935**, *16*, 1–11.

5. Davis, B.H. Fischer–Tropsch Synthesis: Reaction Mechanisms for Iron Catalysts. *Catalysis Today* **2009**, *141*, 25–33.

6. Li, L.; King, D.L.; Liu, J.; Zhu, K.; Wang, Y. Metal-Based Adsorbents for Regenerable Deep Desulfurization of Warm Syngas. In *Proceedings of the 25th Annual International Pittsburgh Coal Conference*; 2008.

7. Schmidt, R.; Cross, J.; Tsang, A.; Sughrue, E.; Kornosky, R. Sulfur Removal from E-Gas Gas Streams with S Zorb Sulfur Removal Technology (SRT). In *Proceedings of the 23rd Annual International Pittsburgh Coal Conference*; 2006.

8. Skoulou, V.; Kantarelis, E.; Arvelakis, S.; Yang, W.; Zabaniotou, A. Effect of Biomass Leaching on H_2 Production, Ash, and Tar Behavior During High-Temperature Steam Gasification (HTSG) Process. *Int. J. Hydrogen Energy* **2009**, *34*, 5666–5673.

9. Arvelakis, S.; Hurley, J.; Folkedahl, B.; Koukios, E.G.; Spliethoff, H. Fluidized-Bed Gasification of High-Alkali and Chlorine Biomass: Effect of Pretreatments on the Agglomeration Behaviour. In *Proceedings of the International Technical Conference on Coal Utilization & Fuel Systems*; Coal Technology Association, 2008; pp 591–601.

10. Nguyen, M.H.; Prince, R.G.H. A Simple Rule for Bioenergy Conversion Plant Size Optimisation: Bioethanol from Sugar Cane and Sweet Sorghum. *Biomass Bioenergy* **1996**, *10*, 361–365.

11. Börjesson, P.I.I. Energy Analysis of Biomass Production and Transportation. *Biomass Bioenergy* **1996**, *11*, 305–318.

12. Arvelakis, S.; Gehermann, H.; Beckmann, M.; Koukios, E.G. Agglomeration Problems During Fluidized-Bed Gasification of Olive Oil Residue: Evaluation of Fractionation and Leaching as Pretreatments. *Fuel* **2003**, *82*, 1261–1270.

13. Arvelakis, S.; Koukios, E.G. Physicochemical Upgrading of Agroresidues as Feedstocks for Energy Production via Thermochemical Conversion Methods. *Biomass Bioenergy* **2002**, *22*, 331–348.

14. Svoboda, K.; Pohořelý, M.; Hartman, M.; Martinec, J. Pretreatment and Feeding of Biomass for Pressurized Entrained Flow Gasification. *Fuel Process. Technol.* **2009**, *90*, 629–635.

15. Ning, W.; Koizumi, N.; Yamada, M. Researching Fe Catalyst Suitable for CO_2-Containing Syngas for Fischer–Tropsch Synthesis. *Energy Fuels* **2009**, *23*, 4696–4700.

16. Gnanamani, M.K.; Shafer, W.D.; Sparks, D.E.; Davis, B.H. Fischer–Tropsch Synthesis: Effect of CO_2 Containing Syngas over Pt Promoted $Co/\gamma\text{-}Al_2O_3$ and K-Promoted Fe Catalysts. *Catalysis Communications* **2011**, *12*, 936–939.

17. Riedel, T.; Claeys, M.; Schulz, H.; Schaub, G.; Nam, S.S.; Jun, K.W.; Choi, M.J.; Kishan, G.; Lee, K.W. Comparative Study of Fischer–Tropsch Synthesis with H_2/CO and H_2/CO_2 Syngas Using Fe- and Co-Based Catalysts. *Applied Catalysis A: General* **1999**, *186*, 201–213.

18. Yao, Y.; Liu, X.; Hildebrandt, D.; Glasser, D. Fischer–Tropsch Synthesis Using $H_2/CO/CO_2$ Syngas Mixtures over an Iron Catalyst. *Industrial & Engineering Chemistry Research* **2011**, *50*, 11002–11012.

19. Yao, Y.; Hildebrandt, D.; Glasser, D.; Liu, X. Fischer–Tropsch Synthesis Using $H_2/CO/CO_2$ Syngas Mixtures over a Cobalt Catalyst. *Industrial & Engineering Chemistry Research* **2010**, *49*, 11061–11066.

20. Ning, W.; Koizumi, N.; Yamada, M. Researching Fe Catalyst Suitable for CO_2-Containing Syngas for Fischer–Tropsch Synthesis. *Energy Fuels* **2009**, *23*, 4696–4700.

21. Yates, I.C.; Satterfield, C.N. Effect of Carbon Dioxide on the Kinetics of the Fischer–Tropsch Synthesis on Iron Catalysts. *Ind. Eng. Chem. Res.* **1989**, *28*, 9–12.

22. Xu, L.; Bao, S.; Houpt, D.J.; Lambert, S.H.; Davis, B.H. Role of CO_2 in the Initiation of Chain Growth and Alcohol Formation During the Fischer–Tropsch Synthesis. *Catal. Today* **1997**, *36*, 347–355.

23. Billet, R.; Schultes, M. Prediction of Mass Transfer Columns with Dumped and Arranged Packings. Updated Summary of the Calculation Method of Billet and Schultes. *Chemical Engineering Research and Design* **1999**, *77*, 498–504.

24. Davis, B.H. Fischer–Tropsch Synthesis: Relationship Between Iron Catalyst Composition and Process Variables. *Catal. Today* **2003**, *84*, 83–98.

25. Strege, J. FT Catalyst Testing in a Continuous Bench-Scale Coal Gasification System: Design and Early Results. Presented at the Clearwater Clean Coal Conference, Clearwater, FL, May 31 – June 4, 2009.

26. Strege, J.; Swanson, M.; Laumb, J.; Folkedahl, B.; Stanislowski, J. Fischer–Tropsch Catalyst Testing in a Continuous Bench-Scale Coal Gasification System: Design and early results. In Proceedings of the *International Conference on Coal Science & Technology*, Cape Town, South Africa, Oct 26–29, 2009.

27. Strege, J.; Swanson, M.; Folkedahl, B.; Stanislowski, J.; Laumb, J. Fischer–Tropsch Catalyst Testing in a Continuous Bench-Scale Coal Gasification System. *Fuel Processing Technology* **2011**, *92*, 757–763.

28. Folkedahl, B.C.; Snyder, A.C.; Strege, J.R. Bjorgaard Process Development and Demonstration of Coal and Biomass Indirect Liquefaction to Synthetic Iso-Paraffinic Kerosene. *Fuel Processing Technology* **2011**, *92*, 1939–1945.

29. Strege, J. Oxygen-Blown Gasification and Fixed-Bed Fischer–Tropsch Synthesis of Coal and Biomass. Presented by Mr. Jason Laumb at the International Freiberg Conference on IGCC & XtL Technologies, Dresden, Germany, May 3–5, 2010.

30. Strege, J. Pilot-Scale Gasification and Fischer–Tropsch Catalyst Testing. Presented at the 36th International Technical Converence on Clean Coal & Fuel Systems, Clearwater, FL, June 5–9, 2011.

31. Strege, J.R.; Laumb, J.D.; Stanislowski, J.J.; Snyder, A.C.; Swanson, M.L. *Fischer–Tropsch Fuels Development*; Final Report to North Dakota Industrial Commission, March 2010.

APPENDIX A

RAW DATA

RAW DATA

The following raw data are provided in chart form for each test. For the gasifier itself:

- Average bed and freeboard temperatures. This allows the reader to see overall trends not readily visible from the individual temperature readouts shown in the main report.

- Flow rates into and out of the gasifier.

- Pressure drops across the fluid bed and freeboard. These indicate bed height (i.e., amount of solids inventory in each section).

- Gasifier pressures.

- Syngas composition as measured by laser gas analyzer (LGA). It should be noted that in Test FBG002, H_2O was measured instead of O_2 as the LGA had not yet been modified to detect O_2.

For the Fischer–Tropsch (FT) reactor:

- Product gas composition exiting the FT reactor as measured by LGA, except for Test FBG021 because sampling was intermittent in this test.

- Flow rates into and out of the FT reactor bed(s)
  – FI901 – Flow rate into FT Bed 1
  – FI901 – Flow rate into FT Bed 2
  – FI903 – Flow rate of recycled FT wax into FT Bed 1 (not used)
  – FI904 – Flow rate of recycled FT wax into FT Bed 2 (not used)
  – FI905 – Flow rate of recycled product gas into FT Bed 1
  – FI906 – Flow rate of recycled product gas into FT Bed 2
  – Flowrate – Exhaust gas flow out of FT reactor system

- Pressure drops across FT reactor
  – DPT901 – Pressure drop across FT Bed 1
  – DPT902 – Pressure drop across FT Bed 2
  – DPT903 – Pressure drop across wax trap (unreliable)
  – DPT904 – Pressure difference between dry gas meter and atmosphere (would indicate plugged outlet line)

- FT reactor pressures
  – PT900 – Pressure downstream of syngas regulator
  – PT901 – Pressure at top of FT Bed 1
  – PT902 – Pressure at top of FT Bed 2
  – PT903 – Quench pot pressure

- FT reactor temperatures

- Conversion of CO and H_2, except for Test FBG021

- Selectivity to light gas, except for Test FBG021

FBG002
Gasifier Trends

FT Reactor Trends

EERC JS36586D.AI

FBG003
Gasifier Trends

EERC JS36591A.AI

EERC JS36591B.AI

EERC JS36591C.AI

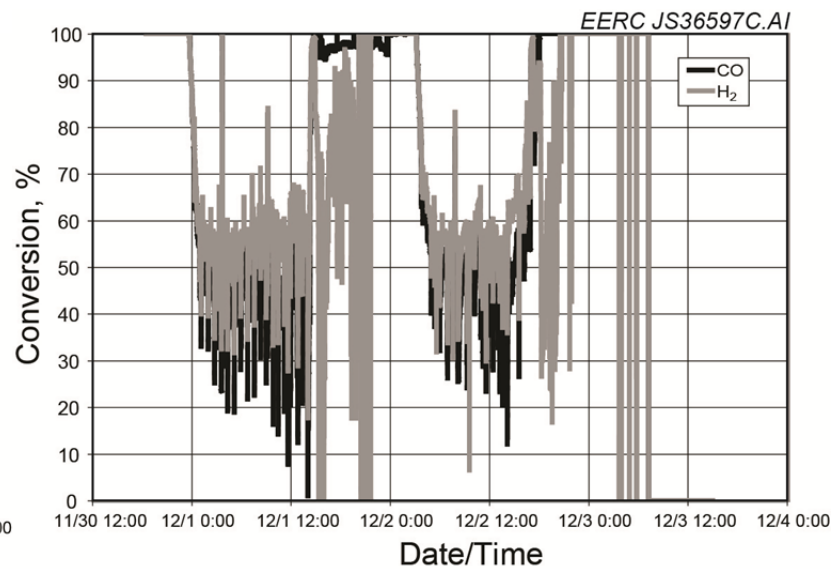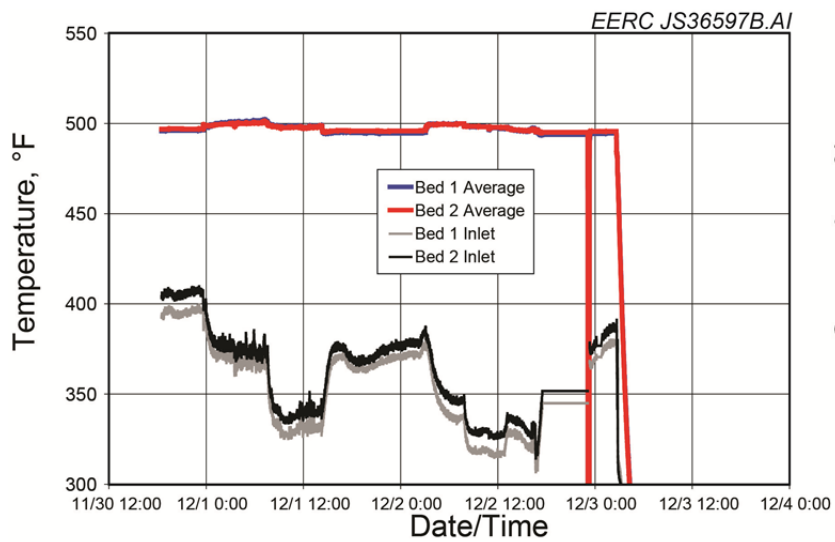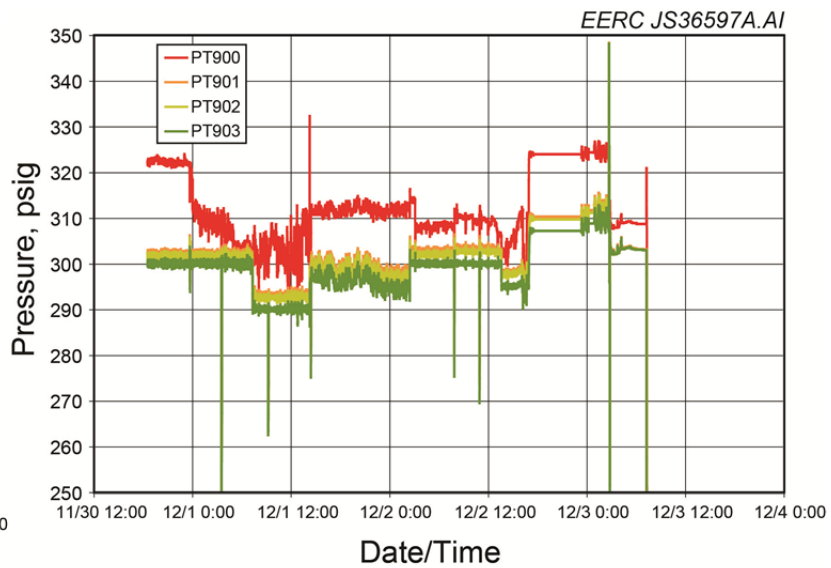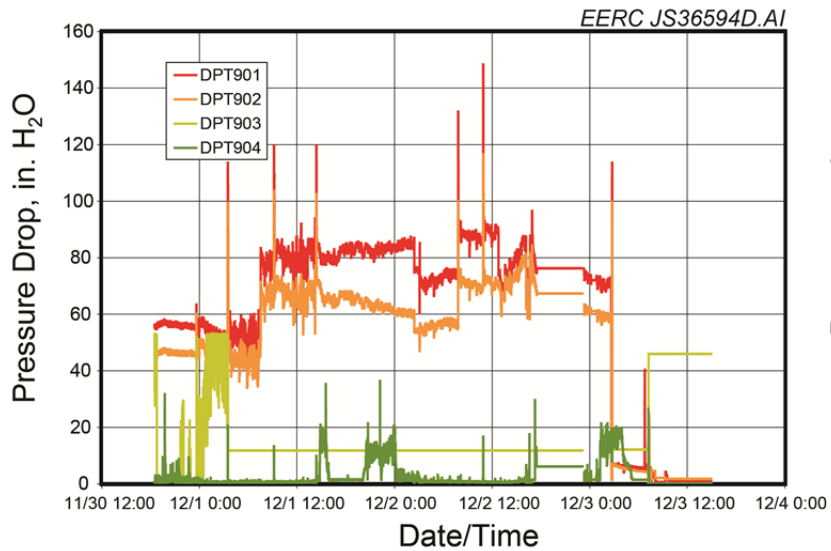*EERC JS36591D.AI*

FT Reactor Trends

EERC JS36589D.AI

A-10
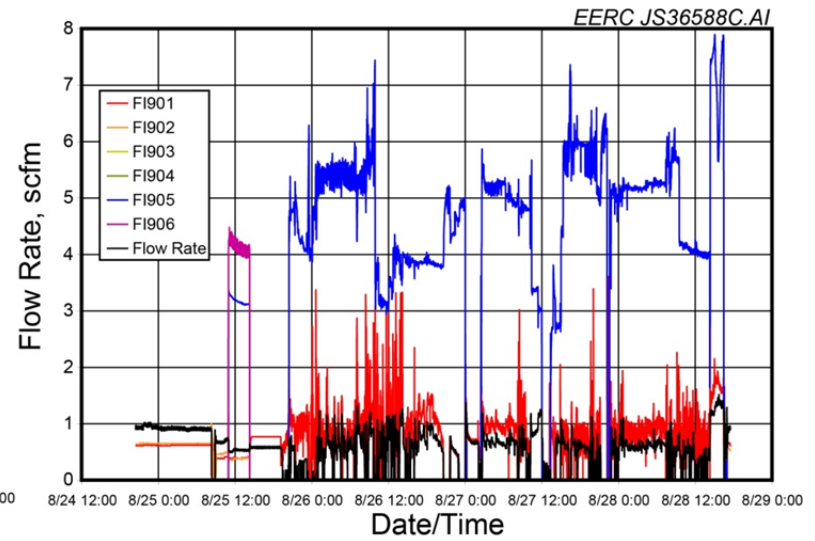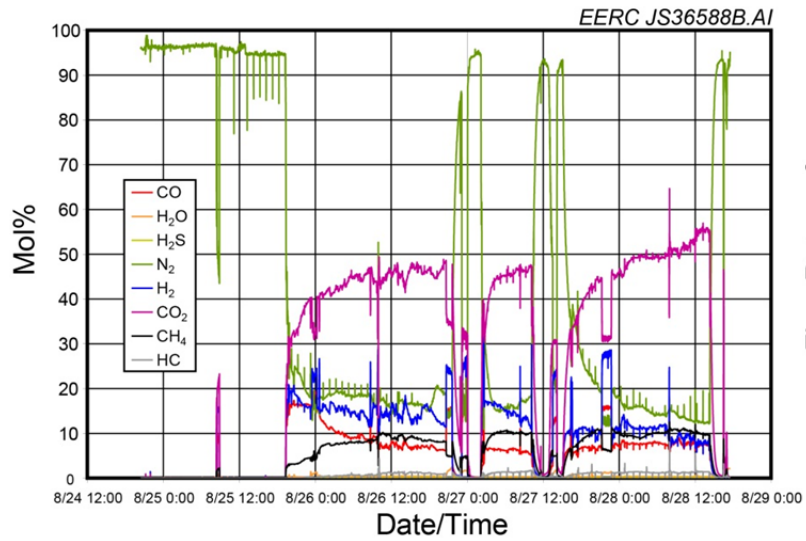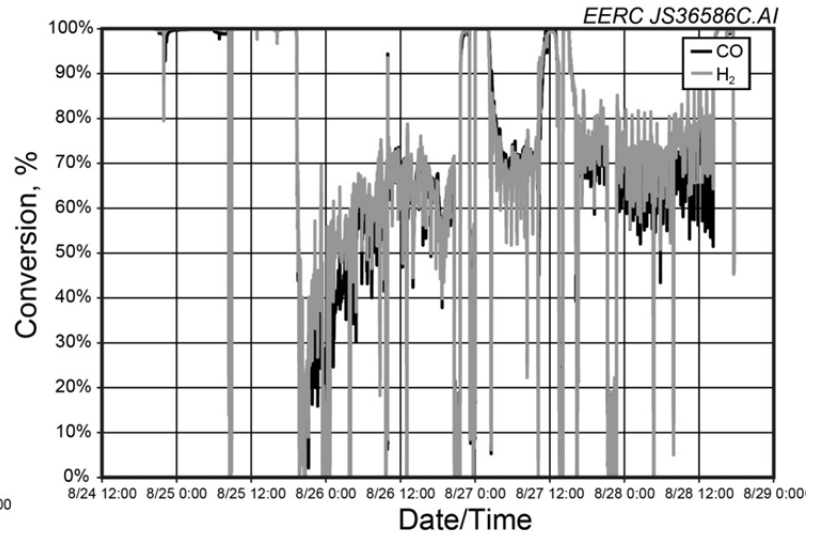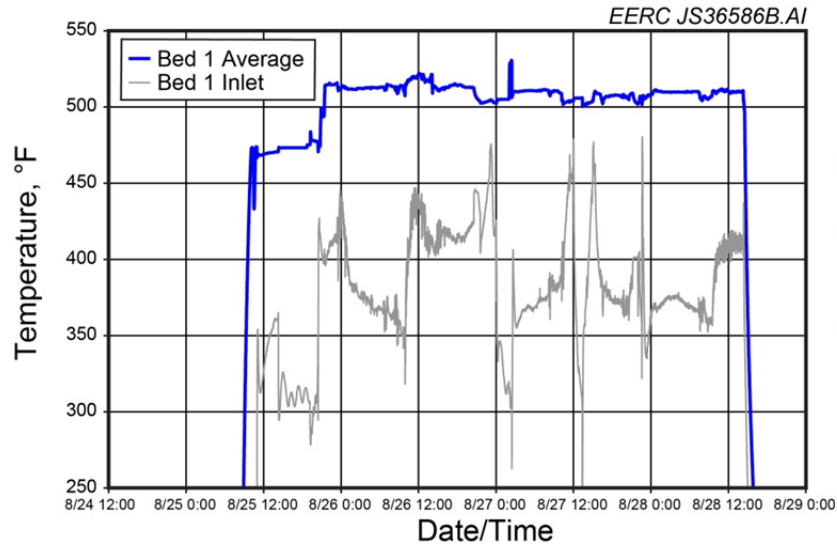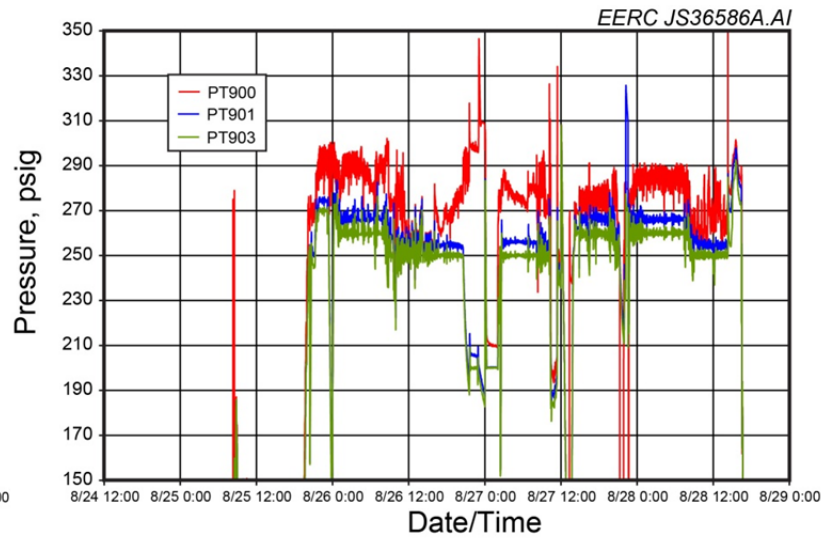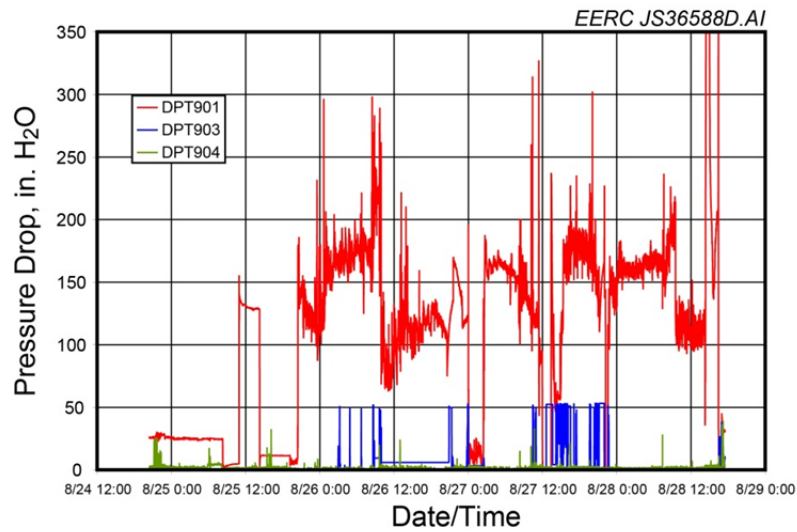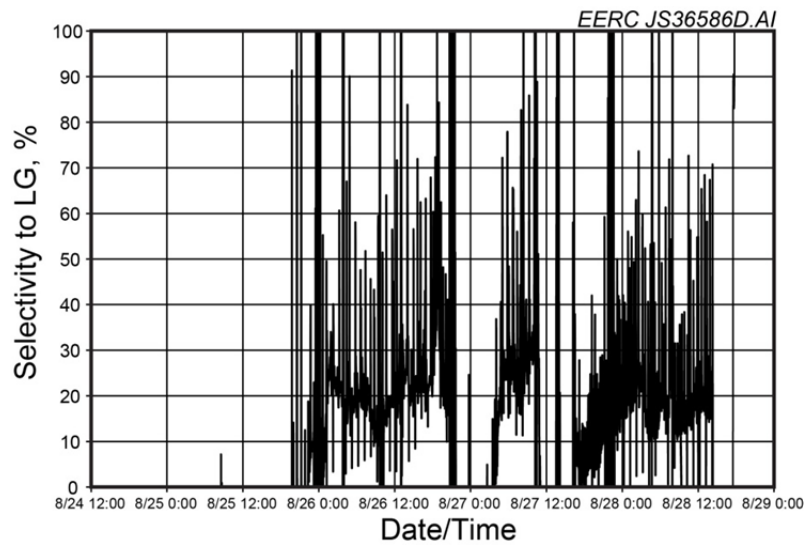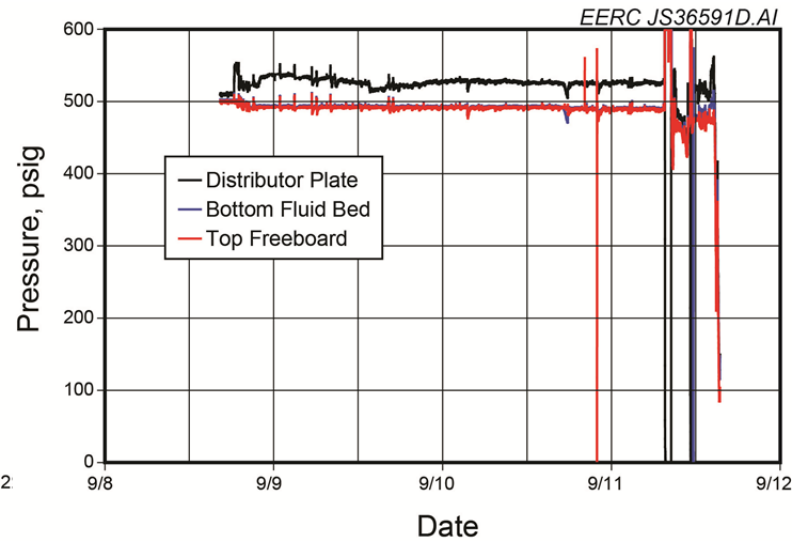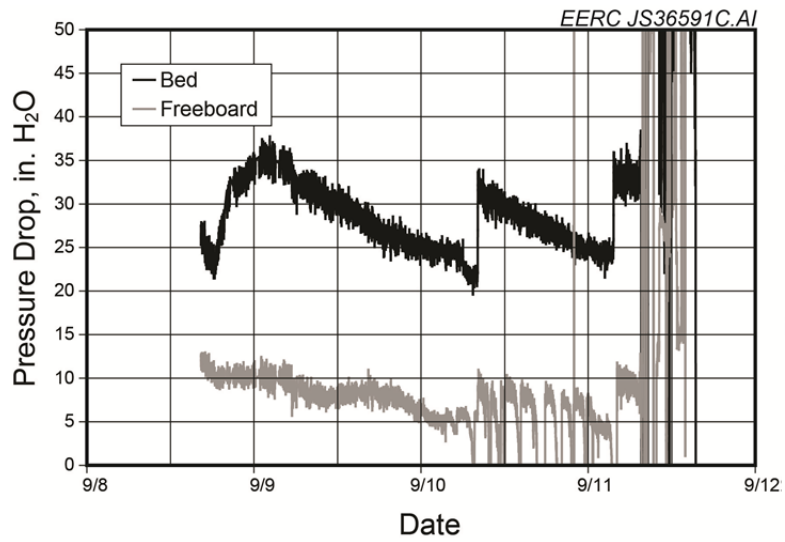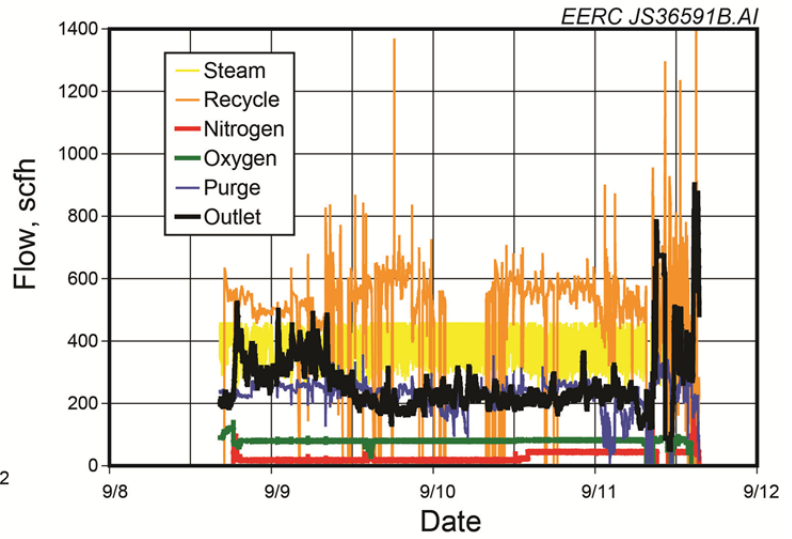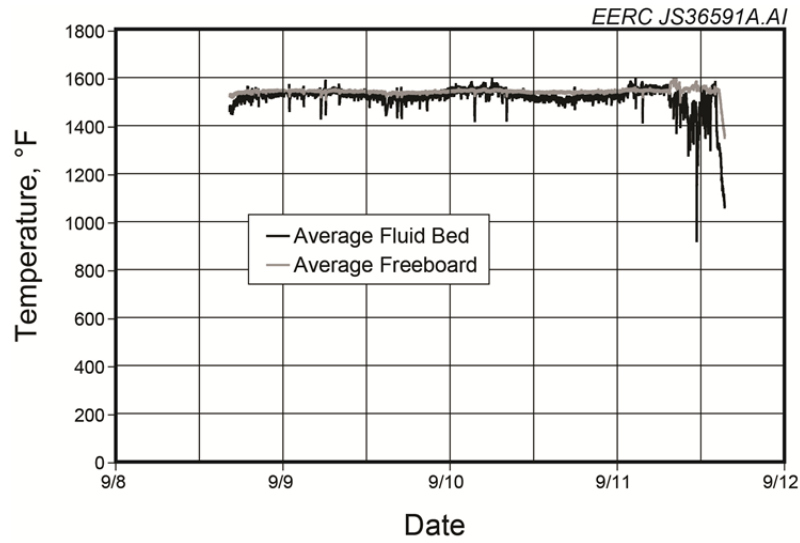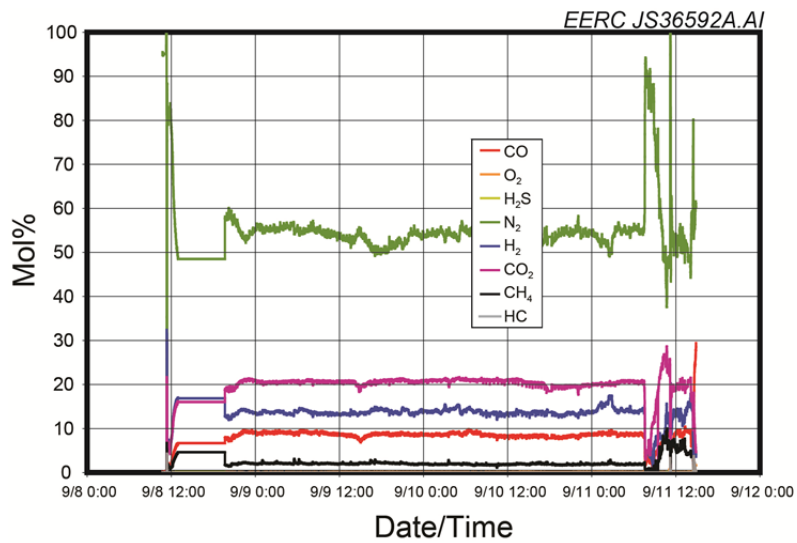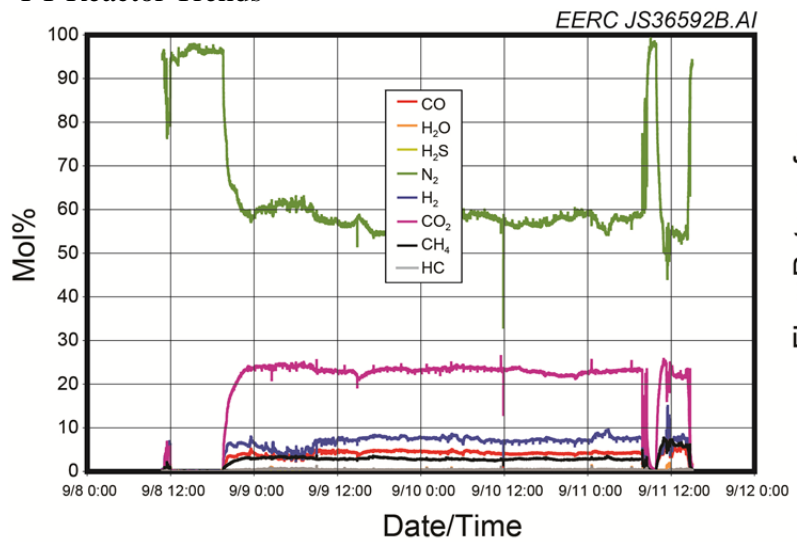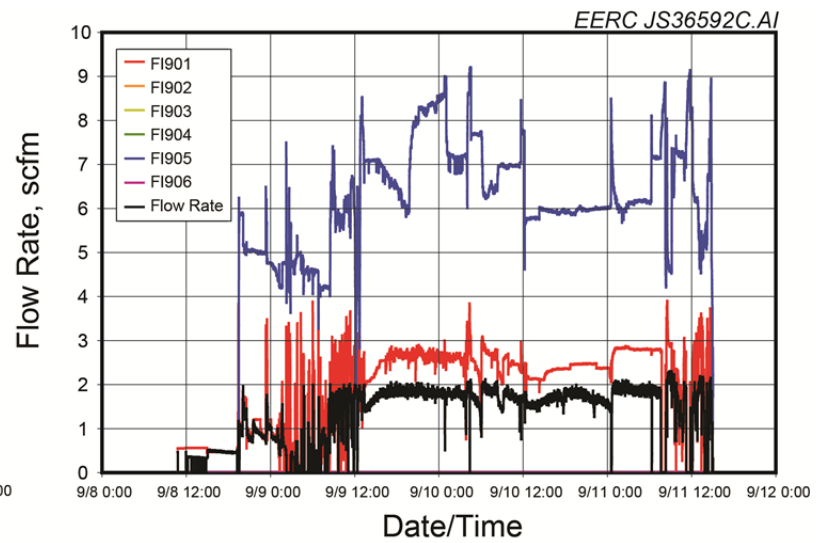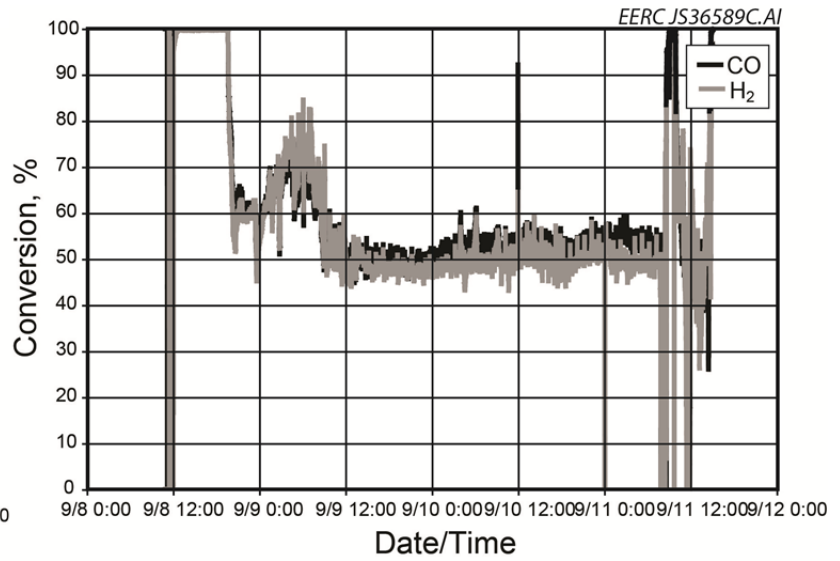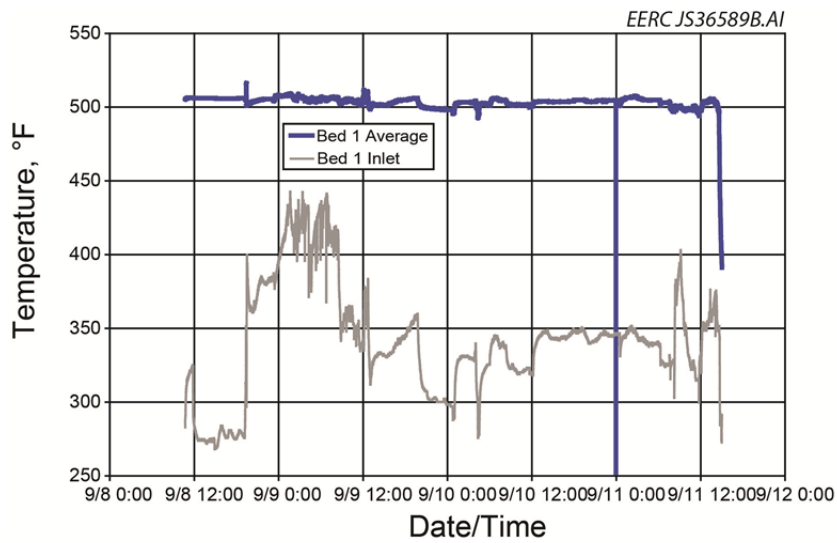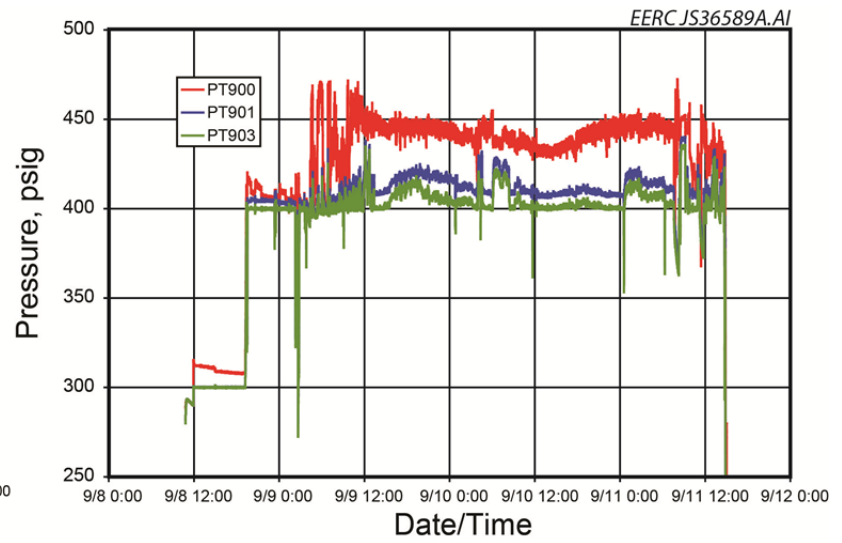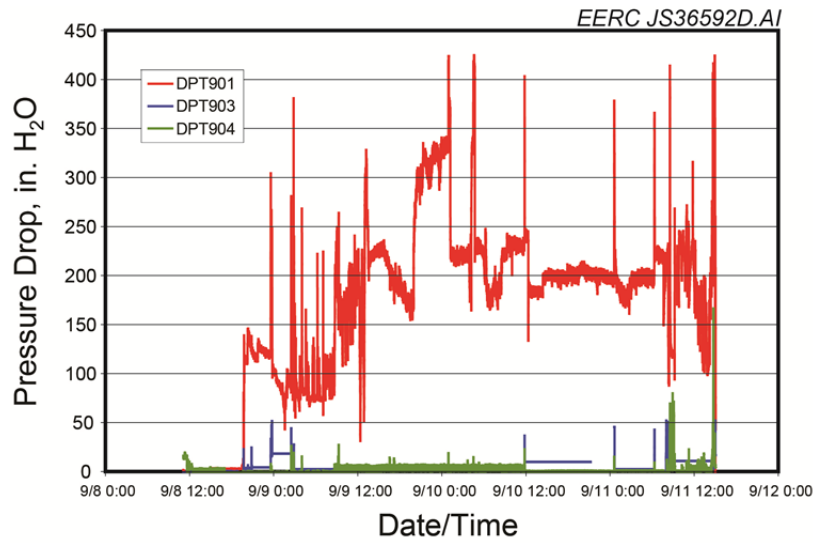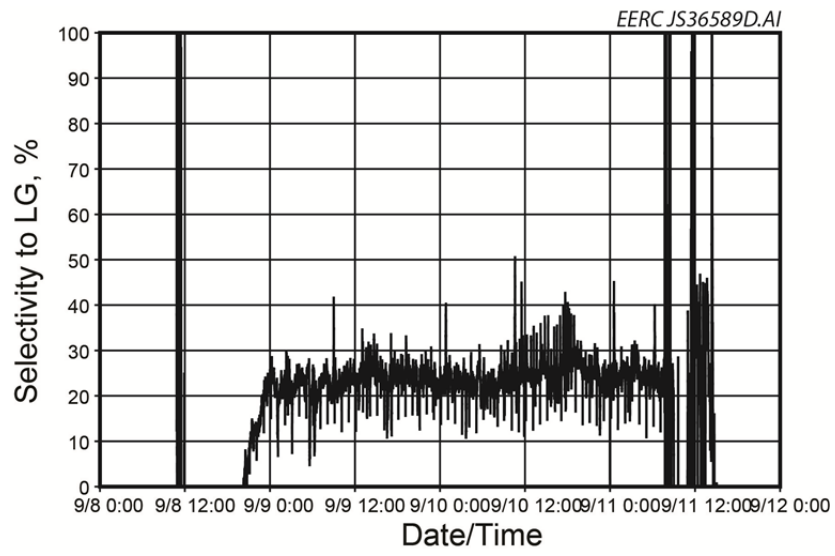
FBG004
Gasifier Trends

FT Reactor Trends

EERC JS36595D.AI

FBG005
Gasifier Trends

EERC JS36596A.AI
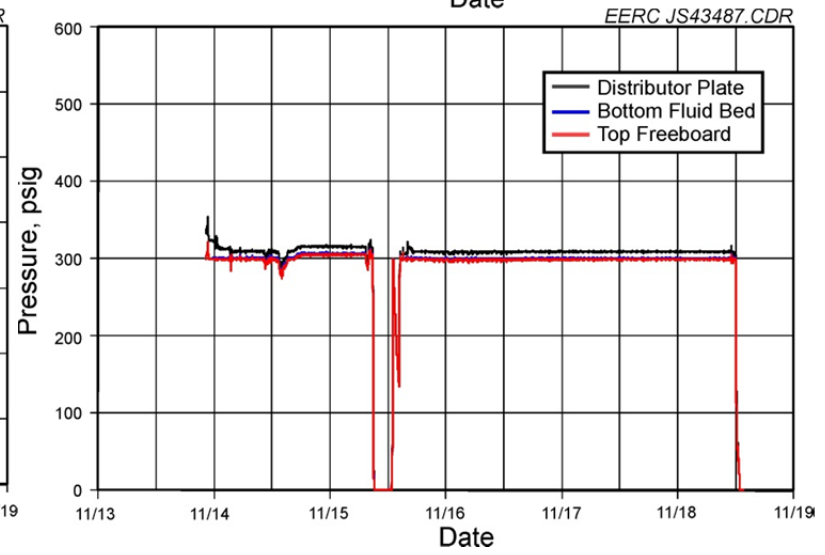
EERC JS36596B.AI

The flow rate of recycle gas is determined in part by the MW of the syngas. This may be inaccurate. Verify with FT file data.

EERC JS36596C.AI

EERC JS36596D.AI
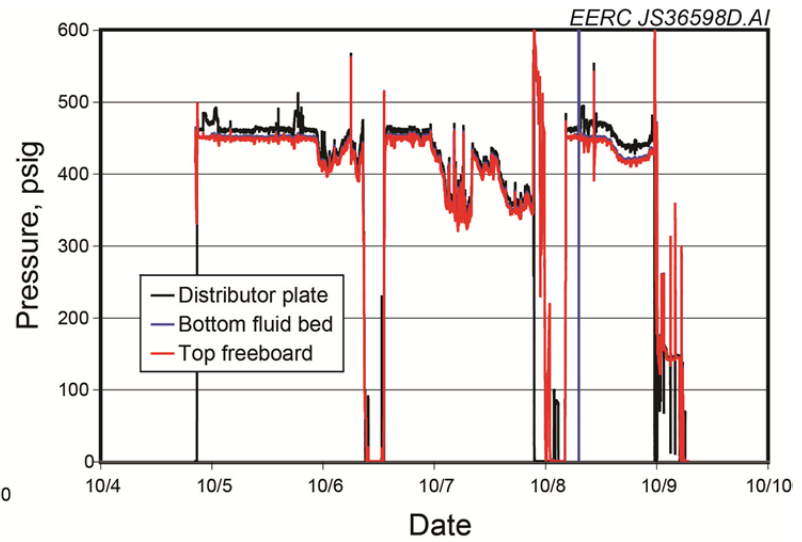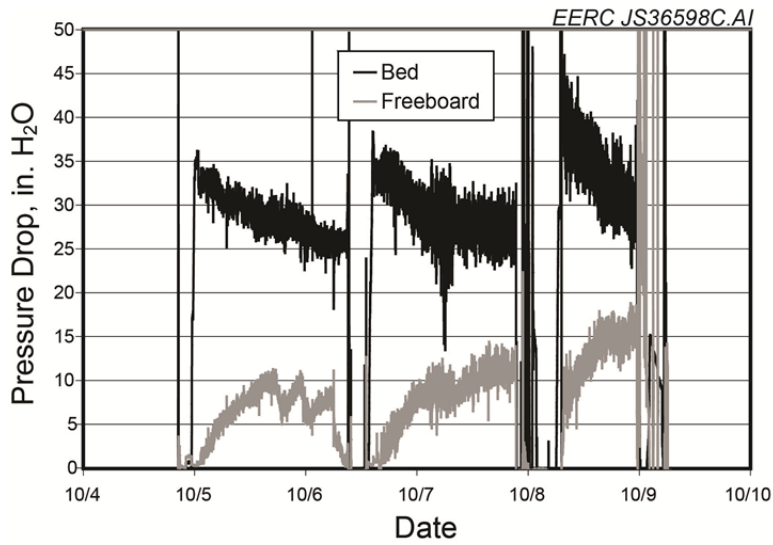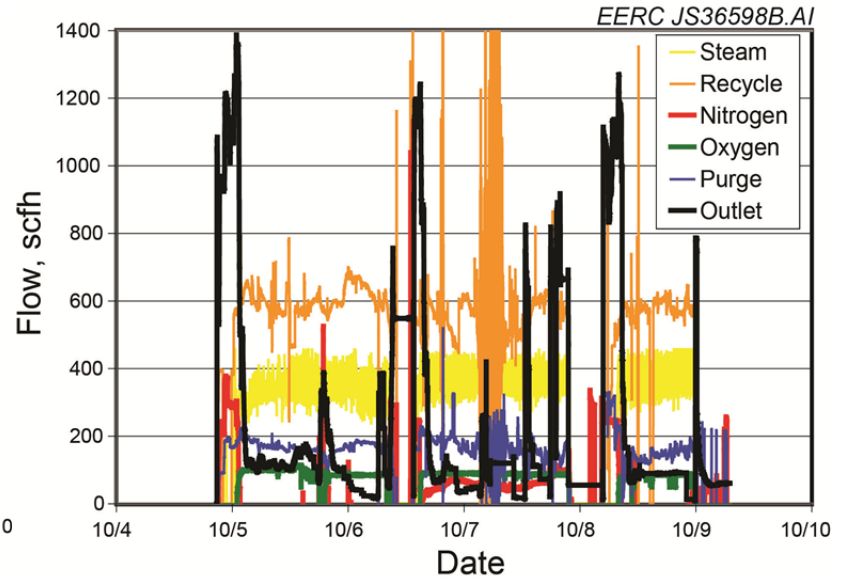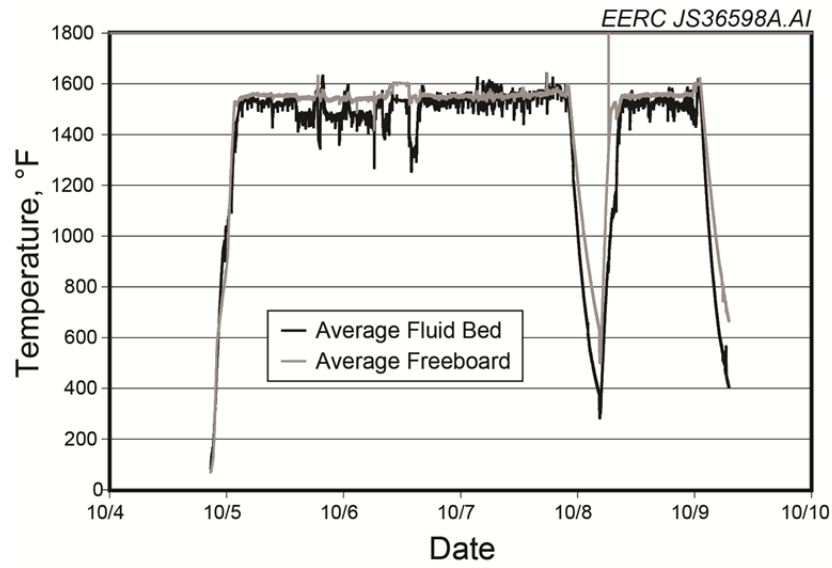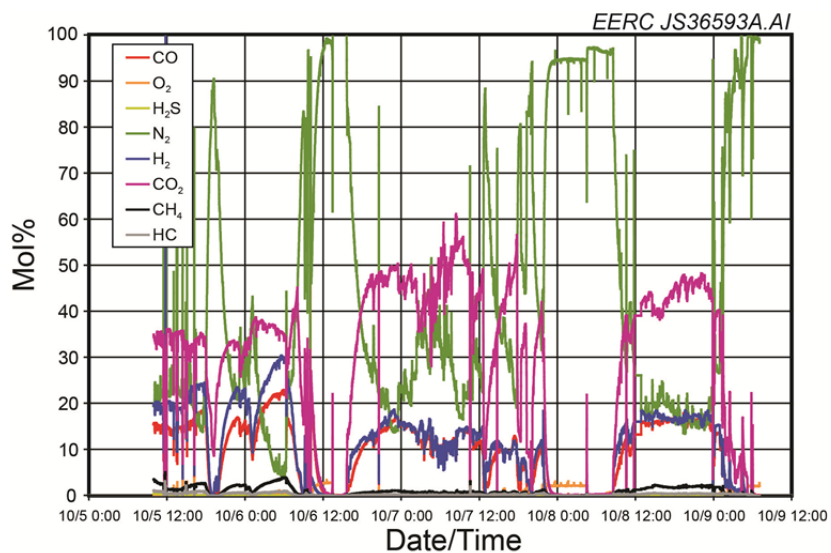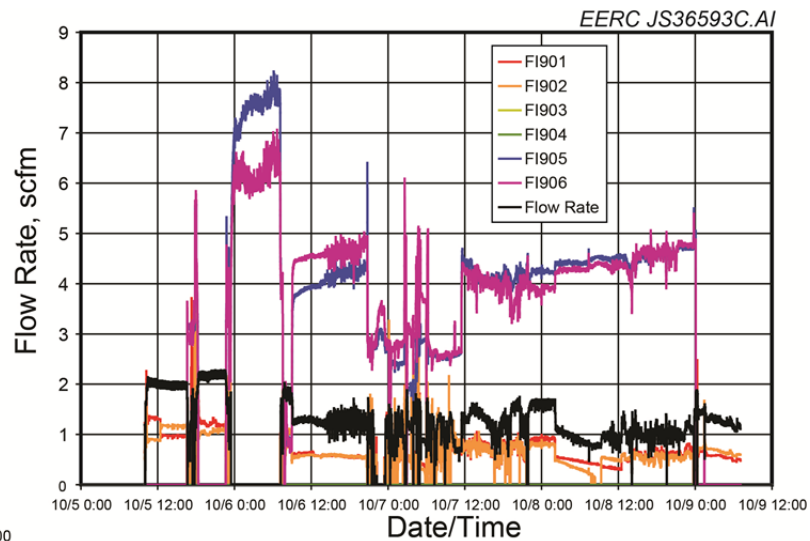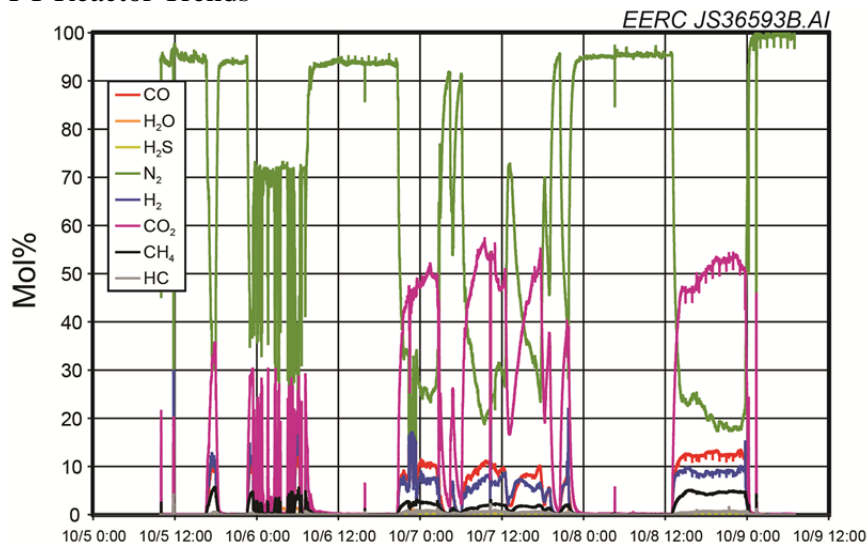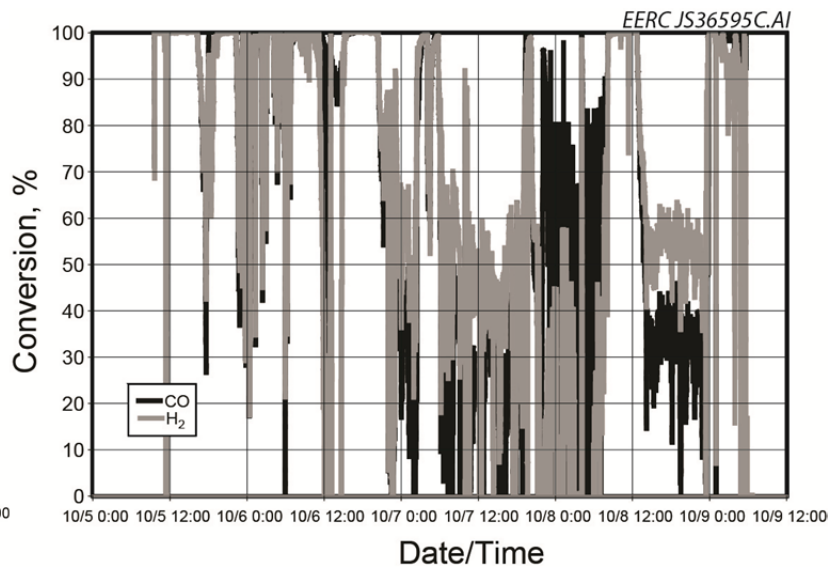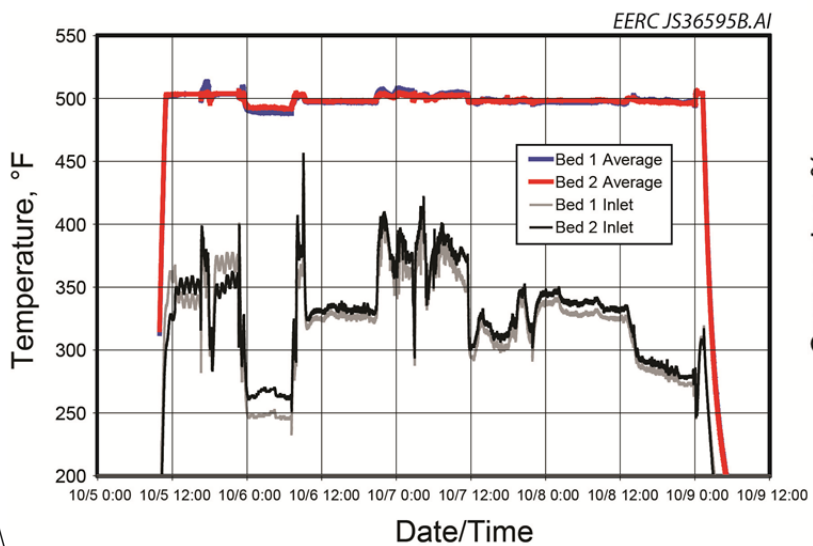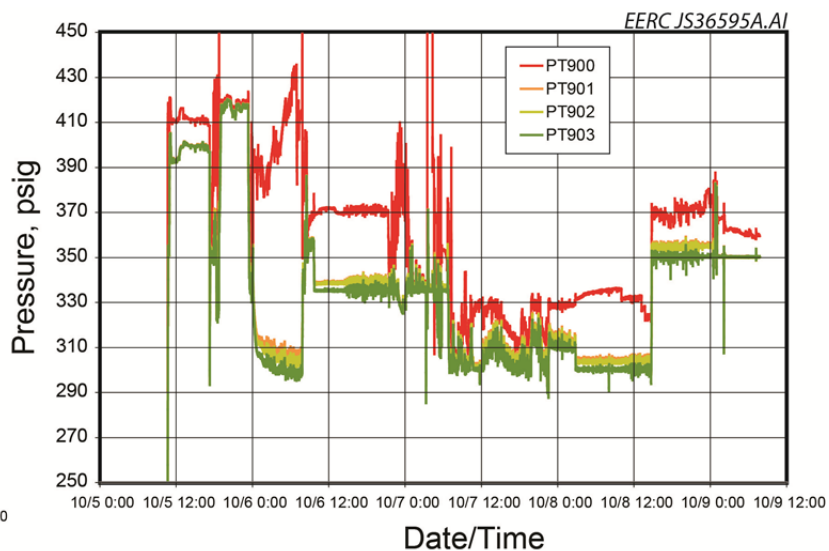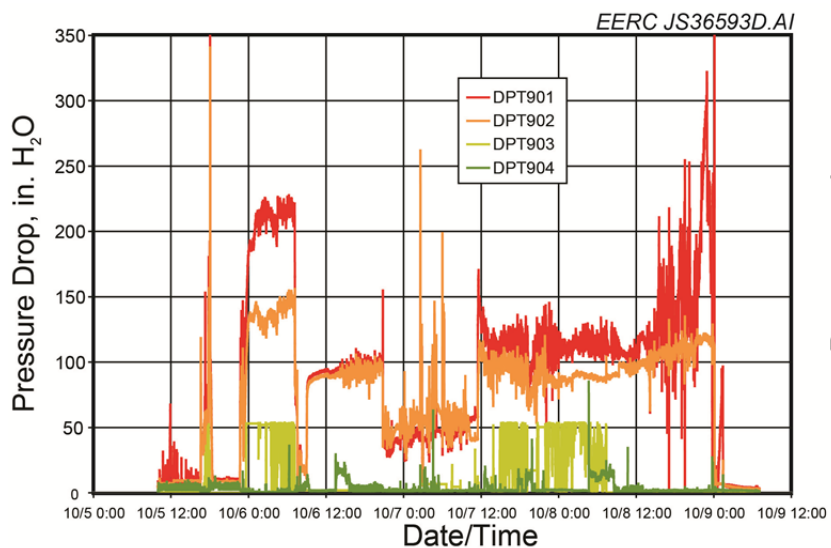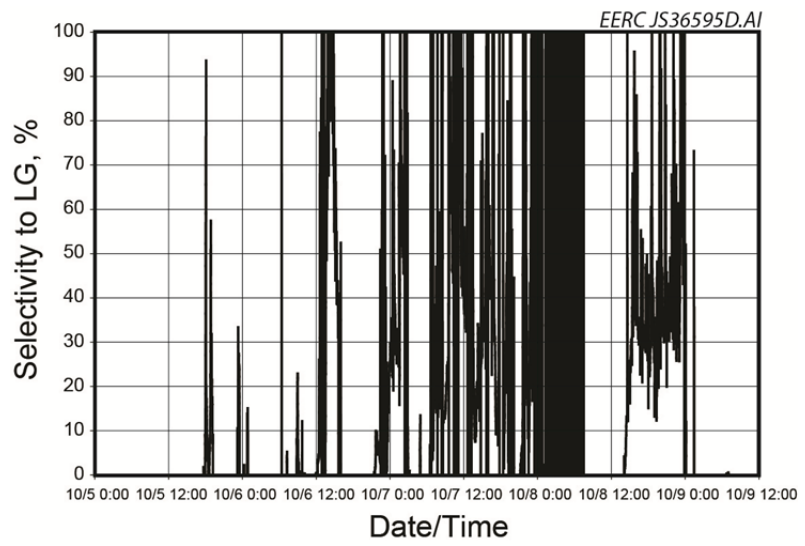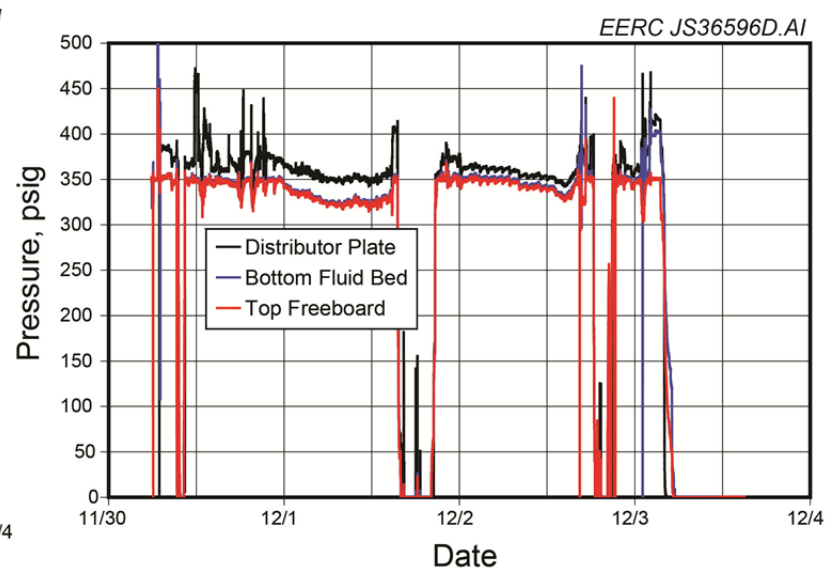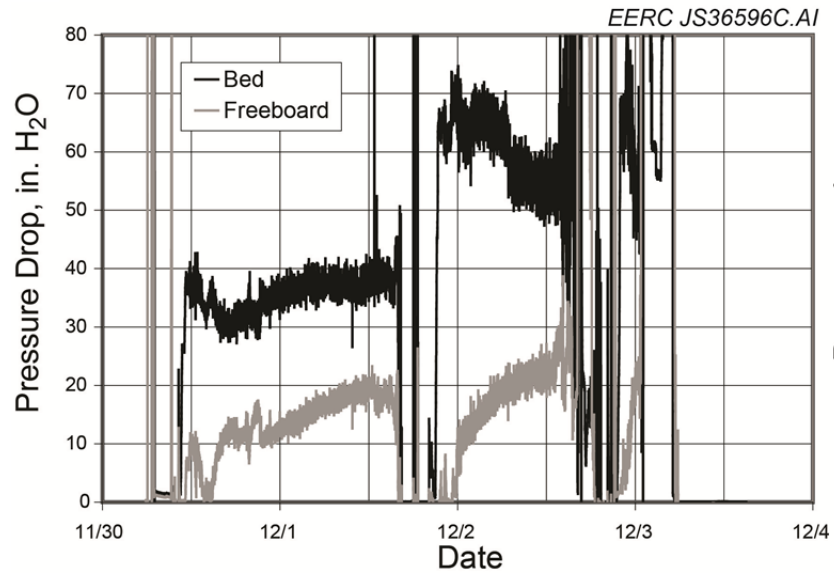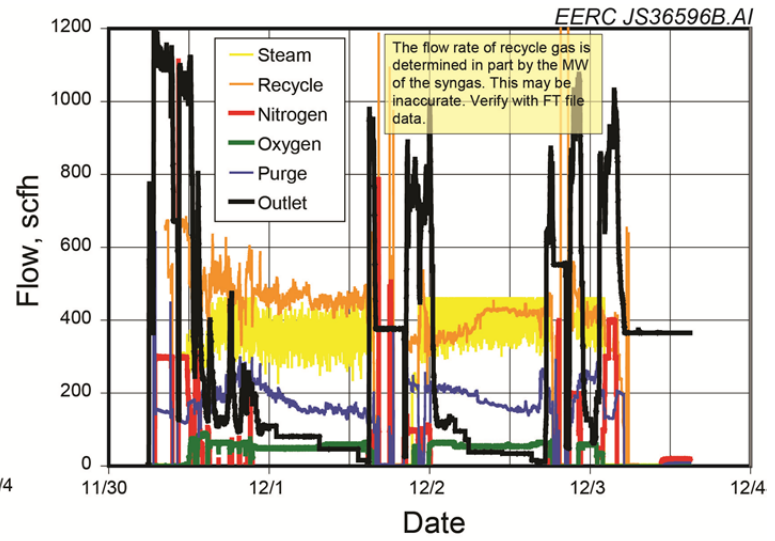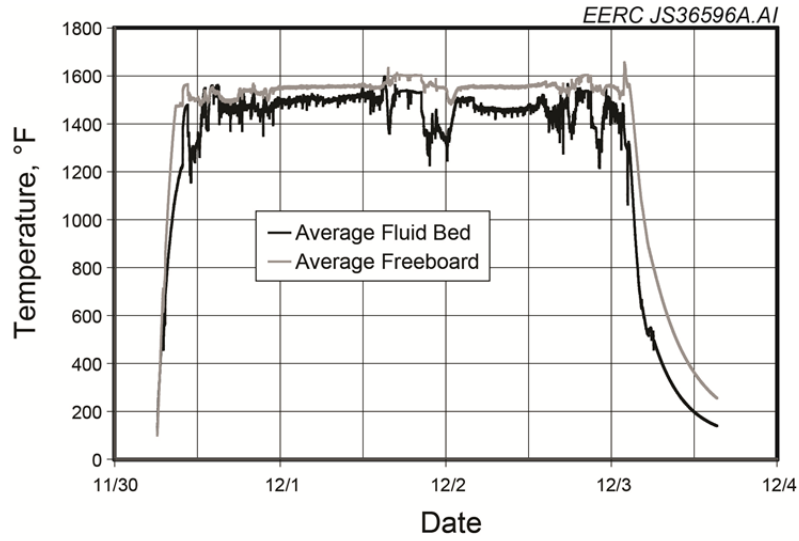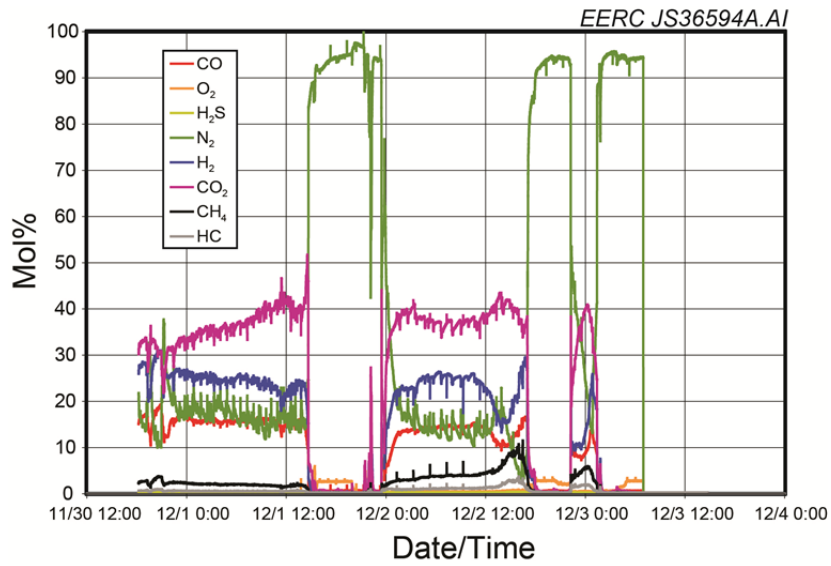
FT Reactor Trends

FBG021
Gasifier Trends

EERC JS43486.CDR
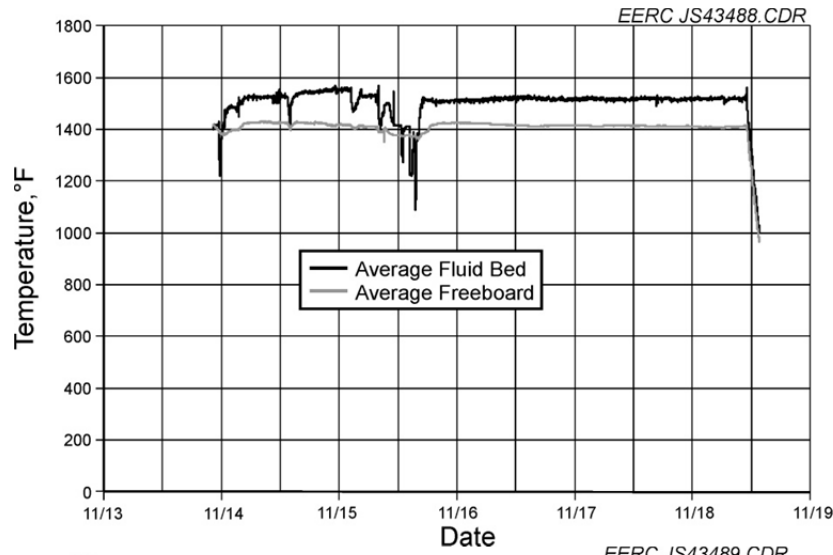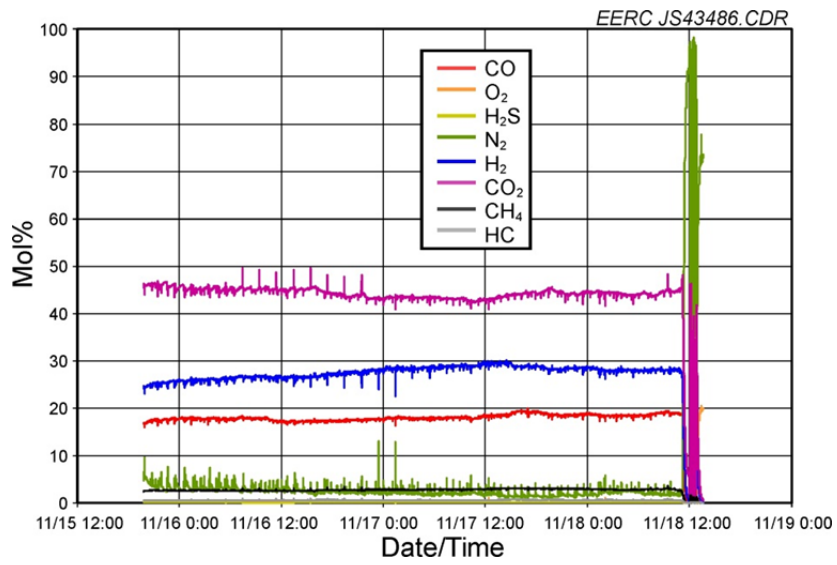
CO
O₂
H₂S
N₂
H₂
CO₂
CH₄
HC

FT Reactor Trends

EERC JS43485.CDR

FI901
FI902
FI903
FI904
FI905
FI906
Flow Rate

EERC JS43484.CDR

DPT901
DPT902
DPT903
DPT904
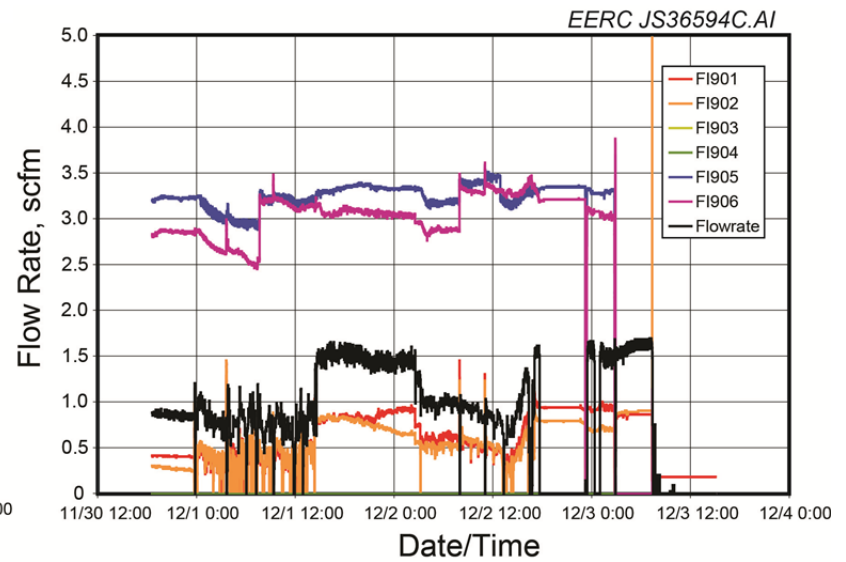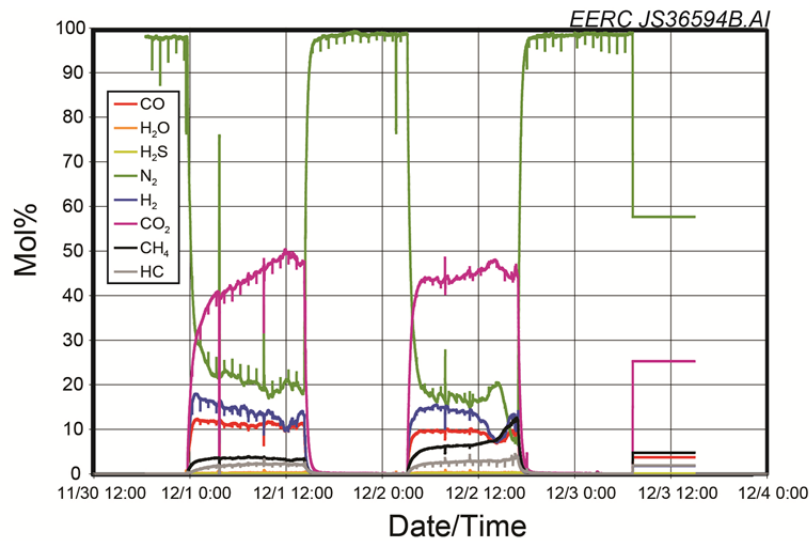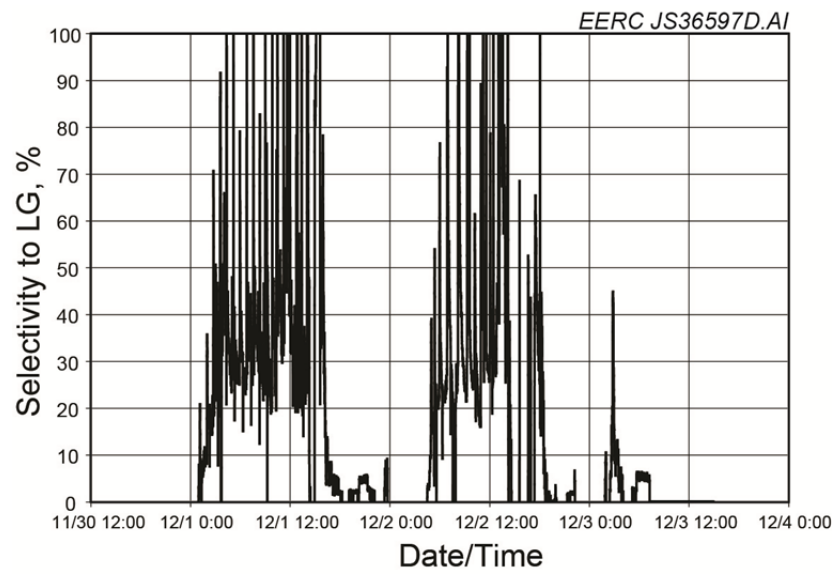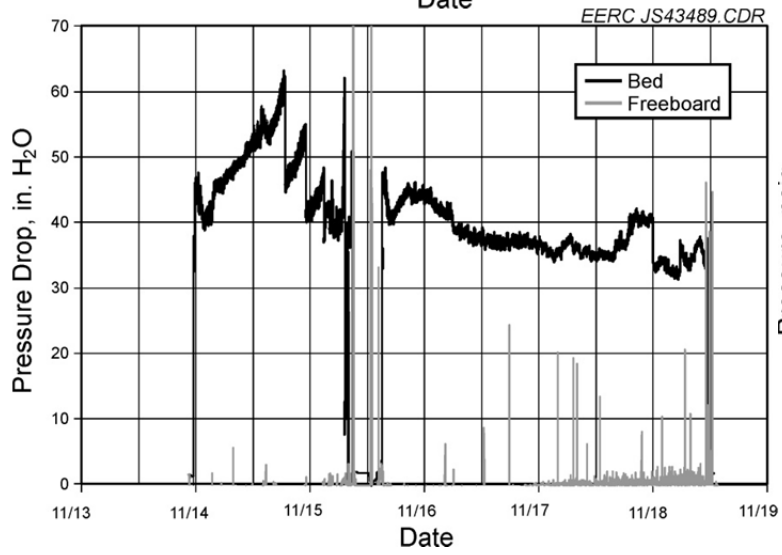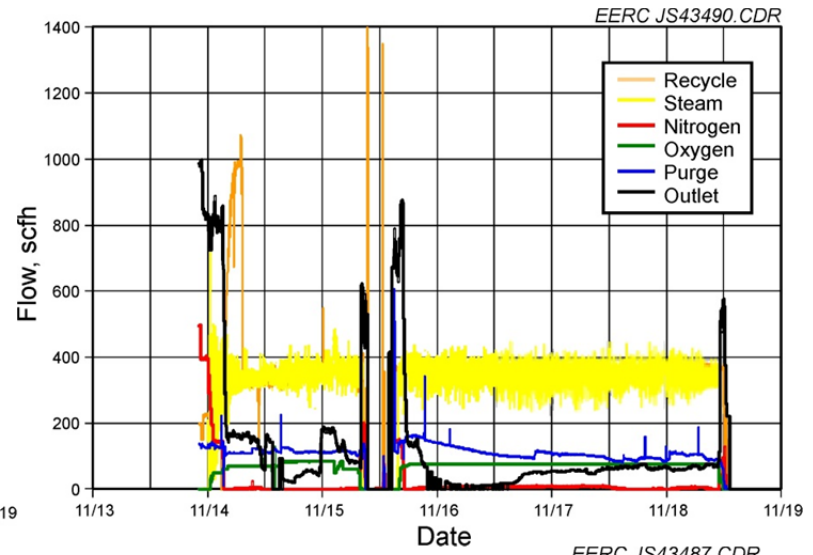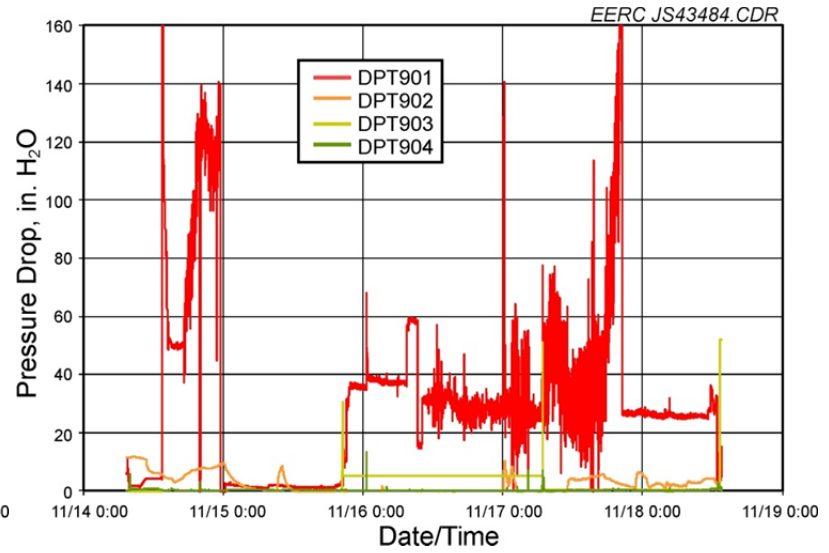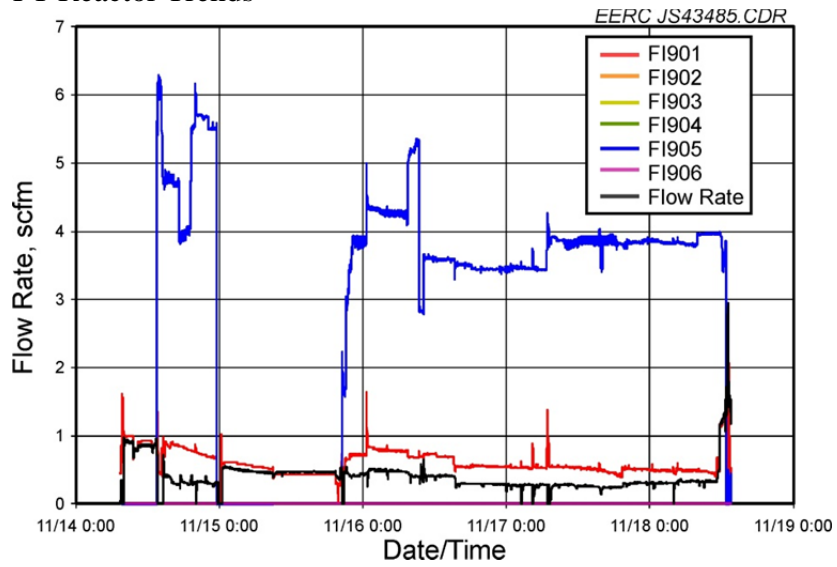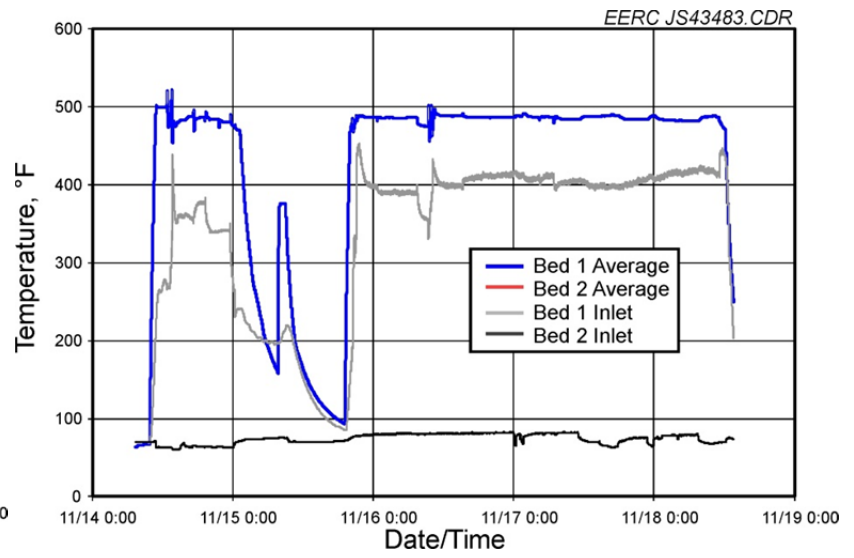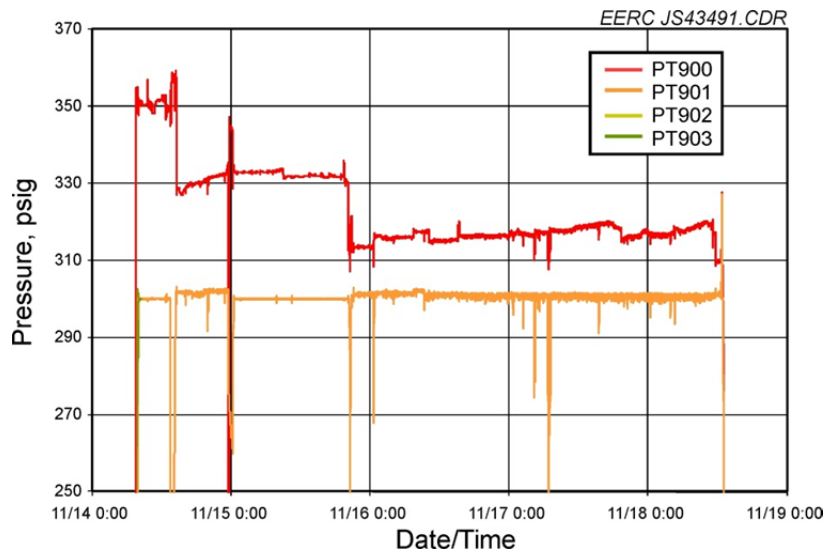
APPENDIX B

EQUIPMENT DESCRIPTION

DESCRIPTION OF EQUIPMENT

LABORATORY-SCALE FISCHER–TROPSH (FT) REACTOR

A laboratory-scale reactor system was designed and built to test potential FT catalysts prepared in the lab (Figure B-1). The system consists of three zones. Zone A is a collection of four bottled gases that are used to simulate a syngas feed stream from a coal- or biomass-fed gasifier. The bottled gases are hydrogen, carbon monoxide, carbon dioxide, and nitrogen. Mass flow controllers are used to regulate the flow and composition of the mixed feed stream. Pressure relief valves are installed before each mass flow controller to protect them in the event of a gas cylinder pressure regulator failure, since the cylinders are pressurized in excess of 2000 psig, while the flow controllers are rated for only 1000 psig. Check valves after each flow controller prevent reverse flow.

Zone B depicts the fixed-bed reactor and clam shell heater. The heater is used to preheat the gas stream (not shown in the diagram) and to heat the reactor to FT reaction conditions. The reactor body consists of a 5/8-in.-outside diameter (OD) stainless steel tube. A 1/4-in.-OD spacer tube is slid over a 1/8-in.-OD multipoint thermocouple that runs axially through the center of the reactor and measures four points for temperature control. The spacer tube may slightly reduce the accuracy of the thermocouple because of heat transfer through the spacer tube. However, the spacer tube also reduces the reactor volume and positions the catalyst closer to the double-helix
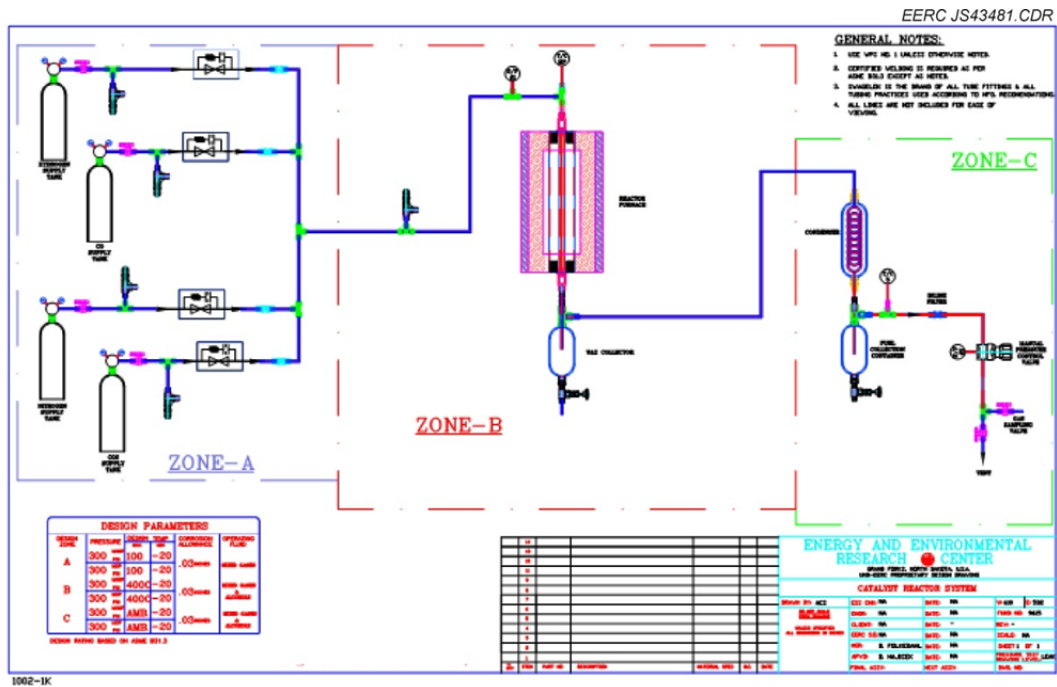

Figure B-1. Schematic of FT laboratory-scale reactor system.

cooling coils, both of which help to control temperature. In previous tests with a larger-diameter reactor tube and no spacer tube, temperature control was impossible even when catalyst was diluted with glass beads.

The gas stream enters the top of the reactor. Hot hydrocarbon liquids, gases, and unreacted syngas exit the bottom of the reactor and collect in a 1-L hot trap, which is maintained at 150°C. This temperature prevents the hot liquid hydrocarbons from solidifying into waxes while still allowing medium-chain hydrocarbon gases to condense to liquids. A 1/8-in. cable heater is installed inside the 1/4-in. tube that connects the reactor to the hot trap to prevent wax plugging. The short-chain hydrocarbon gases, water vapor, and syngas separate and continue to Zone C. The liquids that are collected in the hot trap are periodically drained through a needle valve.

In Zone C, the remaining hydrocarbon gases, water vapor, and syngas flow through an ice-cooled condenser. Water and all but the shortest of hydrocarbon chains (C_1–C_7) condense into liquids and collect in the cold trap. The remaining hydrocarbon gases, carbon dioxide, and unreacted syngas vent into a fume hood and are periodically collected in gas bags for analysis. A back-pressure control valve and two pressure transducers are used to regulate system pressure and monitor pressure drop through the reactor, condenser, and traps. A flowmeter is used to measure the venting gas flow rate. In conjunction with the mass flow controllers and gas bag analysis, a carbon mass balance can be done over the system.

Figure B-2 provides a photograph of the reactor system, illustrating how the reactor system is built onto a mobile metal frame. Mobility allows easy transport of the reactor system from the lab to a coal- or biomass-fed gasifier. The four mass flow controllers are mounted onto a metal plate on the side of the frame. The 18-in. stainless steel tube reactor is supported in the middle of the frame. The clam shell heater that is used to start the FT reaction can be moved out of the way to allow for easy access to the reactor or more aggressive air cooling for the highly exothermic reaction. When used in the laboratory, the entire system is placed under a large fume hood to capture leaking gases.

To remove heat from the reactor, two 1/8-in.-diameter stainless steel tubes are wrapped around each of the three reactor zones in a double-helix configuration (Figure B-3.) Air from one tube is fed into the top of the zone, while air from the other tube in the double helix is fed from the bottom of the zone. This counters the effect of air in the tube heating up as it travels around the reactor so that each zone has a more uniform axial temperature profile. Computer-controlled mass flowmeters continuously adjust airflow to control temperature. Axial reactor temperature can be controlled to less than ±1°C. This automation allows for continuous, unsupervised operation of the reactor.

A data collection program is used to set mass flow controller set points and collect data such as reactor temperatures, system pressures, and gas flow rates. The program also monitors the system for unsafe operating conditions such as excessive reactor temperatures or high pressure. In the event that the reactor exceeds a predetermined unsafe temperature, the program

Figure B-2. FT laboratory-scale reactor system.

Figure B-3. Double-helix reactor cooling coil.

will automatically shut off syngas flow and purge the system with nitrogen. If the system pressure becomes too high or the pressure differential between two transducers spikes because of plugging, then the program shuts off all flow to the reactor system.

HIGH-PRESSURE FLUID-BED GASIFIER (HPFBG)

The Energy & Environmental Research Center's (EERC's) HPFBG can feed up to 9.0 kg/hr (20 lb/hr) of pulverized coal or biomass at pressures up to 70 bar absolute (1000 psig). The externally heated bed is initially charged from an independent hopper with silica sand or, in the case of high-alkali fuels, an appropriate fluidization media. Independent mass flow controllers meter the flow of nitrogen, oxygen, steam, and recycled syngas into the bottom of the fluid bed. Various safety interlocks prevent the inadvertent flow of pure oxygen into the bed or reverse flow into the coal feeder.

After a review of available alloys, Haynes 556® was selected as the material most suitable for fabrication of the high-temperature, high-pressure system as well as for all of the reactor nozzles and the cyclone. The reactor was designed with the capability to operate at a maximum operating pressure (MOP) of 1000 psig at an operational temperature of 1550°F, 650 psig at an operational temperature of 1650°F, and 300 psig at an operational temperature of 1800°F. The 2500-pound 316H stainless steel flanged connections at the top and bottom of the reactor are limited to somewhat lower maximum operating temperatures but do not greatly impact the operation of the gasifier, as they are generally cooler than the reactor bed itself. A design drawing of the reactor is shown in Figure B-4. In the standard 8-ft bed, 16 thermocouple ports are spaced every 4–5 in. up the bed to monitor for loss of fluidization, solids agglomeration, and localized combustion zones, and the feed line extends up two stories to the coal hopper.

Figure B-5 is a photograph of a 15-ft extension that was added to the 8-ft bed between BP1 and BP3. This extension provides longer solids residence times and permits higher bed velocities. Additional thermocouples provide measurements approximately once every foot along the length of the extension. Temperature is controlled in the extension by six independent heaters. Another major change between BP1 and BP3 was installation of a solids recycle auger. This auger returns solids that are collected by the cyclone back into the bottom of the gasifier bed. As seen in Figure B-4, these solids were initially collected in an ash collection pot that required frequent draining. By extending the bed's total height and recycling cycle solids, the carbon conversion of the HPFBG was increased and the tar production reduced. System operability was also improved, as during BP1 the standpipe below the cyclone would sometimes back up with solids and cause the cyclone to plug. This was never an issue in BP3 or in any of the dozen or so unrelated tests conducted after the auger was installed.

Coal is fed to the HPFBG from a pressurized K-Tron® loss-in-weight feeder that provides online measurement of coal feed rate at pressures up to 1000 psig. This feeder allows instantaneous measurement of the fuel feed rate to the gasification system. The feed system electronic controls are interfaced to a data acquisition system that allows for local or remote computer control of the fuel feed rate. Above the main feed hopper is the fuel charge hopper.
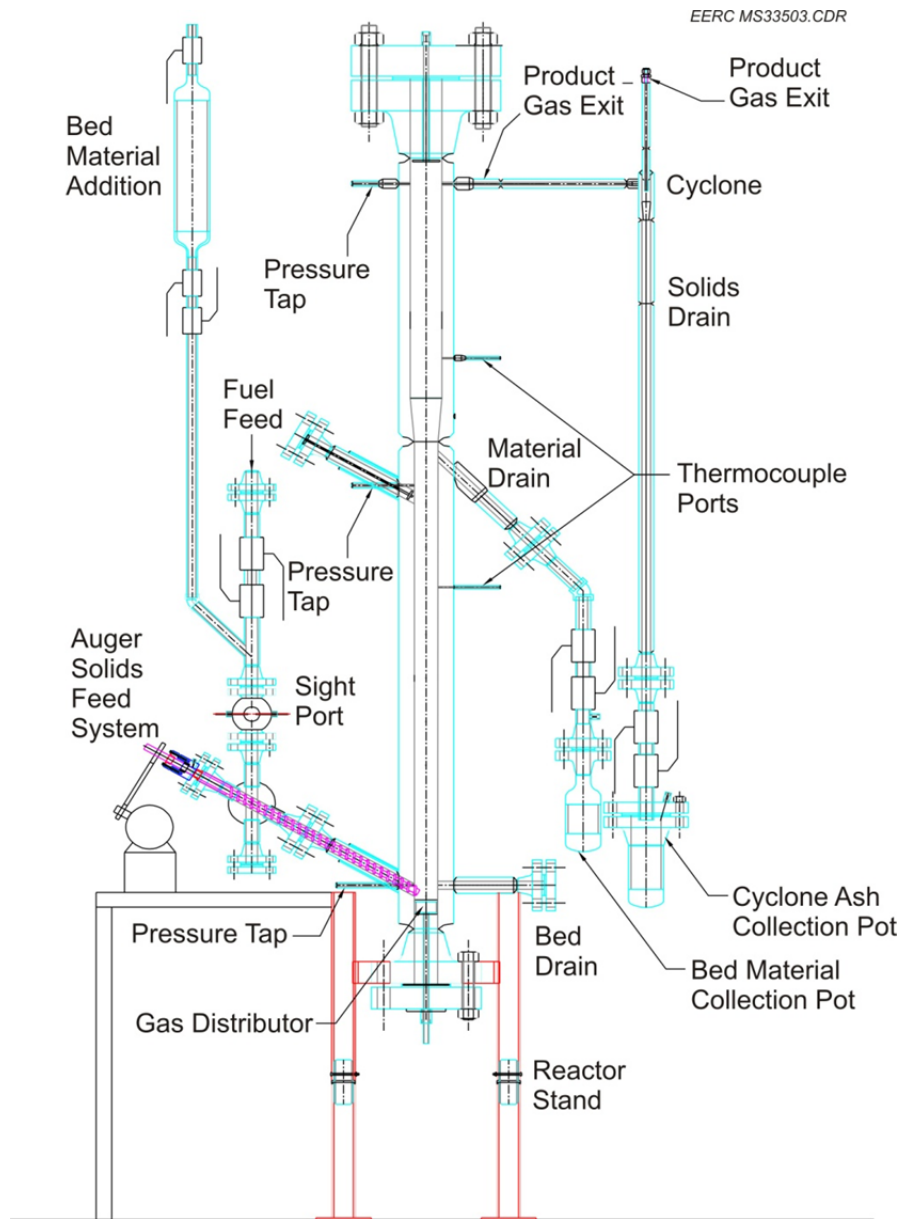
Figure B-4. Design drawing of the pressurized, fluidized-gasification reactor.

The fuel charge hopper is manually charged with fuel through the top valve while at atmospheric pressure. It is then sealed and pressurized. Finally, the fuel feed material is transferred by gravity feed to the weigh hopper inside through the lower dual-valve system. The entire feed system pressure vessel is on a movable platform to allow easy transition from the HPFBG to the EERC's entrained-flow gasifier (which shares common front- and back-end components with the HPFBG).

Figure B-5. Photograph of the top of the HPFBG extension.

Coal feed from the K-Tron system drops through a long section of vertical tubing and is then pushed quickly into the fluid bed through a downward-angled feed auger, as seen in Figure B-4. Syngas exiting the fluid bed passes through a cyclone before optionally flowing into a transport reactor that uses regenerable sorbent to remove sulfur from the syngas stream. The syngas then passes through a hot candle filter to remove fine particulate before entering a series of fixed beds. For warm-gas sulfur removal, the first bed is usually loaded with regenerable sorbent to capture bulk sulfur. The next bed is typically a polishing bed of ZnO that removes all remaining traces of sulfur from the syngas. Other beds can be loaded with water–gas shift (WGS) catalysts, heavy metal sorbent, a chlorine guard, or other sorbents and catalysts. The clean, shifted syngas, still hot and pressurized, is then routed through a series of water-cooled condensers to remove volatile organics and moisture. The clean, dry syngas exiting the condensers is then recycled through a compressor to the bottom of the HPFBG, and a portion is vented through a control valve to maintain system pressure.

The syngas exiting the system passes through a dry gas meter for mass balance. A slipstream of this depressurized, dry gas is also fed to a laser gas analyzer (LGA) and a Varian gas chromatograph (GC) equipped with thermal conductivity detectors (TCDs) for online analysis of major gas components and GC equipped with a pulsed-flame photometric detector (GC–PFPD) for low-level (ppb) analysis of sulfur species. A second LGA and a Yokogawa GC–TCD are also available and can be used either to verify readings from the first LGA and Varian or to measure gas composition downstream of particular units, such as WGS beds or the FT reactor. In addition, operators periodically sample syngas from various points throughout the system using Dräger tubes for H_2S and other trace gases to verify low-level GC–PFPD data. Figure B-6 depicts overall system process layout from HPFBG to the FT reactor using warm-gas sulfur cleanup.

PILOT-SCALE FT REACTOR

Pressurized syngas exiting the fluid-bed system can be routed to several back-end systems, one of which is a pilot-scale FT reactor with an estimated maximum liquid production rate of roughly 4 L (1 gal)/day/reactor bed. The FT reactor system meters up to 3.5 scfm/bed of clean, pressure-regulated syngas from the HPFBG through a preheater and then into a set of
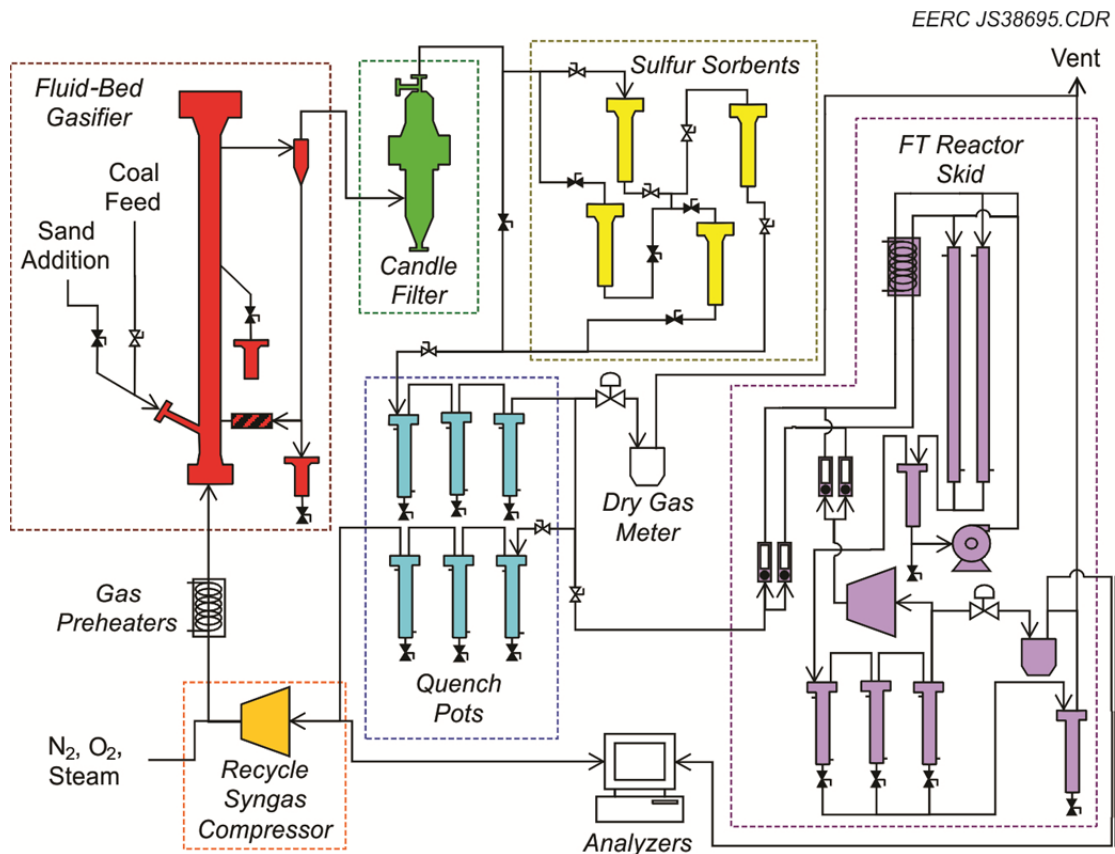

Figure B-6. HPFBG process layout.

down-flow, parallel, packed shell-and-tube reactor beds. Two reactor beds are currently installed on the system, with room for expansion to four. The reactor beds can operate at up to 1000 psig and 570°F, allowing the possibility of methanol or mixed-alcohol synthesis in future tests.

Figure B-7 provides a process flow diagram for the FT reactor skid. The shell-and-tube reactor beds are initially heated to temperature using a countercurrent flow of DOWTHERM™ through the external (shell-side) tube. Syngas passing through the beds is then slowly brought to operating pressure, which begins the exothermic FT reaction. As pressure builds and the beds begin to heat under exothermic reaction, the DOWTHERM heater is turned down and the DOWTHERM begins to function as a coolant. Because the packed-bed design lends itself to runaway exotherms, single-pass conversion is kept low, and product gas exiting the beds is recycled through preheater coils to the bed inlets. This dilutes incoming syngas and achieves higher overall conversion efficiencies. Liquid exiting the bottom of the packed beds is collected in a heated wax trap before passing through a set of water-cooled condensers to remove lighter organic material and water. Hot liquid in the wax trap can be recycled to the top of the reactor to provide further syngas dilution and catalyst cooling, thus bringing the inlet to the packed beds closer to outlet conditions. This design allows the packed beds to function similarly to slurry bed designs more commonly used in large-scale FT synthesis. Unrecycled product gas is depressurized and measured through a dry gas meter, and a slipstream is passed to an LGA and GC to provide online comparison of inlet syngas and outlet product gas composition.
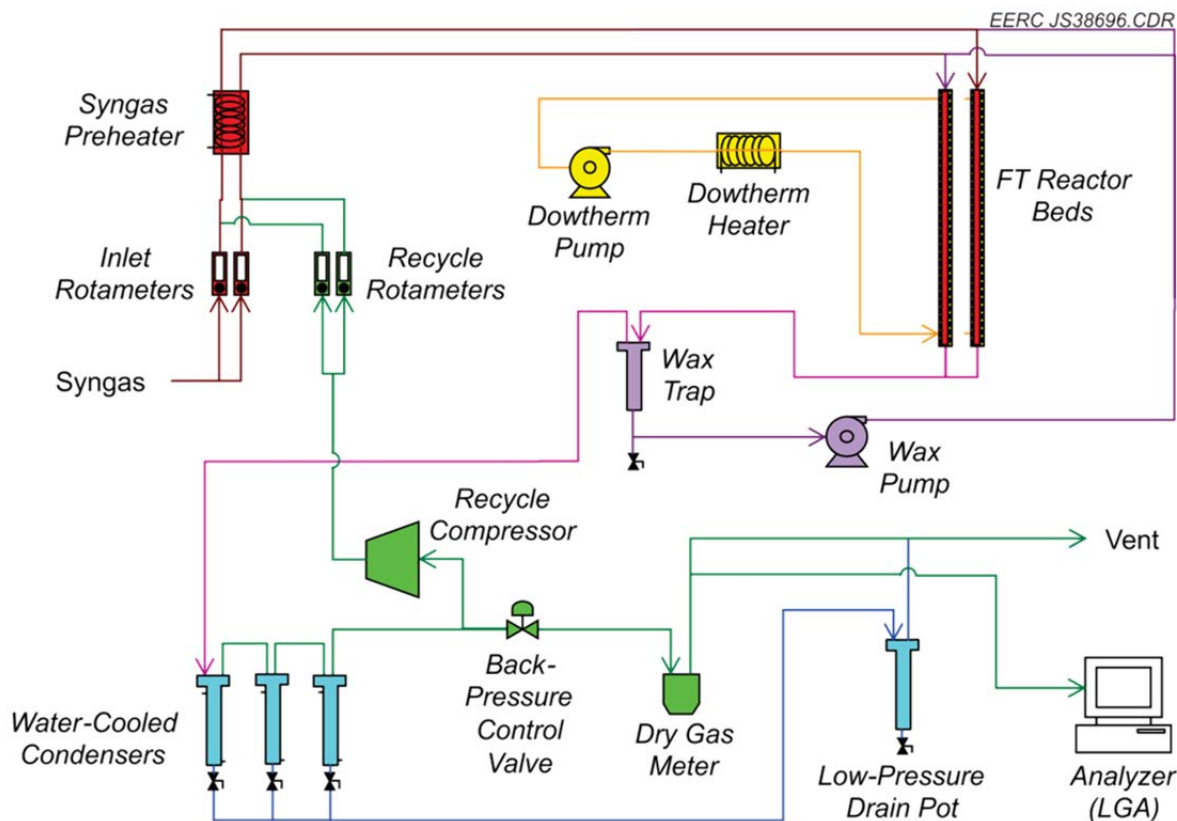

Figure B-7. Process layout for the pilot-scale FT system.

Figure B-8 is a photograph of the FT reactor system included to give a sense of scale. To date, the FT reactor has processed over 10,000 standard cubic feet of gas from a variety of coal and biomass types, including subbituminous, lignite, switchgrass, dried distiller's grains and solubles (a by-product of ethanol production), and olive pits. Gas feed has been processed both with only warm-gas cleanup and with deep gas sweetening. Because the entire unit is compact and skid-mounted, it can be readily moved to any of the different gasification systems located at the EERC or can be loaded into a truck and coupled to an off-site gasifier. This design flexibility in terms of recycle ratio, operating conditions, heat load or heat removal, and placement makes the FT reactor system a valuable tool for testing catalysts under a wide variety of scenarios.

Figure B-8. Photograph of EERC pilot-scale FT reactor.

GAS SWEETENING ABSORPTION SYSTEM (GSAS)

Figure B-9 provides a process flow diagram of the GSAS. The absorption column is constructed of 316SS pipe filled with stainless steel Koch-Glitsch IMTP 15 random packing. The packing is supported at the bottom by a perforated plate. A similar plate at the top of the column holds packing down in the event of a pressure surge. The column diameter expands above the top plate to act as a fluid disengager. Cold, lean solvent sprays down onto the plate in a 60° full-cone pattern from within the top disengager. The top of the disengager is filled with demisting material, similar to steel wool, to catch entrained liquid droplets. Gas exiting the top of the column passes through a coalescing filter to capture very fine mist before being reheated to ensure that the remaining gas is not saturated with moisture or other vapors. The hot, dry, sweet gas then flows through a pressure control valve and a Coriolis meter before being sent to the pilot-scale FT reactor.
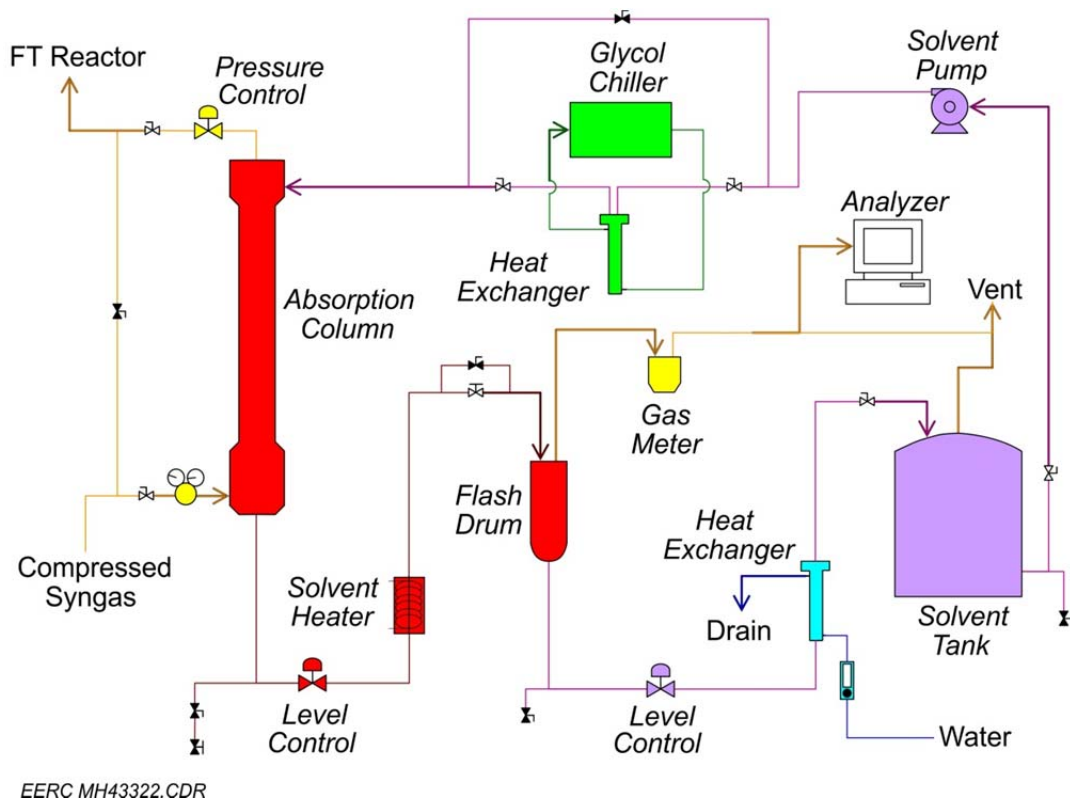

Figure B-9. GSAS process layout.

Below the bottom support plate, the column again expands out to a larger diameter to act as a lower disengager for allowing entrained gas bubbles to rise out of solution. Pressure-regulated sour gas enters the column through a port near the top of the gas headspace in the lower disengager. The inlet flow rate of sour gas is measured by a thermal mass flowmeter. An actuated bypass valve allows the control room engineer to quickly divert sour gas around the column in the event of a sudden emergency or if the pressure drop begins rising uncontrollably, which would indicate that the column is flooding.

Pressure drop is measured and controlled across the lower disengager to ensure continuous solvent flow while giving some liquid hold-up so that bubbles have enough residence time to escape. Rich solvent flows out of the bottom disengager through a hydraulic filter and then through a level control valve. Pressure downstream of the level control valve is monitored and controlled to ensure that excessive cavitation does not occur in the control valve as acid gas begins to flash out of solution. A solvent heater prewarms the rich solvent upstream of a heated flash drum.

Solvent is then depressurized through a metering valve into the single-stage flash drum. The metering valve maintains sufficient pressure in the level control valve and heater that any evolving gas will have a low volume and reduced velocity. This, in turn, reduces the rate of erosion from liquid impingement and cavitation in the control valve and heater.

The heated flash drum is wrapped in a 3000-W cable heater and is submerged in an outer vessel filled with sand. This design helps to insulate the flash drum while distributing heat somewhat evenly along its length. Fittings on top of the flash drum allow for rich solvent inlet, acid gas venting, and pressure and temperature measurement. Pressure is controlled with a metering valve in the acid gas line. The flash drum is maintained at a pressure slightly above atmospheric and a moderate temperature. The pressure and temperature are selected based on solvent properties that allow high acid gas recovery without causing solvent to boil. Acid gas exiting the drum flows through a dip tube in a knockout pot to capture any entrained liquid in case of excessive foaming or boiling. Acid gas then flows through a mass flowmeter before being sent to a natural-gas-fired thermal oxidizer to be fully combusted.

Lean solvent level is controlled with a differential pressure transmitter and control valve. Lean solvent flows through the flash drum level control valve to a water-cooled heat exchanger. The cooled solvent then collects in a 55-gallon reservoir drum with fittings for level measurement, venting, and liquid inlet and outlet. The reservoir includes an independent vent line to allow the reservoir to "breath" as liquid level rises and falls. The reservoir also includes a low-pressure burst disc in case the independent vent line plugs.

A diaphragm pump pulls liquid out of the reservoir through a sieve to collect any large particulate that might fall into the drum. The pressurized solvent exiting the pump flows through a computer-interfaced rotameter before being chilled in a glycol-cooled heat exchanger and then flows back into the top of the column, completing its loop.

The entire GSAS is housed in a Class 1, Division II facility at the EERC with all auxiliary equipment including the HPFBG and FT reactor. Flowmeters, heaters, chillers, and pipes are

sized such that the unit can process up to 1000 scfh of either coal-derived syngas or natural gas at pressures up to 1000 psig. The unit includes extended-bonnet control valves and other features that allow operation well below 0°F. Because the GSAS is skid-mounted and is designed to collapse down to a manageable height, it could also be moved to other gas sources either at the EERC or off-site for solvent testing.

1-L BATCH REACTOR

The EERC also houses a number of batch autoclave systems ranging in size from 250 cm^2 up to 2 gallons. These reactors are used when very high pressures are required or when the feed is a solid or slurry. The 1-L batch reactor, purchased from Parr, can be used at pressures and temperatures up to 5000 psig and 932°F (500°C).

The 1-L reactor is equipped with magnetically driven mixing impellers; internal baffles; a dip tube for gas inlet or liquid sampling; computer-controlled electric heating and water cooling; headspace ports for gas venting and liquid addition; and thermocouples for monitoring the heater, liquid, and gas temperatures, as seen in Figure B-10. The reactor vents through a condenser for recovering volatile matter from the vent gas, then through an inline vent trap for bubbling product gas through liquid scrubbing solutions. The 1-L reactor is also equipped
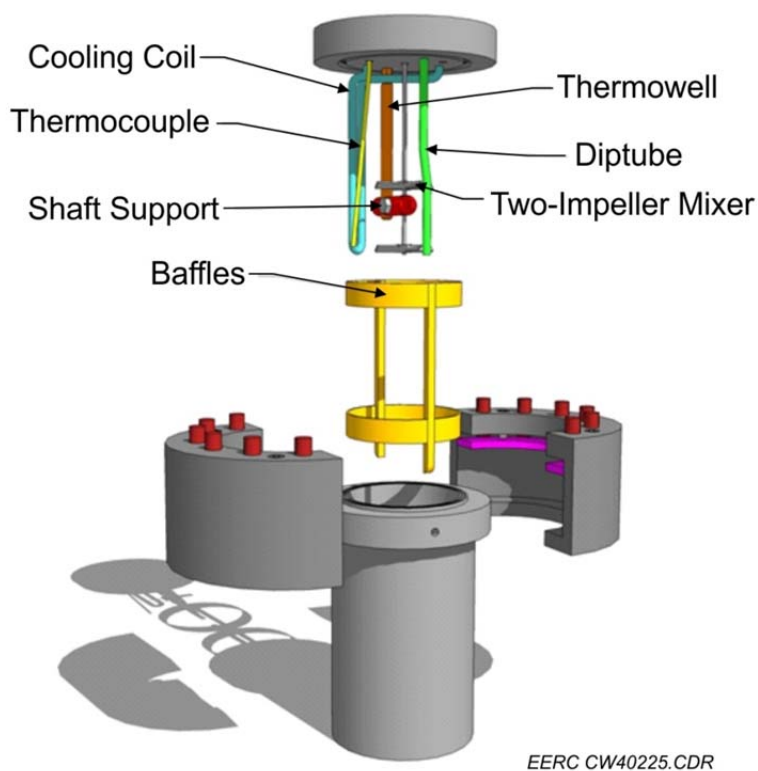

EERC CW40225.CDR

Figure B-10. Computer rendered drawing of 1-L batch reactor.

with a bottom drain for removing liquid without opening or lifting the reactor. All gas and liquid feed can be metered into the reactor manually or by computer control from behind a blast wall. Gas can be automatically metered into the reactor to maintain a pressure set point when constant pressure is required in a gas-consuming reaction.

SMALL CONTINUOUS REACTOR (SCR)

The SCR is a 50–500-mL/hr trickle-bed reactor designed and utilized to carry out two-phase gas–liquid reactions over solid catalysts at the bench scale. It is used primarily for exploratory research or small-scale liquid processing. The reactor body is constructed of Type 316 stainless steel and is fully enclosed in a single-zone electric clamshell heater. The SCR has been tested to temperatures of 600°C and pressures of 1000 psig. All temperatures, pressures, and flow rates are computer-controlled and monitored from behind an explosion-rated blast wall.

Reagents flow to the SCR through an explosion-rated blast wall to minimize the volumes of flammable gas and liquid in and around the heated equipment. The reactor is plumbed to allow top-down (trickle-bed) or bottom-up feed, depending on the desired liquid residence time and flow patterns. All inlet and outlet lines are heated and have independent temperature control to allow reagent preheat or to prevent product condensation.

Multiple thermocouples located throughout the reactor body allow close monitoring of the average bed temperature and of the temperature gradient through the bed. The use of multipoint thermocouples also allows early detection of hot-spot formation during exothermic reactions.

Following reaction, products are carried rapidly away from the heated reactor to a glycol-chilled condenser. The condensed product then flows into a dual-sample bomb system. Each sample bomb in the dual system can be independently pressurized or vented while off-line, preventing any upsets to system pressure during sampling.

A slipstream of the noncondensable product gas can be passed to an online Raman spectrometry LGA. The analyzer is a LGA–SFC–HHC synfuel gas analyzer that measures gas-phase concentrations of H_2, CO, CO_2, CH_4, higher hydrocarbons (C_XH_Y), H_2O, N_2, and H_2S.

Reactions tested in the SCR include:

- Crop oil and fatty acid conversion to distillate fuels.
- Distillate fuel hydrocracking and hydrotreating.
- Paraffin reforming to aromatics under mixed atmospheres.
- Alcohol upgrading.